Orientation Dependence Of Ionization in Ion-Molecule Collisions

A dissertation submitted in partial fulfillment of the requirements for the degree of

DOCTOR OF PHILOSOPHY

By

Deepak Sharma

Department Of Physics

INDIAN INSTITUTE OF SCIENCE EDUCATION AND RESEARCH PUNE

December 2020

To My Family

Declaration

I, **Deepak Sharma**, declare that this written submission entitled **"Orientation Dependence Of Ionization in Ion-Molecule Collisions"** represents my idea in my own words and where others' ideas have been included; I have adequately cited and referenced the original sources. I also declare that I have adhered to all principles of academic honesty and integrity and have not misrepresented or fabricated or falsified any idea/data/fact/source in my submission. I understand that violation of the above will be cause for disciplinary action by the Institute and can also evoke penal action from the sources which have thus not been properly cited or from whom proper permission has not been taken when needed. The work reported in this thesis is the original work done by me under the guidance of Prof Bhas Bapat.

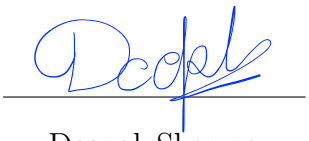

Deepak Sharma

Certificate

I certify that the thesis entitled **"Orientation Dependence Of Ionization in Ion-Molecule Collisions"** presented by **Mr Deepak Sharma** represents his original work which was carried out by him at IISER, Pune under my guidance and supervision during the period from 01 Aug, 2016 to 30 Dec, 2020. The work presented here or any part of it has not been included in any other thesis submitted previously for the award of any degree or diploma from any other University or institutions. I further certify that the above statements made by him in regard to his thesis are correct to the best of my knowledge.

30-Dec-2020

Prof Bhas Bapat

Contents

Acknowledgements

When I think about the first day at the institute and the day I am writing this part, I find myself lost in the beautiful memories. The degree of Ph.D. not only gives you a title of Dr. to your name, and the knowledge of your research field, but also the experience about life. How we grow up during this phase depends on the environment we are living in. This environment is our institution, our collaborator, our friends and family, and most importantly the Ph.D. supervisor.

First of all, I express my gratitude to Prof. Bhas Bapat. He is the right person to define a relationship between a Ph.D. supervisor and his student. I still remember the day when he said that Ph.D. is not just about paper publications but it is more about the research skills and the experience you get. His constant support and trust have made me what I am today. He brought confidence in me, especially in the presentation skills, scientific discussions, and writing of any scientific report. Working with him has always motivated me to stay in academia and do fruitful research. Being his first Ph.D. student at IISER Pune, I find myself lucky and proud. A special thanks to him for his constructive feedback on this thesis.

The work presented in this thesis is performed at IUAC New Delhi. I would like to thank Dr. C P Safvan and Dr. Pragya Bhat. My comfortable stay at IUAC and smooth operation of all the experiments have not been possible without you. Thank you for all your help during the experiments. I would also like to thank Mr. Kedarmal for the smooth operation of the ion beam during all the experiments.

I thank my RAC members Prof. Prasad Subramanian and Prof. M S Santhanam for continuous evaluation of research work.

I am thankful to IISER Pune for the fellowship during my Ph.D. tenure. A special thanks to the Physics department. A partial support of the funds for all of my visits to IUAC, all the conferences and schools I have attended during my

Ph.D. was provided by the department of Physics IISER Pune. I would like to thank the Infosys Foundation for partial support of the funds for my international trip to attend the conference and the Department of Science and Technology India for the travel grant.

I thank Nilesh Dumbre, Sudhir, Santosh, Prashant for technical support at the laboratory at IISER Pune.

A special thanks to Prabhakar Sir, Dhanashree Ma'am from the Physics office, and Tushar Sir and Sayali Ma'am from the academic office for all the help during official work at IISER. I would like to thank the staff at Srinivasa Ramanujan library at IISER Pune. A large group of people contributes to the smooth operation of our life at the campus. I must acknowledge all the non-teaching staff of IISER Pune including the IT section, electrical dept, cafeteria staff, housekeeping staff, and hostel manager Mr. Ramlal Choudhary.

I must acknowledge DISHA organization at IISER Pune. Disha is a platform for IISER students to set and work towards goals of socioeconomic equity. I was a part of this organization for three years. Apart from regular Ph.D. work, teaching school kids and interacting with them was great. This has helped me to grow a leadership skills.

Ph.D. might seem quite tough sometimes. There are ups and downs. A friend in need is a friend indeed. Thank you Mr. Mayur for always be there for me. You know me better than anyone else. I know I can not write everything for which I am so grateful to you. Thanks for understanding me and thanks for all your emotional support.

Ms. Ankita Niranjan, the emotional girl, thanks to you for being there when I needed someone to talk to. The long discussion about the philosophy of life, cooking some special dishes together, help during packing, doing all the crazy audio recording and fancy pieces of stuff, thank you very much. Mr. Yashwant Chougale, the tech guy, my roommate for one year, a special thanks to you for the academic discussion that has always motivated me to do better and better. A special thanks for the misal pav too. Every time I used to say that this is my last but you always brainwashed me for this unhealthy food, and thanks for your recommendation to buy any electronic accessories. Ms. Chinmayee Mishra, my gym buddy, the girl

who is ready to take the challenge, and the very understanding one, thanks to you. After you left IISER, I never felt the same at the gym. No one was there to whom I could say "see I am doing this exercise with a heavier weight than you". Mr. Sumit Srivastav, the singer, my only available groupmate at IISER, I had lotta memories with you. The philosophical talk on Ph.D., singing while doing the experiment, judgment on the presentation skills, playing with laboratory tools, taking random pics, and tea at 3 pm. Thanks to you for listening to me when I was frustrated with Ph.D. work. I would also like to thank my other groupmate Suddho da and Arnab Sen. I thank my friends Tejal, you were the one I knew before coming to IISER. My first air travel to home was with you and that will be memorable. I thank my friend Sayali. She is the most talented and positive person I have ever met. A special thanks to my friends Kriti, Dipti, Punita, Prashant, Naveen, Abhishek, and all of my batchmates for making my campus life fun-loving. A special thanks to my special friend Neelay Mehendele. I can not forget to mention that the whole world is going through a covid-19 pandemic now. The way I imagined my last semester of my Ph.D. was totally different.

I am grateful to Dr. Seema Sharma. Your achievements have always motivated me a lot. I will always remember that day when we had aloo paratha and that crazy story behind Rasmalai. Thanks for asking again and again about my thesis writing and motivating me for doing this as soon as I can. The masala tea at your home will be the special tea of my IISER life.

All of this has not been possible without family support. Growing up in a small village and achieving this level, I am deeply thankful to my parents for believing in me and letting me do what I wanted to. A special thanks to my sister Mamta. She is the one who guided me in this direction. Her suggestion for doing my graduation from Delhi University has changed my life. I will always be grateful to her for this.

Deepak Sharma

Abstract

This work deals with the study of the orientation dependence of ionization in ion-molecule collisions. The orientation of the molecule is defined by the angle between the internuclear axis of the molecule and the velocity vector of the incident ion beam. The interaction potential between the incident ion and molecule is not spherically symmetric and depends on the orientation of the molecule. Thus the outcome of the collision, which can be excitation or ionization, depends on the perturbation created or the energy deposited to the molecule, will thus depend on the orientation of the molecule. This dependence of the outcome of the collision on the orientation of the molecule is called the orientation effect.

The dependence has been studied via the coincidence momentum imaging technique, where, under the axial recoil approximation, the orientation of the molecule with respect to the incident projectile is determined from the measured momentum vectors of fragments. All the experiments were performed at the Low Energy Ion Beam Facility at Inter-University Accelerator Center (LEIBF-IUAC), New Delhi, India. The study is limited to diatomic molecule CO and triatomic molecule OCS. We show that a high degree of ionization is more likely to achieved when a molecule is oriented parallel to the incident projectile as compare to perpendicular orientation. Further we show that the orientation effect is not purely a geometric effect , i.e. it is not merely dependent on the shape of the molecule. An asymmetry in the angular distribution of the fragment ions is observed and quantified, showing that the orientation effect depends on the type of the constituent atoms.

The next question examined is how does the orientation effect change with the projectile? The answer to this is found by performing experiments with different types of projectiles such as p^+, He^{2+}, C^{2+}, Xe^{9+}. The orientation effect is found to depend on the interaction strength of the projectile which is parameterized by

the ratio of charge (q) to velocity (v), both in atomic units. In this work, we have covered all the interaction strength from the perturbative regime ($q/v \ll 1$) to the strong interaction regime ($q/v \gg 1$). For the perturbative regime, a simple model calculation is performed to calculate the probability of multiple ionization, involving hyperbolic trajectories with an orientation-dependent distance of closest approach and an impact parameter dependent single ionization probability. The calculated probabilities show an orientation dependence and match quite well with the experimental observations.

Keywords : orientation effect, ion–molecule collisions, anisotropy, asymmetry, momentum imaging, multiple ionization

List of publications

1. Anisotropy in multiple ionization of CO by ion collisions at intermediate interaction strengths
   Deepak Sharma et al 2018 Journal of Physics B: Atomic, Molecular and Optical Physics 51 195202

2. Orientation dependence of multiple ionization of a diatomic molecule under proton impact
   Deepak Sharma et al 2019 Journal of Physics B: Atomic, Molecular and Optical Physics 52 115201

3. Triple ionization of OCS: orientation dependence in the case of ion impact
   Deepak Sharma et al 2020 Journal of Physics B: Atomic, Molecular and Optical Physics 53 155202

4. Electron beam ion trap/source for ion–molecule collisions in the non–perturbative regime
   B Bapat, **Deepak Sharma** and S Srivastav 2020 J. Phys.: Conf. Ser.1412 152070

5. Fragmentation dynamics of CO_2^{4+}: Contribution of different electronic states [accepted in PRA]
   Sumit Srivastav, Arnab Sen, **Deepak Sharma** and Bhas Bapat

List of Figures

List of Tables

Chapter 1

Introduction

What we see around us is made of small indivisible building blocks. This idea was proposed by an ancient Greek philosopher Democritus in 450 BCE, and he called the blocks *atomos*, which means indivisible. The modern word atom is derived from this. This idea was rejected by Aristotle. He thought that every object comprises four fundamental elements: earth, water, air, and fire. The idea of Aristotle was widely accepted until Dalton proposed the modern atomic theory in 1803 [1]. John Dalton's atomic theory was based on the law of conservation of mass and the law of constant composition, which were formulated on the basis of careful observations of chemical reactions. He proposed that all elements are made of atoms and, atoms of different elements are different and have different masses. But, the internal structure and indivisibility of the atom still remained unquestioned. The discovery of the electron by Joseph John Thomson in 1897 [2] led him to propose that an atom is consist of negatively charged corpuscles accompanied by an equal quantity of positive charge, which are uniformly distributed throughout a sphere. This idea remained a conjecture until 1909. The breakthrough happened with Geiger and Marsden's experimental observation [3]. They studied the deflection of α particles through a thin film of gold and found that a small fraction of incident alpha particles, about 1 in 20000, were deflected by an average angle of 90 degrees. This deflection pattern could not be explained by the atomic model of Thomson. Later, Rutherford explained the observed deflection pattern with a simple calculation and proposed that there must be a nuclear core with a positive charge, and negatively charged electrons uniformly distributed around this [4]. These atomic models could

not explain the stability of atoms. A negatively and positively charged particles in proximity of each other should coalesce instantaneously. Discrete emission spectra of atoms, which were already observed then, could also not be explained by the Rutherford model. In 1913, Niels Bohr proposed an atomic structure model in which the electrons move in a circular orbit with discrete energy levels around a positively charged nucleus [5]. With the development of quantum mechanics [6], the atom is understood consisting of a central nucleus surrounded by a cloud of the electrons. These electron distributions are solutions to the Schrödinger equation and represent the orbital in an atom. Except for hydrogen atom, Schrödinger equation can not be solved exactly. Two or more atom combine to form a molecule. In a molecule there are electron-electron, electron-nucleus, and nucleus-nucleus interaction, and this makes Schrödinger equation very difficult to solve. In section 1.1, various approximation methods used to solve such a complex system and the molecule structure are discussed.

The static properties of atoms and molecules have been studied extensively using spectroscopic methods. An extensive collection of the database is available on NIST [7]. A greater challenge is understanding of dynamics of atoms and molecules under external perturbation. The study of dynamics of atoms and molecules under an ion or electron impact has been strongly motivated by the need of data for ionization cross-sections, testing and developing suitable scattering theories, and obtaining the information on the structure of atoms or molecules [8–12]. In section 1.2, the behavior of a molecule under external perturbation is discussed.

Molecules are not spherically symmetric. They have different shapes and structures. In ion-molecule collisions, the outcome of the collision will depend on the structure of the molecule. This thesis deals with the study of ionization of the molecule under ion-molecule collisions. The ionization of the molecule depends on the orientation of the molecule with respect to the incident ion beam. In section 1.3, the orientation dependence in ion-molecule collisions is discussed briefly. The orientation dependence is a long-studied field of research. A brief historical background is discussed in section 1.4. The questions addressed, and the outline of the thesis is discussed in section 1.5 and 1.6.

1.1 Structure of molecule

In an atom, the electrons are bound together by the central potential of the nucleus. One can write the Hamiltonian for an atom as,

$$\hat{H} = -\sum_i \frac{\hbar^2}{2m_i}\nabla_i^2 - \sum_i \frac{Ze^2}{r_i} + \sum_i \sum_{j>i} \frac{e^2}{r_{ij}} \tag{1.1}$$

where i, j refer to electrons. m, r, Z and e represent electron mass, distance from the nucleus, atomic number and electronic charge respectively. The first term corresponds to the electron's kinetic energy. The second term corresponds to the electron's potential energy, and the third term corresponds to electron-electron interaction in an atom. For a simple one-electron system like a hydrogen atom, the third term is zero, and the Hamiltonian can be solved exactly, and wavefunction can be obtained. For multi-electrons atom, the exact solution to the Schrödinger equation is not possible. An approximate solution to the Schrödinger equation can be obtained using different approximation methods such as Hartree-Fock self-consistent field method. The Hartree-Fock self-consistent method does not consider the Pauli exclusion principle, which says that no two electrons in an atom can have the same value of four quantum numbers n,l,m, and m_s. All electronic wavefunction must be antisymmetric under the interchange of any two electrons. Such an antisymmetric wavefunction can be represented by Slater determinants, and then an approximate solution can be obtained using the Hartree-Fock method [13].

In a molecule, the potential seen by the electron lacks spherical symmetry. This is readily seen for a simple diatomic molecule, where, the potential seen by the electrons is two-centred. The general form of Hamiltonian for any molecule can be written as,

$$\hat{H} = -\sum_\alpha \frac{\hbar^2}{2m_\alpha}\nabla_\alpha^2 - \sum_i \frac{\hbar^2}{2m_i}\nabla_i^2 - \sum_\alpha \sum_i \frac{Z_\alpha e^2}{r_{i\alpha}} + \sum_\alpha \sum_{\beta>\alpha} \frac{Z_\alpha Z_\beta e^2}{r_{\alpha\beta}} + \sum_i \sum_{j>i} \frac{e^2}{r_{ij}} \tag{1.2}$$

where α, β refer to nuclei, and i, j refer to electrons. m, r, Z and e represent mass, distance, atomic number and electronic charge. The first two terms correspond to the kinetic energy of nuclei and electrons. The last three terms correspond to the system's potential energy arising from electron-nucleus, nucleus-nucleus, and

electron-electron interaction.

1.1.1 Potential energy curve

As the nuclei are more massive than electrons, they can be considered fixed relative to electrons' motion. Born and Oppenheimer gave this approximation of neglecting the nuclear motion in 1927 [14]. For a fixed nuclear separation, the Schrödinger equation for an electron can be written as

$$[\hat{H}_e + V_{NN}]\psi_e = U\psi_e \tag{1.3}$$

Where

$$\hat{H}_e = \sum_i \frac{\hbar^2}{2m_i}\nabla_i^2 - \sum_\alpha \sum_i \frac{Z_\alpha e^2}{r_{i\alpha}} + \sum_i \sum_{j>i} \frac{e^2}{r_{ij}} \tag{1.4}$$

$$V_{NN} = \sum_\alpha \sum_{\beta>\alpha} \frac{Z_\alpha Z_\beta e^2}{r_{\alpha\beta}} \tag{1.5}$$

$$U = E_e + V_{NN} \tag{1.6}$$

The Hamiltonian in equation 1.4 looks similar to the one in equation 1.1, with a slight difference in the second term. The electrons are bound together by the multi-centre potential of α number of nuclei. Equation 1.5 corresponds to nucleus-nucleus repulsion, and equation 1.6 corresponds to the total potential energy of the system, which includes electronic energy E_e and nucleus repulsion energy V_{NN}. Following Born-Oppenheimer approximation, and for a fixed value of internuclear separation, the Schrödinger equation 1.3 can be solved in a manner similar to the atomic case. The potential energy U then becomes a function of internuclear separation $r_{\alpha\beta}$. This results in a potential energy surface for a polyatomic molecule and potential energy curve for a diatomic molecules.

1.1.2 Molecular orbitals

By separating the nuclear motion, the Born-Oppenheimer approximation simplifies solving the Schrödinger equation for a molecule. To solve the molecular wave-function, there are two significant approximations beyond Born-Oppenheimer ap-

proximation. First was proposed by Heitler and London in 1927 is known as the valance-bond method. Hund and Mulliken proposed the second in 1930 is known as the molecular orbital (MO) theory. Valance bond theory is based on a localized bond approach where electrons in a molecule occupy the atomic orbital of an individual atom. Whereas in molecular orbital theory, each electron is assumed to be in a molecular orbital, and the net wavefunction is a product of such one-electron wavefunctions. One can always use either of the approximations; the valance bond method or molecular orbital theory to generate the wavefunction of any complicated molecule. The significant characteristic of MO theory is that one can construct a set of molecular orbitals where electrons can be filled following the Pauli exclusion principle. The molecular orbital can be written as a linear combination of atomic orbital (LCAO). For a better understanding, let us discuss the case of H_2 molecule. A trial wavefunction can be written as,

$$\psi = c_1\phi_{1s,A} + c_2\phi_{1s,B} \tag{1.7}$$

where $\phi_{1s,A}$ is the atomic orbital of the hydrogen atom. Solving this equation for c_1 and c_2, it can be shown that it has two solutions $\psi_\pm$ such that

$$\psi_\pm = c[\phi_{1s,A} \pm \phi_{1s,B}] \tag{1.8}$$

where c is some normalization constant, ψ_+ describes a state that exhibits stable chemical bond, called bonding orbital, ψ_- describes a state which is repulsive, and is called an antibonding orbital. MO theory gives a set of molecular orbitals by combining atomic orbitals. Just like the atomic orbital $s, p, d, ...$, molecular orbitals are named $\sigma, \pi, \delta....$ These orbitals can also be distinguished based on the inversion symmetry of the molecular wavefunction. If the wavefunction does not change the sign under inversion, it is called gerade (even), and subscript g is added to molecular orbitals. If it changes sign, it is called ungerade (odd) and subscript u is added to molecular orbitals for example σ_g and σ_u.

Graphical visualization of atomic orbitals is common in textbooks [13], eg. s orbital is spherical, p orbital has two lobes, etc. A pictorial presentation of electron density in molecular orbital for a few diatomic molecule is computed by A C

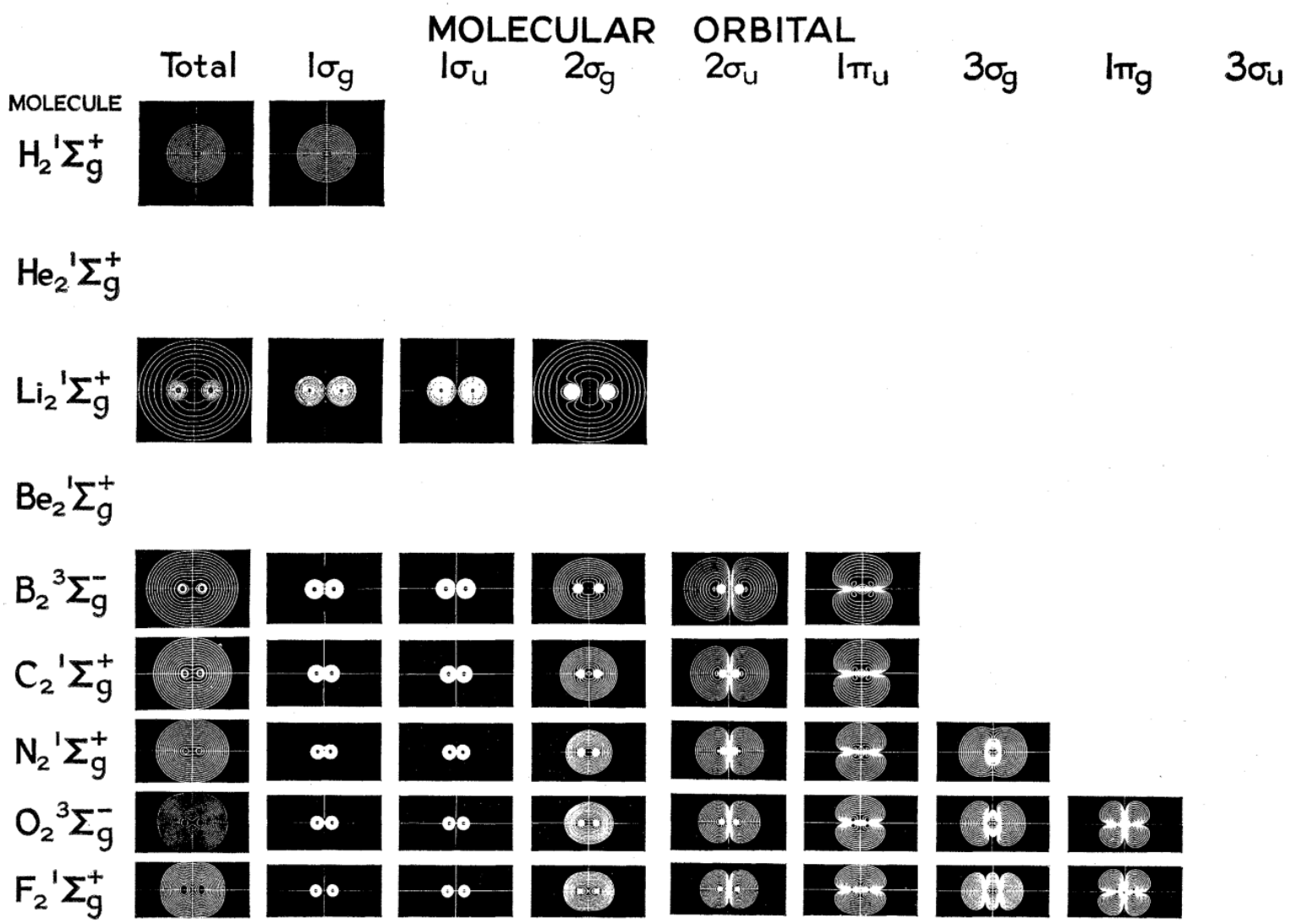

Figure 1.1: Contour map and total electron density of various molecular orbitals for different homo-nuclear molecule for a fixed internuclear distance [From A C Wahl Science 151, 961 1966 [15] Reprinted with permission from AAAS]

Wahl [15] and shown in Fig. 1.1. Let us construct the molecular orbital of a simple diatomic molecule N_2. Nitrogen atom has a total of seven electrons and the electronic configuration of nitrogen atom is $(1s)^2(2s)^2(2p_x)^1(2p_y)^1(2p_z)^1$. Following MO theory, the molecular orbital of nitrogen molecule can be constructed as $(1\sigma_g)^2(1\sigma_u)^2(2\sigma_g)^2(2\sigma_u)^2(1\pi_u)^4(3\sigma_g)^2$. The electronic state of a diatomic molecule is represented by term symbol ${}^{2S+1}\Lambda^{+/-}_{g/u}$, where Λ is the projection of orbital angular momentum on the internuclear axis, $+/-$ shows the reflection symmetry along a plane containing internuclear axis, g/u shows the parity and $2S+1$ represents the multiplicity. The term symbol for the ground state of the nitrogen molecule is ${}^1\Sigma^+_g$. For other diatomic molecules, the term symbol is also given in Fig. 1.1.

1.2 Molecule under external perturbation

A molecule is a stable assembly of electrons and nuclei moving in the mean-field of each other. Under Born-Oppenheimer approximation, the Schrödinger equation is solved, and the potential energy curve/surface for the molecule can be obtained. A typical potential energy curve for a diatomic molecule AB is shown in Fig. 1.2. The curve U_1 represents the ground electronic state of the molecule. It has a minima R_0, which we call the bond length of the molecule. In the ground electronic state, a molecule can rotate or vibrate around its center of mass, which gives rotational and vibrational energy to the molecule. The rotational and vibrational energy levels lie in the well of the ground electronic state.

Under external perturbation, when a sufficient amount of energy is transferred to the molecule, it can be excited to different electronic states. For a diatomic molecule AB, two excited state U_2 and U_3 are shown in Fig. 1.2. The transition from ground state U_1 to repulsive state U_3 is shown by a vertical transition under Franck–Condon principle. It relates the interaction between the vibrational and electronic levels of the molecule. The electronic transition is so rapid, and their timescale is so fast that the nuclei can be considered fixed during the transition. The electronic state U_3 is purely repulsive such that if the molecule is excited to this state, it will break apart into its fragments. $E(A)$ and $E(B)$ represent the internal energy of fragments A and B of diatomic molecule AB when they are far apart. The

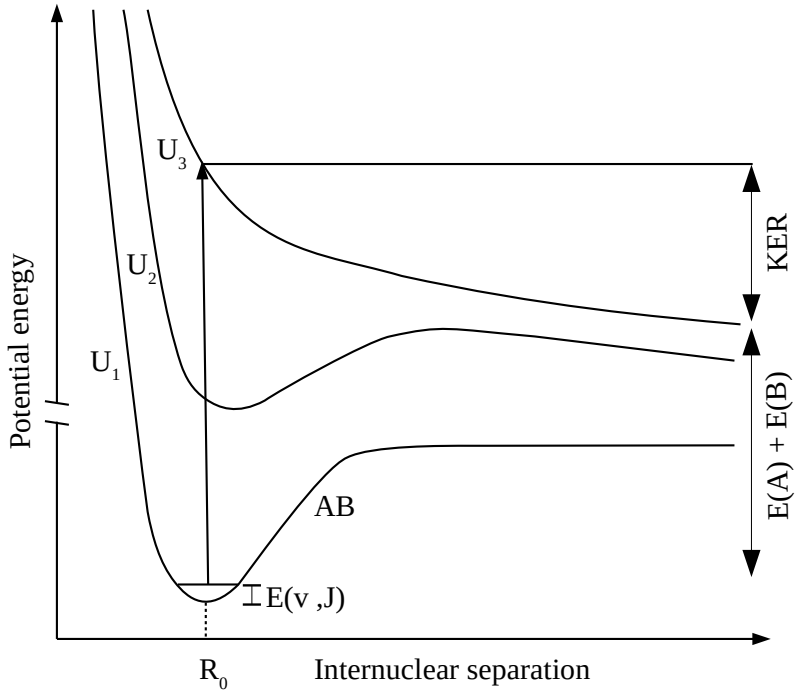

Figure 1.2: A typical potential energy curve for a diatomic molecule AB.

extra energy which is the energy difference between the asymptotic limit of curve U_3 and the point on the curve where the molecule is excited, is converted into the kinetic energy of the fragments. The total sum of the kinetic energy of all the fragments is called kinetic energy release (KER). KER carries information about that particular potential energy curve of the molecule. As shown in Fig. 1.2, the molecule can also be excited to the electronic state U_2, which has minima representing the metastable state. It may happen that a molecule tunnels through the barrier and dissociate into its fragments. We have discussed only two excited electronic states of the molecule. In general, the case is quite complicated.

A molecule can be perturbed by an external agent that can be a photon, electron, or positively charged ions. Depending on the energy deposited into the molecule, different processes can happen within the molecule. There can be excitation to different vibrational or rotational level but within the same potential well. The molecule can simply dissociate into its neutral fragments. A few electrons can be removed, which is called ionization, or an ionized molecule can further dissociate, which is known as dissociative ionization of the molecule. The effect of different types of perturbing agents on the molecule is discussed further.

1.2.1 Photon impact

A photon is a quanta of the energy of an electromagnetic field. When a molecule is irradiated with photons, depending on the energy of the photon, it can be excited or ionized. If the energy of the photon is greater than the binding energy of the electron, the electron may be removed, and the process is called photoionization as shown in equation 1.9

$$\hbar\omega + AB \rightarrow AB^{n+} + ne^{-} \tag{1.9}$$

This is in the domain of perturbation theory. In a special case, the ionization or excitation can happen when the total energy available within a short interval is large enough, even though the energy of a single photon is very small. More than one photon can be used to remove the electron, and this is called multiphoton ionization. The energy and intensity of the photon play an essential role. In an intense electric field, the potential barrier of the molecule is distorted. An electron can tunnel through the barrier and escape the potential. This process is called tunnel ionization. To distinguish between these two different ionization regime, an important parameter was given by Keldysh in 1965 [16]

$$k = \sqrt{\frac{E_b}{2U}} \tag{1.10}$$

where E_b is the binding energy of the electron, and U is the ponderomotive energy (time average energy gain by a charge particle under external electric field) of the electron under an external electric field. $k > 1$ corresponds to multiphoton ionization (MPI) regime and $k < 1$ corresponds tunnel ionization regime.

Photoionization of atom and molecule is a long-studied process [17, 18]. Samson had given a great review of this field [19]. The information about the energy level of the molecule can be obtained from the photoelectron spectrum [20]. With the advancement in technology, molecular dynamics is studied in a more controlled way using pump-probe technique [21, 22]

1.2.2 Electron impact

When a molecule is bombarded with electrons, the interaction in terms of energy of the electron can result in excitation or ionization of the molecule. At low energy, the electron can be captured by the molecule forming a transient negative molecular ion, and the process is called resonant attachment. Depending on the nature of the potential of the negative molecular ion, it can dissociate into a negative ion, and neutral atom, which is known as dissociative electron attachment (DEA) [23] or the attached electron can auto detach, which is called resonant scattering [24].

The interest and the advances in electron impact study of atoms and molecules is represented in the diverse field of research such as stellar physics, plasma, and atmospheric physics, etc. [25–27]. Dissociation dynamics of the molecule, lifetime of metastable state, the energy level of the molecule are studied under electron impact [28, 29].

1.2.3 Ion impact

Ion impact is another method of perturbing the molecule. The interaction between ion and molecule can take place in many different ways. The molecule can be excited or ionized by an ion X^{q+}, as in the case of photon and electron impact.

$$X^{q+} + AB \rightarrow X^{(q-p)+} + AB^{n+} + (n-p)e^{-} \tag{1.11}$$

But, together with direct ionization, charge exchange processes can take place between ion and molecule. Ionization mechanism for a diatomic molecule AB under ion impact X^{q+} is shown in equation 1.11. If p is zero, the charge of the projectile is the same before and after the collisions, which is called direct ionization. Non zero value of p represents charge exchange processes. Incident ion has two basic properties *i.e.* charge and velocity of the ion. The interaction strength of the projectile ion is parameterized by Sommerfeld parameter k,

$$k = \frac{q}{v} \tag{1.12}$$

where q and v are the projectile charge and velocity, respectively, in atomic units. A large value of k, corresponds to strong interaction regime and $k \ll 1$ represents the perturbative regime. Multiple ionization and dissociation of molecules under the impact of charged particles is a long studied process. Various features have been experimentally studied in detail, focusing on the ionization cross-sections [30–34] , kinetic energies of the fragments [35–37], dissociation sequences from multiply charged precursors [38–40] and electron emission patterns [41]. Theoretical studies have attempted to explain the dependence of the total and differential ionization cross-sections and energy transfer on the nature of the projectile and for different ionization channels [42–47].

1.3 Orientation dependence

In Fig. 1.3, a schematic of the collision geometry of a charged particle colliding with a diatomic molecule is shown. Based on a simple geometric argument, the interaction

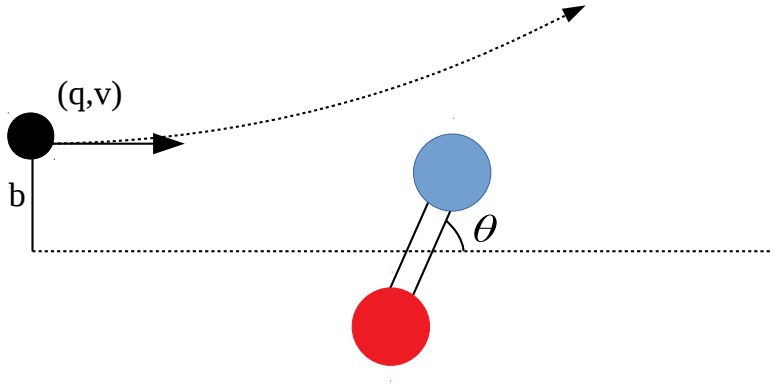

Figure 1.3: A schematic for collision geometry of a charge particle with a diatomic molecule. The molecule is oriented at an angle θ wrt the incident projectile.

time of the colliding ion with the molecule, which can be defined as R/v (where R is the bond length of the molecule and v is the velocity of the ions) will be different for different orientation of the molecule. Roughly speaking, for parallel orientation, the colliding ion will interact with both the atoms, and for perpendicular orientation, it will interact with only one atom. Perturbation caused by the ion will be different for different orientations of the molecule. The second geometric argument is based on the structure of the molecule. As discussed in section 1.1, the electron clouds

in the molecule are not spherically symmetric. Depending on the orientation of the molecule, the potential felt by the colliding ion will be different. This dependence is called the orientation effect. In ion-molecule collisions, the velocity vector of the incident projectile defines the reference, and the molecule orientation is determined with respect to that.

1.4 Earlier studies

The absence of spherical symmetry in a molecule is expected, in principle, to lead to an anisotropy in the ionization cross-sections of molecules subject to ion impact. This anisotropy was observed as early as in 1935 by Sasaki and Nakao [48, 49]. They studied the orientation dependence of dissociation probability of H_2 molecule under electron impact. They measured the angular distribution of protons with respect to incident electrons beam for the dissociation process where H_2 breaks into H^+ + H + e^-. They found that the molecule dissociates seventy times as easily in parallel orientation as compared to perpendicular orientation. The angular distribution of proton from dissociation of H_2 molecule under electron impact is studied extensively both theoretically and experimentally [50–57] and anisotropy in the distribution is reported.

Anisotropy in multiple ionization can be quantified using the coefficients of the multipole expansion of the angle-differential cross-section:

$$\frac{d\sigma^{(n)}}{d\theta} = \frac{\sigma^{(n)}}{4\pi}\Big[\sum_{L=0}^{L=\infty} \beta_L P_L(\cos\theta)\Big], \tag{1.13}$$

where θ is the angle between the projectile direction and the internuclear axis, $\sigma^{(n)}$ is the total cross-section for n-fold ionization and P_L are the Legendre polynomials. For a homonuclear diatomic molecule, only even-L terms will contribute, rendering the differential cross-section symmetric around $\theta = \pi/2$. For a heteronuclear diatomic molecule odd-L terms will contribute, resulting in an asymmetry around $\theta = \pi/2$ due to different atoms. To the lowest order of asymmetry, $d\sigma^{(n)}/d\theta$ can be approximated as

$$\frac{d\sigma^{(n)}}{d\theta} \approx \frac{\sigma^{(n)}}{4\pi}\Big[1 + \beta_1 P_1(\cos\theta) + \beta_2 P_2(\cos\theta)\Big]. \tag{1.14}$$

where β_2 represent deviation from spherical symmetry, but still reflecting a symmetry around $\theta = \pi/2$, whereas non-zero values of β_1 represent an asymmetry around $\theta = \pi/2$.

1.4.1 Theoretical studies

Theoretical investigations have confirmed the anisotropy in multiple ionization of molecules. Wohrer and Watson [58] gave a simple geometric argument for the anisotropy: it is expected because the spatial extent of the electron cloud along the direction of the projectile velocity is different for different orientation of the molecule. The anisotropy should be strong for diatomic and linear triatomic molecules since their electron clouds have a greater spatial extent along the molecular axis than in the direction perpendicular to the axis. They calculated the ionization cross-section of the O_2 molecule orientated parallel to and perpendicular to the projectile direction. Their model was based on binomial distribution of ionization probabilities under independent atom approximation [59–61], and electron correlation was ignored. Caraby *et al.* [62] have calculated the angular distribution of n-fold ionization of CO for different orientations of the molecule by extending the Wohrer–Watson model to an arbitrary orientation. Their model treats the two atoms of the molecule independently and identically. However, for a given trajectory, the effective impact parameters for the two atoms depend on the orientation of the molecule relative to the projectile, and hence the probability of ionization becomes angle-dependent. Their calculations matched the experimental data of Horvat *et al.* [63] fairly well.

Kaliman *et al.* [64] developed a model that predicted the dependence of anisotropy of different degrees of ionization on the projectile energy. In this model ionization probabilities are calculated using the statistical energy deposition model of Kabachnik *et al.* [65, 66]. The trajectory of the projectile is assumed to be linear. Molecular orbital wavefunctions are employed to calculate the various matrix elements for electron emission. Energy transfer is calculated under the unitary-convolution approximation of Schiwietz and Grande [67]. Collisions result in electronic excitations within the molecule, the deposited energy being statistically distributed among all target electrons. The probability distribution of the deposited energy is assumed to be Gaussian, with mean energy that is impact parameter and orientation de-

pendent. Depending on the energy received, some electrons escape the molecule, leaving behind a multiply charged molecule. The anisotropy in ionization cross-sections decreases with increasing projectile energy. The resulting anisotropy in multiple ionization is quantified by the parameter A, given by

$$A = \frac{\sigma(0) - \sigma(90)}{\sigma(0) + \sigma(90)} \tag{1.15}$$

Interpreting $\sigma(\theta)$ in the above equation as the differential cross-section $d\sigma^{(n)}/d\theta$ at the chosen value of θ in degrees, we can write A in terms of β_1, β_2 appearing in equation 1.14 as

$$A = \frac{2\beta_1 + 3\beta_2}{4 + 2\beta_1 + \beta_2} \tag{1.16}$$

$$= \frac{3\beta_2}{4 + \beta_2} \quad (\text{for } \beta_1 = 0). \tag{1.17}$$

It should be noted, that the β parameters are based on the entire angular distribution, while the A parameter is based only on the values of the differential cross-section at two angles. Furthermore, the parameter A will fail to capture any forward-backward asymmetry in the process. This model was primarily developed for N_2, but the authors have presented the dependence of A on the projectile energy for different degrees of ionization of F_2, CO and CO_2 subject to collisions with He^{2+} ions, and the conclusion of their work is, that the observed anisotropy is largely independent of the details of the species, and is mainly a geometric effect.

1.4.2 Experimental studies

Experimental and theoretical work go in parallel. In 1935, Sasaki *et al.* [48] presented the first experimental study. They measured the angular distribution of protons which were produced from dissociation of H_2 molecule under electron impact. In the same year, this experimental work was well supported by theory [49]. Edwards *et al.* [68, 69] reported the angular distribution of proton from dissociative ionization of H_2 molecule under proton, D^+ and He^+ impact for two specific orientation of the molecule. Later on, several experiments have confirmed the anisotropy in

multiple ionization of different diatomic molecules. Varghese *et al.* [70] studied the orientation dependence of ionization of N_2 molecule under 19 MeV F^{9+} ion beam. They showed that the highly ionized fragments are preferentially produced when the molecule is aligned with its axis parallel to the beam.

The orientation effect is also found to depend on the interaction strength (k) of the projectile. A projectile with large k can transfer the same energy at a large impact parameter as a projectile with small k at a small impact parameter (b) since the energy transfer depends approximately on k^2/b^2 [71]. Thus, when integrated over the impact parameter, the anisotropy for a given degree of ionization will tend to vanish for a projectile with large k, but will be significant for a projectile with small k. The experimental study of Siegmann *et al.* [72, 73] shows that the orientation dependence becomes stronger with increasing degree of ionization and is inversely dependent on the interaction strength of a projectile. For a given degree of ionization, anisotropy tends to vanish as the interaction strength increases. In another work, Siegmann *et al.* [74], demonstrated a clear relationship between the interaction strength and the anisotropy for varying degrees of ionization. For example, the formation of N_2^{10+} was seen to have a stronger orientation dependence for projectiles with $q/v \approx 1.2$, as compared to projectiles with $q/v \approx 2.8$. Adoui *et al.* [37] showed that for the CO molecule the orientation dependence of the ionization cross-section is very weak for large interaction strengths. Zhou *et al.* [75, 76] calculated the absolute multiple ionization cross sections for H_2O and CO for fast, highly charged projectiles. Anisotropy was observed for CO at higher degrees of ionization, while the distribution for H_2O was isotropic. The orientation effect has also been studied in charge exchange processes. Cheng *et al.* [77] obtained the angular distributions of the D^+ for electron capture and ionization of deuterium target under 2-16 MeV O^{8+} ion impact. They showed that the cross-section for the electron capture process is higher when the molecule is aligned perpendicular to the incident beam than parallel to it. Mizuno *et al.* [78] studied the orientation effect in fragmentation of CO molecule induced by charge changing process under 6 MeV O^{4+} ions. Strong anisotropy was observed for e^- loss process as compared to e^- capture by the projectile. Lüdde *et al.* [79] and Hong *et al.* [80] studied e^- capture and loss for different orientations of H_2O molecule under proton impact, and found

an orientation dependence in the case of low energy collisions.

1.5 Questions addressed in the thesis

This work deals with the study of the orientation dependence of ionization in ion-molecule collisions. As discussed in the previous section, earlier studies have looked into this aspect and many trends have been observed mostly for H_2, N_2, O_2, and CO molecule. Specifically, no study has made a distinction between the homonuclear and heteronuclear molecules, and the orientation dependence has been attributed purely to the geometry of the molecule.

In our study, we have measured the orientation dependence of ionization for diatomic molecule CO and triatomic molecule OCS resulting from the collisions with a variety of ion beams, e.g. p^+, He^{2+}, C^{2+}, and Xe^{9+}. For CO, we show that the heteronuclear nature of the molecule gives rise to an asymmetry in the ionization process. A higher degree of ionization is likely to be achieved in the collision when the incident ion first encounters the oxygen atom rather than the carbon atom. Thus, the orientation effect is not purely a geometric effect rather it also depends on the constituents of the molecule.

For molecules with differing bond lengths, the longer molecule is likely to show greater asymmetry and anisotropy in the angular distributions of the fragment ions. For this, we choose a triatomic molecule OCS to further extend our study of orientation dependence in ion-molecule collisions. For the triatomic molecule OCS, it is difficult to determine the orientation of the molecule with respect to the ion beam because of additional degrees of freedom. We provide an alternative method to determine the orientation of the molecule and quantify the anisotropy and asymmetry in the distribution.

Furthermore, the dependence of the orientation effect on the interaction strength ($k = q/v$), where q and v are the charge and velocity of the ion beam in atomic units, is studied. For a given degree of ionization, the orientation effect decreases as one moves towards either the perturbative regime ($k < 1$), or towards the strong interaction regime ($k \gg 1$). For the perturbative regime, a semi-classical model is used to calculate the orientation dependence of ionization probability.

1.6 Outline of thesis

This work presented here is divided into six chapters. In chapter one, we have discussed the structure of the molecule and historical background devoted to the study of the orientation dependence in ion-molecule collisions.

Chapter two deals with the experimental technique and data analysis methodology. The ion source used to create the incident ion beam is discussed. The principle of time of flight mass spectrometer and the experimental setup at Low Energy Ion Beam Facility (LEIBF) at IUAC used to perform all the experiments is described. The data analysis procedure followed to determine the orientation of the molecule with the incident direction of the beam is discussed.

The next three chapters are based on the publications. In chapter three, the orientation effect in multiple ionization of CO molecule under the perturbative regime ($k \leq 1$) is discussed. We show that for a heteronuclear molecule CO, there is a forward-backward asymmetry in the distribution. The orientation effect is not purely a geometric effect but depends on the constituents of the molecule. With an increase in projectile energy or when we go to a highly perturbative regime, the orientation effect decreases. For the perturbative regime, a semiclassical model calculation is performed to obtain the orientation dependence of the ionization cross-section. The applicability of this model is checked with earlier reported results.

In chapter four, we discuss the orientation effect in multiple ionization of CO under intermediate ($k \approx 1$) and strong ($k \gg 1$) interaction regime. For the intermediate interaction regime, we show that the orientation effect or the anisotropy and asymmetry parameters, decrease as we go to to the perturbative regime or the strong interaction regime. A comparison is made with earlier theoretically calculated results. For a strong interaction regime, a separate set of experiments is performed. No orientation effect is observed for high k projectiles.

In continuation of this, the orientation effect for a triatomic molecule OCS is presented in chapter five. For a two-body break-up, the measurement of the molecule orientation is straightforward. The situation is quite complex for a three-body breakup. The two major challenges to determine the orientation of the molecule, 1. The mixing of concerted and sequential dissociation channels and 2. the bond angle distribution in the ground electronic state of the molecule, which results in

the asymptotic angular distribution to be different than the actual bond angle of the molecule, are discussed. A representation to quantify the orientation effect for triply ionized OCS is discussed in this chapter.

All of the results are summarized in chapter six. A future outlook in the continuation of this work is also discussed.

Chapter 2

Experimental tools and data analysis methodology

This thesis deals with the dependence of the ionization cross-section on the orientation of the molecule with respect to the incident beam direction. The orientation angle is defined as the angle between the internuclear axis of the molecule and the velocity vector of the incident beam. In most of the ion-molecule collisions experiments, target molecules are randomly oriented in space, so the experimental measurement of this orientation angle is not straightforward. But for the special case of dissociative ionization of a diatomic molecule by fast ions, it is possible to measure the angle between the molecular axis and the incident ion beam by a coincidence measurement of the angular distribution of the two fragmenting ions. In this chapter, the experimental technique used to perform this type of experiment is discussed. All the experiments presented in this thesis were performed at Low Energy Ion Beam Facility at the Inter-University Accelerator Centre, New Delhi, India [81]. The experimental setup at the facility is described briefly. The steps followed for the data analysis are discussed in the last section.

2.1 Requirements

A schematic of the interaction between the incoming charge particle and target molecule before and after the collision is shown in Fig. 2.1. Incident charged particle interacts with the molecule and there can be elastic scattering, excitation–

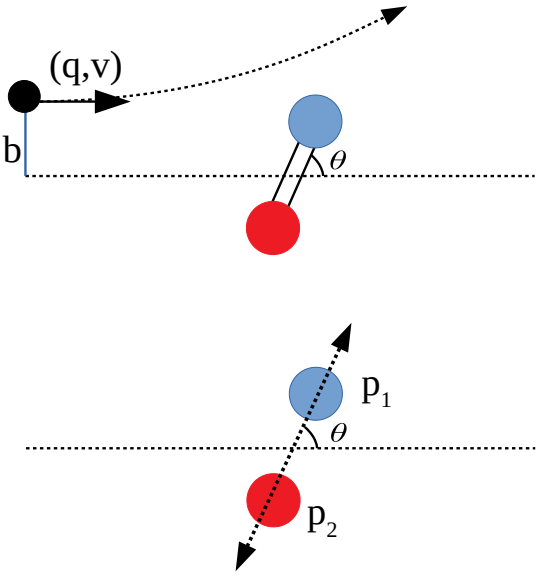

Figure 2.1: A schematic of collision between incident charge particle and target molecule oriented at an angle θ. After collision, the fragment ion fly back to back with momenta $\vec{p_1}$ and $\vec{p_2}$. Two different coloured atoms represent heteronuclear molecule.

fluorescence, charge exchange or a few or more electrons can be removed. Here our focus is on the ionization of the molecule. For the experiments presented in this work, the interaction time scale between the incident ion and the molecule is of the order of ≈100 as. The interaction time is much shorter than the vibrational time scale, which in turn is much shorter than the rotational time scale of the molecule. The dissociation time scale of the molecule is of the same range as the vibrational timescales for low charge states, and shorter for higher charge states. Hence we can make the assumption that the molecules are frozen in space for the purpose of describing the dissociative ionization. This is called axial recoil approximation, i.e. when a molecular ion is formed in a dissociative state, the dissociation products can be assumed to move apart along the straight line defined by the internuclear axis of the molecule at that instant. Thus the orientation of the molecule at the instance of fragmentation can be derived from the directions of the measured momentum vectors of the fragments. In the next few sections, we will describe the individual components of the experimental setup used to perform this type of experiments. First, we will discuss the ion source used to create highly charged ions. The principle of time of flight spectrometer and the technical details of the recoil ion momentum spectrometer used for the experiments will be discussed in the subsequent section.

Then we will briefly discuss the working principle of various types of detectors and data acquisition systems. The analysis procedure followed to obtain the orientation angle is discussed in the last section.

2.2 Ion source

There are different techniques to create an ion beam for ion-molecule collisions experiments. In this section, we will briefly discuss the ion source present at the Low Energy Ion Beam Facility at IUAC New Delhi. The projectile ions are created using Electron Cyclotron Resonance (ECR) ion source. The ion source provides multiply charged ion beams at a wide range of energies from 25 to 350 keV/q. The ECR ion source can be described as a plasma reservoir for electrons, neutral atoms, and ions. Production of highly charged ions occurs in a sequence of ionization steps under electron impact. An electron, in a static and uniform magnetic field, moves in a spiral orbit due to the Lorentz force. For an arbitrary initial velocity vector there are two components of motion of the electrons. The velocity component along the magnetic field lines, superimposed with the circular motion in the plane perpendicular to the same field, results in the cyclotron motion with gyration frequency ω. When microwave of the same frequency is injected into a volume containing low-pressure gas, then the electrons are resonantly accelerated or decelerated, depending on the phase of their transverse velocity component with respect to the electric field. The ECR ion source makes use of this electron cyclotron resonance condition to energize the plasma. The injected microwaves heat free electrons in the gas which in turn collide with the atoms or molecules of the gas in the volume and cause ionization. Highly charged ions are produced in successive collisions. By using a suitable extraction electrode one can extract those ions from the ECR ion source and further accelerated by a DC acceleration column.

2.3 Time of flight mass spectrometer

Time of flight is a unique technique to separate the ions according to their mass (m) to charge (q) ratio. The time of flight of the ions depends on the configuration of electric field through the spectrometer. In a single field time of flight mass spec-

trometer, the ions are extracted using an extraction field and pass through a field free drift tube. The discussion here will be on the double field time of flight mass spectrometer since we have used a double field spectrometer in our experiments. A schematic of double field time of flight mass spectrometer is shown in Fig. 2.2. It consists of the extraction region, the acceleration region, and field-free region along the same axis. The full details and principle of a double field time of flight mass spectrometer are well described by Wiley and McLaren [82].

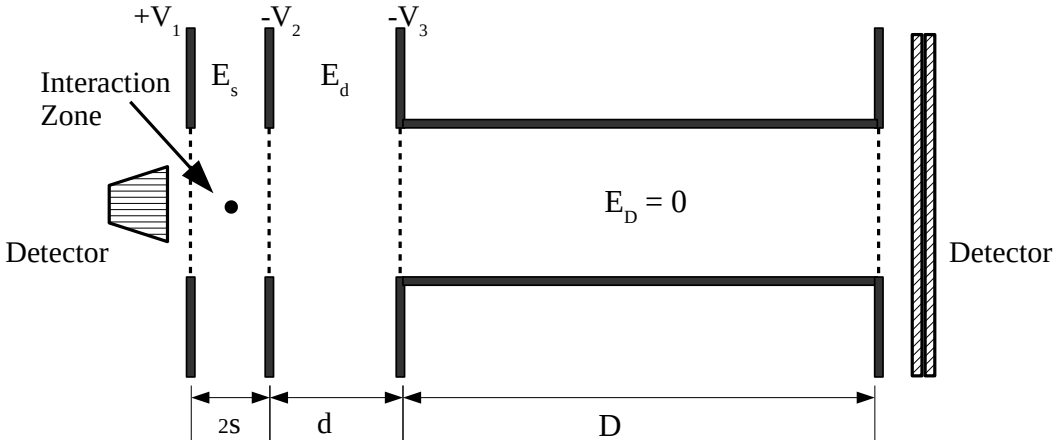

Figure 2.2: A schematic of the double field time of flight mass spectrometer.

After the collision between projectile and target molecule, ions and electrons are created at the interaction zone. The extraction field E_s is applied to separate the ions and electrons. The ions are further accelerated by electric field E_d, pass through to the field-free region, and detected by a detector. The length of extraction, acceleration, and field-free regions are shown as $2s$, d, and D respectively. The double field spectrometer can be operated as a single field spectrometer by setting E_s equal to E_d. The time of flight will be decided by the velocity component $(v_z)$of the ion parallel to the time of flight axis taken as Z-axis. The time of flight of the ion in different regions is given by

$$T_s = \frac{m}{qE_s}\Big[\pm v_z + \sqrt{v_z^2 + \frac{2qsE_s}{m}}\Big] \tag{2.1}$$

$$T_d = \frac{m}{qE_d}\Big[-\sqrt{v_z^2 + \frac{2qsE_s}{m}} + \sqrt{v_z^2 + \frac{2qsE_s}{m} + \frac{2qdE_d}{m}}\Big] \tag{2.2}$$

$$T_D = \frac{D}{\sqrt{v_z^2 + \frac{2qsE_s}{m} + \frac{2qdE_d}{m}}} \tag{2.3}$$

The total time of flight of the ion is

$$T = T_s + T_d + T_D \tag{2.4}$$

The $\pm$ signs in v_z correspond to initial velocity directed away from and towards the detector. It is clear from the above equations that time of flight of the ion is proportional to $\sqrt{m/q}$ and ions with different $\sqrt{m/q}$ will have characteristic time of flights.

The interaction zone or the source of the ions is not exactly a point type. Due to initial spatial spread in the interaction zone, ions of same energy will arrive at different time which gives rise to spread in the time of flight distribution. The resolution of time of flight spectrometer is given by the ratio $t_0/\Delta t$ where Δt denotes the full width half maximum value of the ToF distribution. Since the time of flight is proportional to $\sqrt{m/q}$, the mass resolution is given by

$$\frac{m}{\Delta m} = \frac{1}{2}\frac{t_0}{\Delta t} \tag{2.5}$$

To improve the resolution of time flight mass spectrometer different focusing conditions are applied, one of them is space focusing which reduces the effect of the spatial spread of the interaction volume on the time of flight. The space focusing condition is given by [82]

$$D = 2s_0 k_0^{\frac{3}{2}}\left[1 - \frac{1}{k_0 + \sqrt{k_0}}\frac{d}{s_0}\right] \tag{2.6}$$

where

$$k_0 = \frac{s_0 E_s + dE_d}{s_o E_s} \tag{2.7}$$

For a fixed s_0, d, and D, k_0 is the only variable. The focus condition for a double field time of flight spectrometer is obtained by the ratio of E_d to E_s. The focusing condition for a single field ($d = 0$, $k_0 = 1$) time of flight mass spectrometer is given as $D = 2s_0$. As we can see, this a purely a geometric condition.

The second factor which introduces a spread in the time of flight distribution is initial energy of the ions. The target molecules at room temperature have a distribution of energy. The ions created at the same position but with different initial energy will give a spread in time of flight distribution. This spread can be minimized by accelerating the ions to high energy as compared to the initial energy of the ion.

2.4 Experimental setup

The experimental setup used in this thesis is based on a double field time of flight mass spectrometer. With the development in coincidence momentum imaging technique [83, 84], it is possible to measure the momentum vector of all the fragments ions. The experimental setup used in this work is well described in [85]. We will briefly discuss the setup here.

2.4.1 Recoil ion momentum spectrometer

A schematic of the experimental setup with all the lengths and voltages applied is shown in Fig. 2.3. A collimated beam of energy selected projectiles extracted from

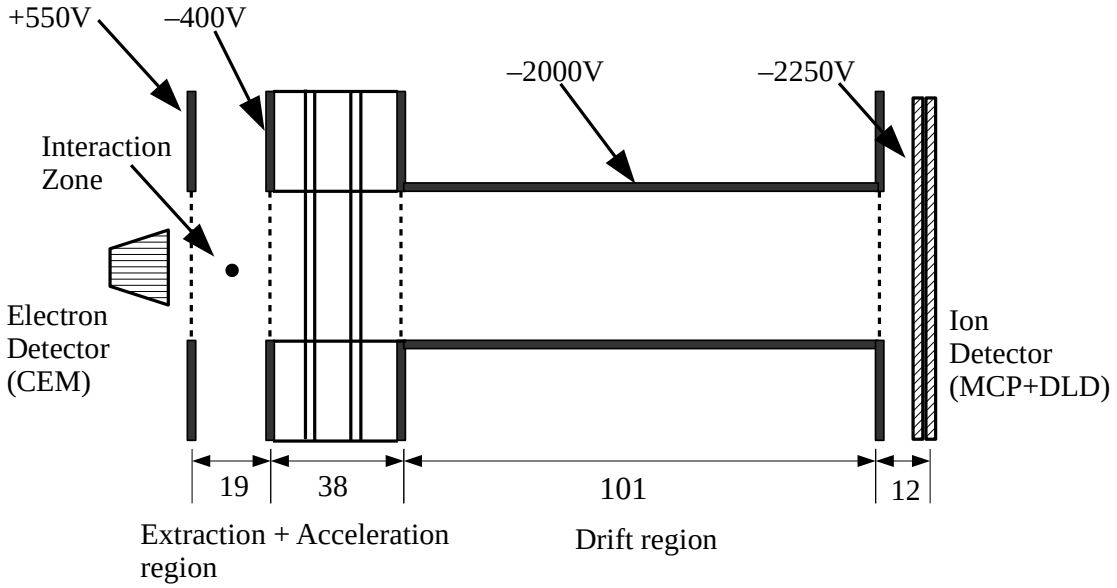

Figure 2.3: A schematic of the experimental setup. All the lengths are in mm.

an electron cyclotron resonance ion source is made to collide with an effusive beam of target molecules in a crossed beam geometry (at room temperature). The pressure

in the chamber is maintained low enough to ensure single collision condition in the interaction zone (base pressure of the chamber is around 1.8×10^{-8} Torr, while the operating pressure with the effusive gas target is maintained around 2.5×10^{-7} Torr).

The interaction zone is shown as a dot in the schematic. An electric field of strength $\approx 50\times10^{6}$ V/mm is applied in the interaction zone for the extraction of ions and electrons perpendicular to the projectile direction. Electrons are extracted on one side of the interaction region. A Channel electron multiplier (CEM) is used as an electron detector. Ions are extracted on the opposite side, fly through a time-of-flight spectrometer. They are further accelerated and detected by a time and position-sensitive detector based on a microchannel plate and a delay line anode. The working principle of all the detectors is discussed in the next section. Ion arrival times and positions are recorded in coincidence with the ejected electrons. Event-by-event position and time-of-flight data were recorded during the experiment. The molecule can be multiply ionized by direct ionization or charge exchange collisions. The charge exchange process results in a charge change of the projectile. These processes cannot be separated using this set-up.

Trajectories of the fragment ions in the spectrometer were determined by simulation using the SIMION suite of programs [86], and it was found that ions with energies up to 19 eV/q are transported without loss to the detector, irrespective of their direction of emission from the interaction volume. The typical time resolution of the spectrometer was measured to be 2.9×10^{-3} (Δt/t). The angular resolution of the spectrometer is estimated to be 12 degrees based on the width of the momentum-sum distribution of ion pairs.

2.4.2 Electron and ion detectors

In the current experimental setup, channel electron multiplier is used as an electron detector and an assembly of micro-channel plate with delay line anode is used for the arrival time and position information of the fragment ions.

Electron detector

A Channel Electron Multipliers (CEM) usually has a cone-like structure that is built from glass as shown in Fig. 2.4. The inside coating is done from a material that has a low work function. The wider end of the CEM funnel serves as the electron

input side while the narrower end is the detection side. The coating material is usually a semiconductor that is highly resistive. In the end, there is a metallic anode from which the electron detection pulse is collected. A potential difference is created within the CEM by biasing the narrower end of the cone with a positive high voltage with respect to the wider end of the cone. The typical voltages applied during the experiment are +300 V on the cone and +2500 V at the end.

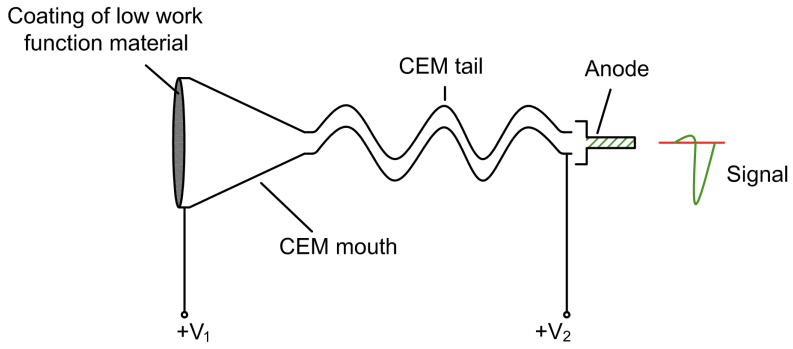

Figure 2.4: A schematic of channel electron multiplier (CEM).

When an incoming electron hits the inner surface of the CEM cone, the secondary electrons from the coating material is produced. These secondary electrons are accelerated due to the potential difference within the CEM and they, in turn, hit the CEM inner wall to produce more electrons. Due to the potential gradient, the electrons move towards the narrower end of the CEM with a cascade of more and more electrons. Due to multiple avalanches, for a single electron hit on the CEM surface, an electron shower containing about 10^7 – 10^8 electrons is generated within the CEM. This electron shower is collected by the anode when it emerges out of the CEM and hence a pulse corresponding to the electron detection is recorded. In the experiment, the electron detector from Sjuts Optotechnik Gmbh, Model KBL 10RS is used.

Ion detector

The ion detector is a combination of the micro-channel plate (MCP) and delay line anode. Similar to CEM, MCP works on the principle of electron multiplication. A micro-channel plate is a closed pack assembly of millions of miniature electron multipliers oriented parallel to one another. Each channel act as a separate electron multiplier. Center to center distance and diameter of these channels in micrometer range can be achieved. A schematic of the micro-channel plate is shown in Fig. 2.5.

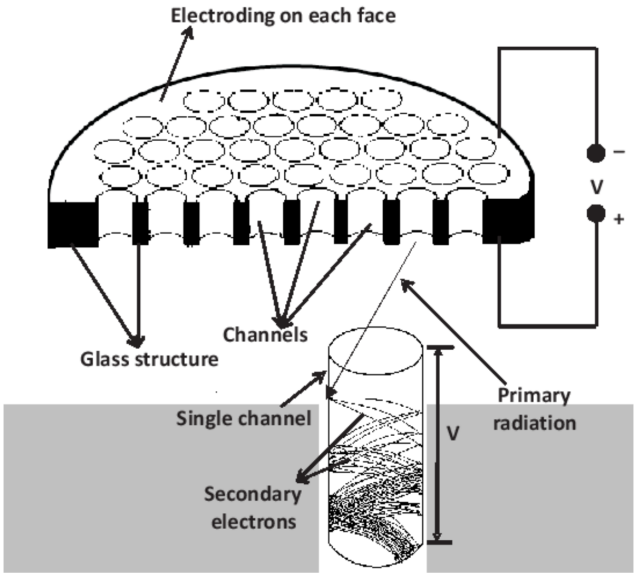

Figure 2.5: A schematic of microchannel plate.

Each channel's inner wall is made of semiconducting material. Metal electrodes are evaporated onto the two surfaces to get electrical contact to individual channels. Length to diameter ratio is an important factor which is 40/60/80 for standard commercial MCP. MCPs are sensitive to ionizing radiation with a penetration depth between 1 nm to 20 nm. When a charged particle hits the MCP, the electrons are removed from the semiconducting surface of the electrode. The potential gradient pulls the electrons to the backside of MCP. This results in a further avalanche of secondary electrons and a shower of electrons is generated at the end of MCP.

After MCP, the electron shower hit another detector called delay line anode. This is a very unique technique to extract information about the position of the charge cloud with good resolution. The details of the delay line anode can be found [87, 88]. As shown in Fig. 2.6, it consists of two sets of wires that are wound around rectangular support in many loops with wire spacing of approximately 0.5 mm. When a charge cloud hit the detector, the signal travel to four corners named x_1, x_2, y_1, y_2. The position information is encoded by the measurement of time a signal needs to travel along these wires to the corners. The time difference between the signals arriving at both ends of the wire is proportional to the position coordinate of the charged cloud centroid. For example, if the charge cloud hits the delay line anode exactly at the center, the time difference between the signal arriving on either

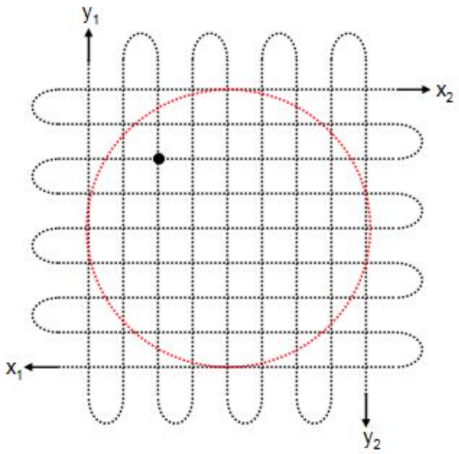

Figure 2.6: A schematic of delay line detector.

delay line is zero, and the coordinate of the charge cloud will be $(0, 0)$. The time signal at both ends extracted by both sets of wire gives the coordinate information. The crossed pair of delay lines form the x and y grid, and the position is derived from the time differences between the pairs of pulses reaching the ends of the two delay lines:

$$x = (t_{x1} - t_{x2})v_{sig} \tag{2.8}$$

$$y = (t_{y1} - t_{y2})v_{sig} \tag{2.9}$$

For a given length of a delay line, the time sum $(t_{x1} + t_{x2}$) of the signal traveling at both end is constant. This is called the sum condition. The time sum will be different for different anode depending on the length of the delay line. The time sum condition is used to distinguish between true and false events.

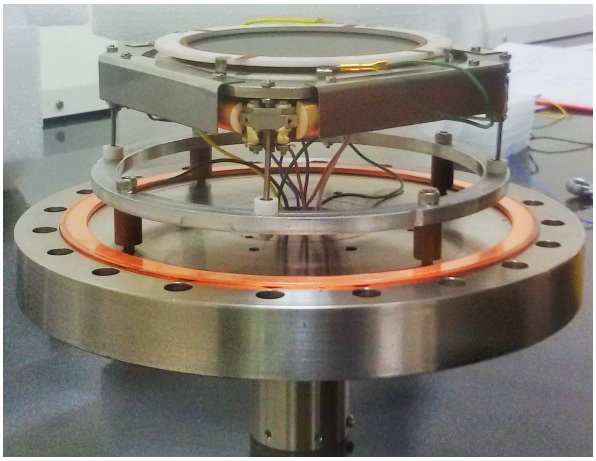

Figure 2.7: Actual photograph of a MCP equipped with position sensitive delay line anode.

The actual photograph of the MCP and delay line anode detector combined is shown in Fig. 2.7. The photo is captured from the detector assembly of the recoil ion momentum spectrometer at IISER Pune.

2.4.3 Data acquisition

The signal from the detector travels via a preamplifier (PA), constant fraction discriminator (CFD), and collected by a VME based multi-hit data acquisition system. The detail of signal processing and data acquisition can be found in [89, 90]. A schematic of the data acquisition is shown in Fig. 2.8. The electron detector signal is used as the start/stop trigger for the data acquisition. During data acquisition, the signal from the electron detector was delayed by 22 μsec. The recoils ions are detected within a specific time window from the detection of the electron. The multiple signals can be processed simultaneously using the data acquisition system.

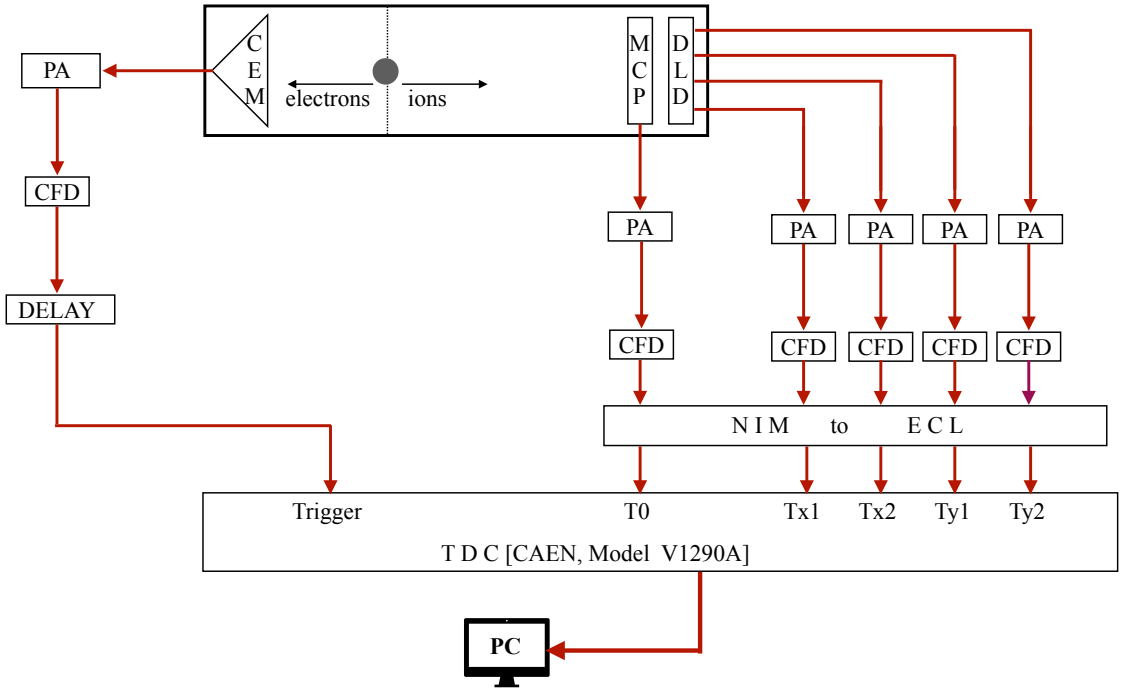

Figure 2.8: A schematic of data acquisition. PA=pre-amplifier, CFD=constant fraction discriminator, TDC=time to digital convertor, MCP=micro-channel plate, CEM = channel electron multiplier, DLD = delay line detector

For each fragment the five signals are generated, one from MCP which gives the time of flight of the ion, four from DLD which provides the information about the position of the ion, and the detection of each electron generates one signal. The

electron and the ion signals from their respective detectors are processed and fed to a multihit time-to-digital convertor (CAEN, Model V1290A). The multi-hit capability of the time to digital converter (TDC) enables us to collect information about not only the first but several ions arriving at the detector from a collision event. The multihit data acquisition system enables us to collect and identify fragment ions from a collision event. The digital data is stored in a computer in ROOT format.

2.5 Data analysis platform: ROOT

The event-by-event analysis of the acquired multihit coincidence data is done using the ROOT platform [91]. The ROOT is a framework for data processing and analysis, mainly designed for multiparticle data acquisition and analysis in high-energy physics. The scripting, or macro, and the programming language are all C++. The ROOT system provides a framework with all the functionality needed to handle and analyze large amounts of data in a better and very efficient way. The curve fitting, histogram, function evaluation, graphics, and data visualization classes are easy to build to interact and process the data effectively. From an event by event analysis of the time and position information of each recoil ion, all three momentum vectors for all correlated ions are determined.

2.6 Analysis procedure

The raw data contains both real as well as false events. The false events are inherently present in any coincidence experiment. The factors such as detection efficiency and dead time of the detectors, unequal count rates for electrons and ions, the influence of the background, etc. can give false counts in the data. The raw data is analyzed after the experiment employing different methods to bring out the information about the orientation of the molecule. In this section, we will discuss the analysis procedure followed to determine the orientation of the molecule with beam direction.

2.6.1 Calibration of spectrometer

The first step is to calibrate the time of flight spectrometer. Before all the experiments, the spectrometer is calibrated with argon gas. Argon gas is easily available and yields multiply charged ionic species upon ionization. Molecular gases are less suitable as they produce fragments with large kinetic energy, and few multiply charge parent molecular ions. Since the time of flight varies linearly with $\sqrt{m/q}$, the centroid peak positions of the various argon ions is fitted and this gives the calibration equation for the spectrometer. The plot to obtain the calibration equation is shown in Fig. 2.9. The calibrated equation is

$$t_0(\mu sec) = 0.351 \times \sqrt{m/q} - 0.058 \tag{2.10}$$

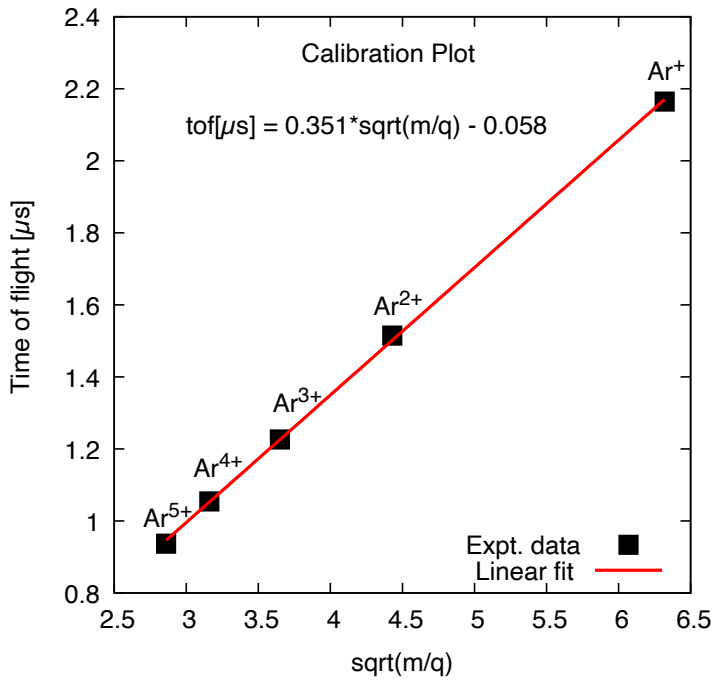

Figure 2.9: Plot for calibration equation. Experimental data shown as square box is the centroid peak position of various argon ions in time of flight spectrum.

In general, the intercept of the time of flight calibrated equation should be zero. But in practice, due to uncertainties in the extraction field and length of various regions of the time of flight spectrometer and due to signal processing delays of the electronics used, the situation deviates from the ideal condition. The time of flight equation is used for the identification of the fragment ions created after the collisions.

2.6.2 Time of flight spectrum

When a target molecule is bombarded with external charge particle, a few or large number of electrons can be removed. Depending on the stability of the molecular ion it can dissociate into its fragments. As discussed in the previous section, the time of flight of the ions is proportional to $\sqrt{m/q}$. The time of flight information is used for identification of the fragment ions created after the collisions. A typical time of flight spectrum of CO molecule under proton impact at 100 keV is shown in Fig. 2.10. The first major peak corresponds to the molecular ion CO^+. The other fragments like C^+, O^+ and molecular dication CO^{2+} can be seen in time of flight spectrum.

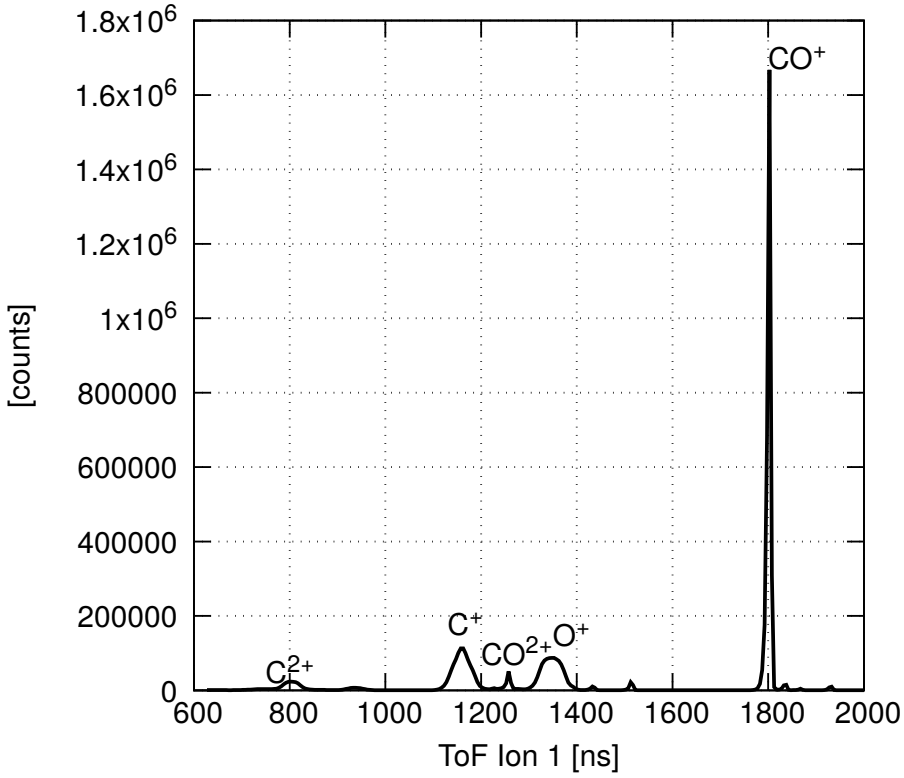

Figure 2.10: Time of flight spectrum of CO under p^+ impact at 100 keV.

2.6.3 Time of flight coincidence map

The fragments shown in the time of flight spectrum of CO molecule can arise from various dissociation channels. The CO molecule may get multiply ionized and depending on the stability of molecular cation, it can dissociate into various fragments ions. For example, the dissociation channels of multiply ionized CO molecule are as

follows

$$CO^{2+} \rightarrow C^{+} + O^{+} \tag{2.11}$$

$$CO^{3+} \rightarrow (C^{2+} + O^{+}), (C^{+} + O^{2+}) \tag{2.12}$$

$$CO^{4+} \rightarrow C^{2+} + O^{2+} \tag{2.13}$$

The fragment ions shown in the time of flight spectrum can arise from any of the dissociation channels. For example, the C^{+} ion can be created from doubly or triply ionized CO molecule. This spectrum shows the fragments of the multiply ionized CO molecule. These fragments can result from different dissociation pathways of the CO molecule. The identification of the dissociation pathways and final charge state of fragment ions are needed to obtain information about the total degrees of ionization of the parent molecule.

When a diatomic molecule dissociates, the two fragment ions will fly back-to-back because of the momentum conservation. Their times of flight will be anti-correlated. If one of the fragment ions is arriving first at the detector, the other fragment ion produced in the same event will reach later. If we plot a time of flight correlation diagram for the first and second hit, the island-like shapes with a negative slope will appear. This is called the time of flight coincidence map. The time of flight coincidence map for CO fragmentation is shown in Fig. 2.11. Since the time of flight of the second ion is always larger than the first ion, the lower half of the figure is empty. The island-like shapes at different positions corresponds to different dissociation channels of multiply ionized CO molecules. As we can see, the fragment C^{+} produced from doubly or triply ionized CO molecule will act as the first hit for the dissociation channel C^{+}:O^{+} and second hit for the dissociation channel C^{+}:O^{2+} and the corresponding islands will be different for dissociation pathways. The shape of the island is a narrow bar with slope equal to $-q_2/q_1$, where q_2 and q_1 are the charge states of second and first hit respectively. The total counts in each island or the intensity of the island carries information about the branching ratio of the particular dissociation channel. It can be seen that the intensity of C^{2+}:O^{+} channel is greater than the C^{+}:O^{2+}, which implies the higher branching ratio for that channel from dissociation of CO^{3+}. Up to four-fold degree of ionization is observed.

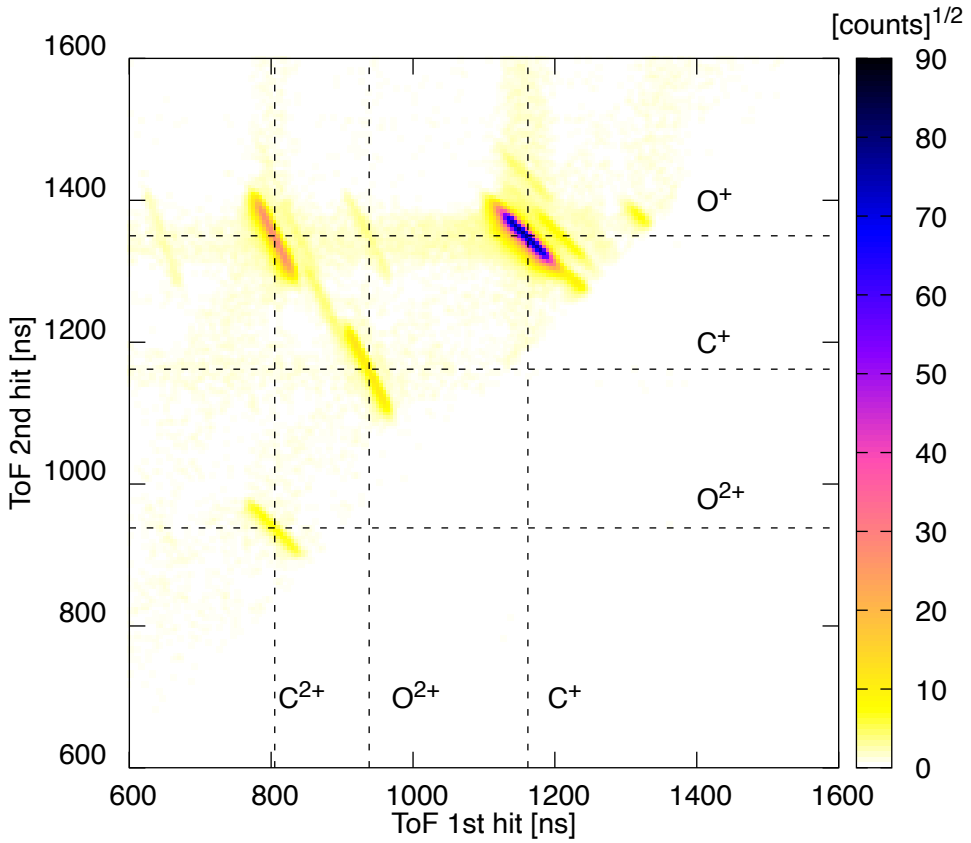

Figure 2.11: Time of fight coincidence map for CO fragmentation under p^+ impact at 100 keV. Different islands corresponds to different dissociation pathways.

For a triatomic molecule or larger molecule, the dissociation pathways can be very different than a simple two body breakup. The two types of mostly observed dissociation pathways are concerted and sequential pathways. For a concerted breakup, all the bonds break simultaneously. Sequential breakup is a two-step process. One of the molecular bond breaks first leaving behind an atomic ion and intermediate molecular cation. The molecular cation can rotate and dissociate after some time. For such a breakup channel the time of flight is not anti-correlated. The shape of the islands can be very different from a simple narrow bar as observed for diatomic molecule CO. The shapes of the islands for different dissociation mechanism are described very well by Eland [92].

2.6.4 Momentum calculation

To determine the orientation of the molecule, we need to find the momentum vector of the individual fragments ion from a dissociation event. The time of flight coinci-

dence map provides information about the dissociation channel for a given degree of ionization. For a given fragment ion, the information we get from the experiment is the position and time of flight. Once the time of flight (t) and the position (x, y) is obtained, the momentum vector of each registered ion can be derived easily. Only the z component of the momentum vector will be affected by the extraction field. The momentum vector along the time of flight axis (z axis) is given by

$$p_z = qE_s(t_0 - t) \tag{2.14}$$

where t_0 is the peak position of the time of flight distribution for a given fragments which corresponds to $p_z = 0$. The other two components are calculated from the position spectrum (x, y) of the fragments ions.

$$p_x = m\frac{x - x_0}{t} \tag{2.15}$$

$$p_y = m\frac{y - y_0}{t} \tag{2.16}$$

where t is the time of flight of the fragment ion and (x_0, y_0) is the centroid of the projection of the interaction volume on the detector plane. The momentum vector of the individual fragment ion from the dissociation of multiply ionized CO molecule from each collision event is calculated by this method.

2.6.5 Orientation measurement

The initial orientation of the molecule with respect to the beam axis can be derived from the momentum vector of fragments. For this, first, we need to know the beam direction. Since the projectile ion will ionize the residual gas molecule along its track, the trace of the molecular ions will be obtained on the position-sensitive detector. The parent molecular ions have very low energy as compare to the fragments ions. For molecular ions, the deviation from the centre position (interaction volume) will be very small when they are detected on the position sensitive detector. The position spectrum of the molecular ions (CO^+) or atomic target ion (Ar^+) can be used to find the projection (x_0, y_0) of interaction regime and the direction of the projectile. The direction of the projectile in our experiments is taken to be along the x-axis.

In this work, the main focus is on the dependence of the ionization cross-section on the orientation of the molecule with the incident beam direction. As discussed earlier, the multiply ionized molecular ion can dissociate into its fragment ions. For example, the molecular ion CO^{3+} can dissociate via two-channel C^{2+}:O^{+} and C^{+}:O^{2+}. After the selection of a particular dissociation channel from the time of flight coincidence map, we can determine the orientation angle of the molecule by measuring the relative angle between one of the fragment ions and projectile direction. This will give the orientation angle of the molecule for that particular channel only. In a similar manner, the procedure can be repeated for other dissociation channels that results from the same molecular parent ion. For a particular degree of ionization, all the dissociation channels are added and orientation angle of the molecule is obtained. For example, the orientation of the molecule for CO^{3+} is derived by measuring the relative angle between carbon ion and the projectile direction for both the dissociation pathways. In the next three chapters, we will discuss the orientation dependence of multiple ionization of diatomic molecule CO and triatomic molecule OCS under the impact of different types of projectiles.

Chapter 3

Orientation effect for CO in the perturbative regime

In chapter one, we have discussed the earlier works devoted to the study of orientation dependence of multiple ionization of molecule, which were mainly focused on H_2, O_2, N_2, and CO molecules. The main conclusion was that a highly charged molecular ion state is more likely to be achieved when the molecule is oriented parallel to the beam direction than when it is oriented perpendicular to the beam direction. But, no attention seems to have been given to the distinction between the homo-nuclear and hetero-nuclear nature of the molecules, and the orientation dependence was recognized purely as a geometric effect. To verify the differences if such a distinction can be made, we have investigated the orientation dependence in multiple ionization of a hetero-nuclear molecule CO. Orientation effect is found to depend on the interaction strength of the projectile [74], which is defined by Sommerfeld parameter $k = q/v$, where q and v are the charge and velocity of the projectile in atomic units. If the value of k is less than one, it corresponds to a perturbative regime, and if it is greater than one, it corresponds to a strong interaction regime. This chapter deals with the orientation effect in multiple ionization of CO under the perturbative regime. A simple model is used to calculate the ionization probability, involving Rutherford-like trajectories with an orientation-dependent distance of closest approach and an impact parameter dependent single ionization probability. The calculated probabilities show a good agreement with the experimental observations.

3.1 CO molecule

CO is a heteronuclear diatomic molecule with a bond length of 112.8 pm and a molecular mass of 28 amu. The carbon atom has four and the oxygen atom has six electrons in the valence shell. Following the octet rule, two atoms combine to form a CO molecule with a triple bond between them. One of the bonds is dipolar where both the bonding electrons are shared by the oxygen atom. This causes a small positive charge on the oxygen end and a negative charge on the carbon end. The other two bonds are covalent where two pairs of electrons are shared between the atoms. Since oxygen is more electronegative than carbon, this covalent bond gives a small negative charge on the oxygen end and a positive charge on the carbon end. Overall, CO is a polar molecule with a small net negative charge on the carbon and a small positive charge on the oxygen atom resulting in a small dipole moment of 0.122 Debye.

3.2 Experimental results

The perturbative regime can be achieved when the charge (q) of the projectile is small and velocity (v) of the projectile is high such that $q/v \leq 1$. We have carried out experiments with p^+ (proton) beam at different energy such that the interaction strength $k \leq 1$. The projectile energy, velocity, and interaction strength are tabulated in Table 3.1

Energy (keV)	Velocity (au)	Interaction strength (k)
25	1	1
50	1.42	0.704
100	2	0.50
200	2.83	0.353

Table 3.1: Energy, velocity and interaction strength for p^+ beam

3.2.1 Dissociation channels

The dissociation channels can be obtained from the time of flight coincidence map. The time of flight coincidence map for the first and second hit is shown in Fig. 2.11

and the dissociation channels that are observed for various degrees of ionization are

$$CO^{2+} \rightarrow C^{+} + O^{+} \tag{3.1}$$

$$CO^{3+} \rightarrow (C^{2+} + O^{+}), (C^{+} + O^{2+}) \tag{3.2}$$

$$CO^{4+} \rightarrow C^{2+} + O^{2+} \tag{3.3}$$

3.2.2 Orientation effect for CO under p^+ impact

The interaction time between the projectile ion and target molecule can be estimated from R/v, where R is the length parameter for the molecule and v is the projectile velocity. In our experiment, the interaction time between the projectile and the molecule is approximately 100 as. This timescale is much shorter than the vibrational time scale, which in turn is much shorter than the rotational time scale of the molecule. The dissociation time scale of the molecular ions is of the same order as the vibrational timescales for low charge states, and shorter for higher charge states. Hence the molecule can be considered frozen in space for the purpose of describing dissociative ionization. For a stationary diatomic molecule, the dissociating fragments will always fly back-to-back due to momentum conservation. The orientation of the molecule at the instance of fragmentation can be derived from the directions of the measured momentum vectors of the fragment ions.

At the time of the collision, the target molecules are randomly oriented, and the resulting fragment ions have been detected by projecting them onto a planar detector. In this situation, the observed angular distribution of the ions will be given by

$$N(\theta) \approx N_0 \Big[1 + \beta_1 P_1(\cos\theta) + \beta_2 P_2(\cos\theta)\Big] \sin\theta \tag{3.4}$$

where θ is the angle between internuclear axis of CO molcule and incident velocity vector of the p^+ beam, N_0 is the normalisation constant, β_1 and β_2 are the asymmetry and anisotropy parameters, and the $\sin\theta$ factor is the solid angle correction. Non-zero values of the parameter β_2 represent deviation from spherical symmetry ($\sin\theta$), but still reflecting a symmetry around $\theta = \pi/2$, whereas non-zero values of β_1 represent an asymmetry around $\theta = \pi/2$ (reference Fig. 3.2).

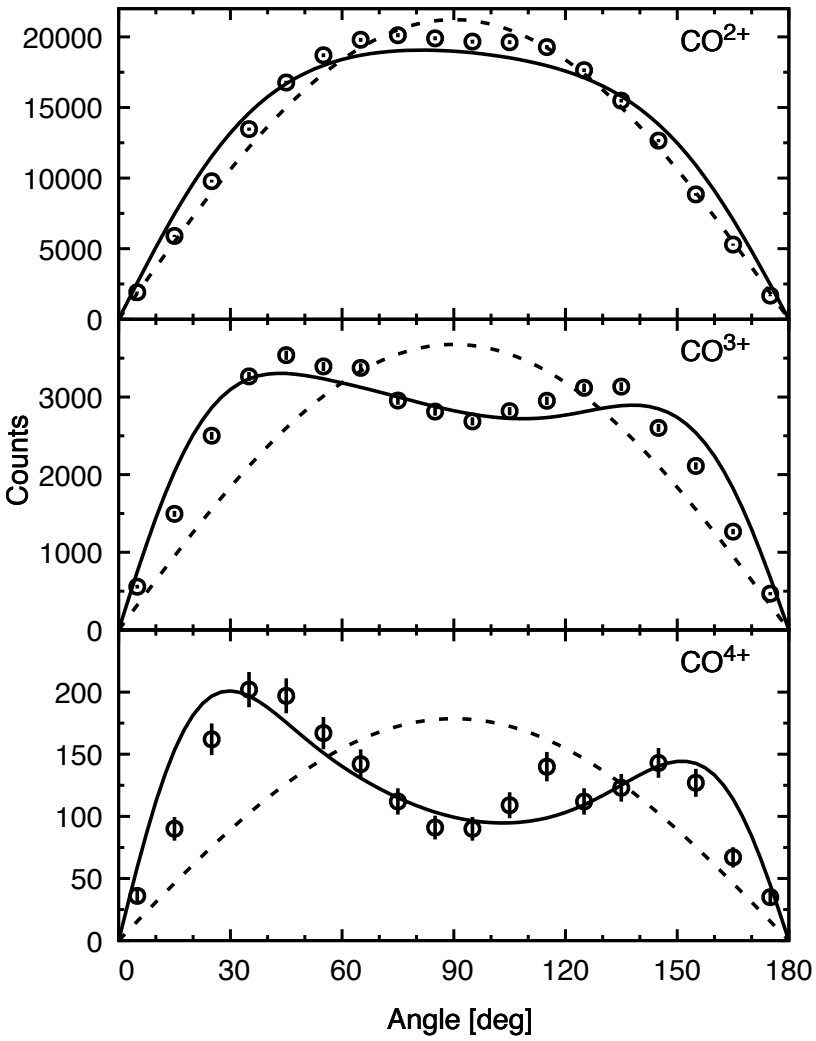

Figure 3.1: Orientation angle dependence for multiple ionization of CO under p^+ impact at 100 keV. Observations—circles with error bars (statistical errors), Model—continuous curve, Isotropic case —dashed curve ($\sin\theta$).

The experimental results for orientation angle dependence multiple ionization of CO molecule under 100 keV p^+ impact are shown in Fig. 3.1. It is clear that for a low degree of ionization the angular distribution has a mild anisotropy. With an increase in the degree of ionization, the anisotropy increases. This implies that a high degree of ionization predominantly occurs when the molecule is oriented parallel to the beam. For parallel orientation, the heteronuclear nature of the molecule is expected to influence the ionization probability. In other words, a forward-backward asymmetry is expected in multiple ionization when the molecule is oriented parallel to the projectile direction. Depending on whether the projectile faces the carbon atom first or the oxygen atom first, the net ionization probability for the molecule will be altered. Thus, a process with high anisotropy can also be expected to show

asymmetry in angular distribution. Over the entire energy range of incident projectile i.e. 25-200 keV, we find a strong orientation dependence of the ionization cross-sections, especially at lower incident energies and a higher degree of target ionization.

The observed angular distribution of the fragment ions is fitted to equation 3.4 and the values of the anisotropy and the asymmetry parameters, β_2 and β_1, are obtained for each incident energy. The observed values of these parameters are shown in Table 3.2 and will be discussed in a later section. We can see that with an increase in projectile energy, the values of anisotropy and asymmetry parameters decrease.

3.3 Model calculation

For the perturbative regime, we have performed a simple model calculation to obtain the orientation dependence of ionization probabilities of CO molecule. This model is based on the idea of Wohrer and Watson [58]. They calculated the ionization cross-section of the O_2 molecule orientated parallel to and perpendicular to the projectile direction. We have extended the model to the CO molecule and included all orientations of the molecule. The simple classical model produces remarkably good results. The anisotropy and asymmetry predicted by the model show good agreement with the experimental observations. In this section, we will discuss the model calculation in detail.

3.3.1 Assumptions

The two basic assumptions for the model calculation are 1. Independent atom approximation and 2. Independent electron approximation. Under the first approximation, the interaction of projectile is considered separately with the atoms of the molecule. Under the second approximation, the electron-electron correlation is ignored. In the perturbative regime, the single ionization probability $p(b)$ of an atom impacted by a projectile following a linear trajectory with an arbitrary impact parameter b is given as

$$p(b) = p_0 \exp(-b/r), \tag{3.5}$$

where p_0 is the single ionization probability for a certain projectile–target pair at zero impact parameter, r is an effective radius of the shell from which the electron is removed. For any atom, the effective radius r can be determined using the Slater formula [93]. Under the independent electron approximation, the probability of removal of n electrons from an atomic shell containing N electrons will be given by the binomial distribution

$$P_n^N(b) = {}^N C_n \left[p(b)\right]^n \left[1 - p(b)\right]^{N-n}. \tag{3.6}$$

Under independent atom approximation, the probability of removal of n electrons from a diatomic molecule, such as CO, will be given by

$$P_n^{\mathrm{CO}}(b) = \sum_{j=0}^{j=n} P_j^{\mathrm{C}}(b^{\mathrm{C}})\, P_{n-j}^{\mathrm{O}}(b^{\mathrm{O}}) \tag{3.7}$$

where the superscripts to P refer to the individual atoms or to the molecule, and $b, b^{\mathrm{C}}, b^{\mathrm{O}}$ are the distances of the projectile from the molecular center of mass, and two atomic nuclei respectively.

3.3.2 Straight line and hyperbolic trajectory

Wohrer and Watson calculated the ionization cross-section of the O_2 molecule orientated parallel to and perpendicular to the projectile direction. Caraby *et al.* [62] extended their calculation and obtained the differential cross-section as a function of orientation of the molecule. The differential cross-section depends on the orientation angle. Nonetheless, their model did not take into account the hetero-nuclear nature of the molecule and predicted differential cross-sections that are symmetric around $\theta = \pi/2$ (angle between the internuclear axis and the direction of the incident velocity of the projectile, or θ in Fig. 3.2).

The two assumptions made in their models were that the trajectory is a straight line and that ionization occurs only at a specific point ($z = 0, y = b$) on the trajectory. This precludes any forward-backward asymmetry in the overall ionization cross-section. For a straight-line trajectory, the asymmetry that is expected in the orientation angle dependence of the ionization of a heteronuclear molecule will not

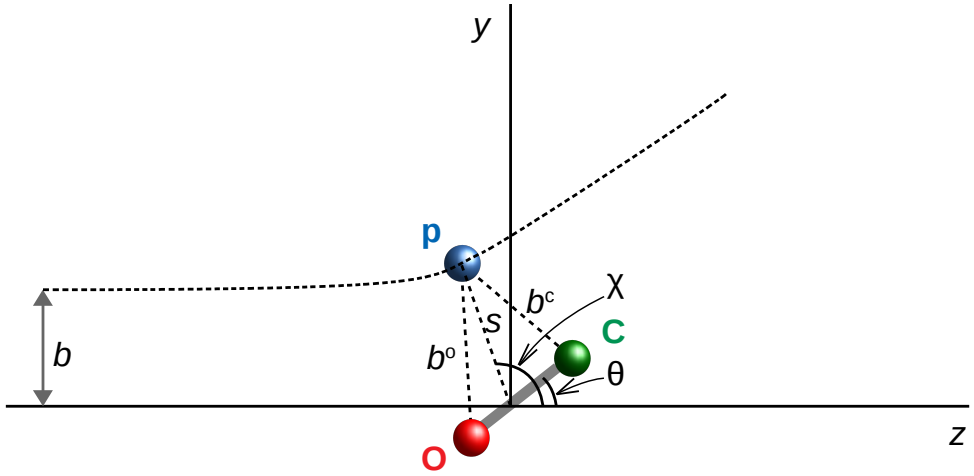

Figure 3.2: Trajectory of the projectile, molecular orientation, and various distances and angles.

emerge, since the problem is exactly symmetric in the forward and backward hemispheres.

In our calculation, we propose a modified trajectory. This is based on a Rutherford-type trajectory in which ionization may occur at any arbitrary distance s from the molecular center of mass, with the probability vanishing exponentially with the distance, similar to that in equation 3.5. The classical Rutherford trajectory is for a spherically symmetric potential. The trajectory is defined uniquely by the impact parameter b and the distance of closest approach $D_{\min}$, in the case of zero impact parameter ($b = 0$). For pure Coulomb potential $D_{\min} = q_P q_T/E$, where q_P, q_T are the projectile and target charge, respectively, and E is the kinetic energy of the projectile with respect to the target. The scattering angle is given by $2\tan^{-1}(D_{\min}/2b)$ in the centre of mass frame (See Fig. 3.2).

The interaction potential between a point charge projectile and a target molecule deviates from spherical symmetry especially for close encounters. Thus, we need to account for the non-spherical nature of the scattering potential in terms of an orientation-dependent value of $D_{\min}$. As given by equation 3.5 the ionization probability is greater for close encounters compared to distant encounters. Since the Rutherford trajectory is determined by the value of $D_{\min}$, we consider modifying its definition to obtain an orientation-dependent ionization probability. In the work by Wohrer and Watson, and Caraby *et al.*, we saw that the ionization probability is larger for the parallel orientation as compared to the perpendicular orientation. The

same pattern emerges from the statistical energy deposition model-based study by Kaliman *et al.* [64], the ionization probability is large for close encounters and small for distant encounters. From the results of previous work, the value of $D_{\min}$ should be large for $\theta = \pi/2$ and small for $\theta = 0, \pi$. Further, the values of $D_{\min}$ should be such, that the closest distance that a projectile may approach the molecule be no smaller than the typical radius of ionization, to ensure that the probability of ionization does not exceed 1 at any distance. Based on these considerations, we define $D_{\min}$ as

$$D_{\min}(\theta) = g(v)\left[r_{\mathrm{m}}^2 + (\frac{1}{2}\, R \sin\theta)^2\right]^{1/2} \tag{3.8}$$

in which r_{m} is an effective ionization radius of the molecule, R is the internuclear separation and $g(v)$ is a projectile velocity-dependent scaling function. For the present set of observations, which are in the perturbative regime ($k \leq 1$), we have taken $g(v)$ to be $(1/v)^{1/2}$, as it is found to give a close match to the trend in the anisotropy and asymmetry parameters over the energy range. The trajectory is calculated in the same manner as in Rutherford scattering, and due to the θ-dependence of $D_{\min}$, the trajectory becomes θ dependent and, in turn, the ionization probability become dependent on the orientation of the molecule.

3.3.3 Differential cross-section

The cross-section for removing n electrons for a particular orientation of the molecule is given by

$$\frac{d\sigma^{(n)}}{d\theta} = \int_{b=0}^{\infty}\int_{\chi=\alpha}^{\pi}\int_{\phi=0}^{2\pi} P_n(\mathbf{s})\, b \sin(\chi)\, d\chi\, db\, d\phi; \qquad \mathbf{s} \equiv \mathbf{s}(\theta; b, \chi, \phi) \tag{3.9}$$

The probability $P_n(s(b, \chi, \phi))$ is given by an expression based on equation 3.6, 3.7

$$P_n(\mathbf{s}) = \sum_{j=0}^{j=n} P_j^{\mathrm{C}}(\mathbf{s}^{\mathrm{C}})\, P_{n-j}^{\mathrm{O}}(\mathbf{s}^{\mathrm{O}}) \tag{3.10}$$

where $\mathbf{s}^{\mathrm{C}}$ and $\mathbf{s}^{\mathrm{O}}$ are the instantaneous positions of the projectile from the two atoms of the molecule. For both atoms, the distance of the projectile is dependent on the orientation of the molecule for every value of the impact parameter b. It is clear from Fig. 3.2, and from equation 3.10, the ionization probabilities for the

two atoms are not equal, owing to differences in distances $\mathbf{s}^{\,\mathrm{C}}$ and $\mathbf{s}^{\,\mathrm{O}}$ and between probabilities p_0^{C} and p_0^{O} for a given trajectory of the projectile.

If the ionization cross-section does not depend on the orientation of the molecule, the fragments arising from the multiply-charged molecular ion will be emitted isotropically, and the observed fragment ion counts N will follow the distribution $N(\theta) \propto \sin\theta$. The $\sin\theta$ distribution is due to the solid angle correction in the observations. If there is some dependence of the ionization cross-section on the orientation of the molecule, deviations from the isotropic case are quantified by two parameters β_1, β_2 in the multipole expansion of the differential cross-section:

$$\frac{d\sigma^{(n)}}{d\theta} \approx \frac{\sigma^{(n)}}{4\pi}\Big[1 + \beta_1 P_1(\cos\theta) + \beta_2 P_2(\cos\theta)\Big]. \tag{3.11}$$

The model calculation does not directly predict the values of asymmetry and anisotropy parameters β_1, β_2. They are obtained by a least-squares fit to the predicted values of $d\sigma^{(n)}/d\theta$ (i.e. equation 3.9). The values of β_1, β_2 thus obtained are compared with the values of β_1, β_2 obtained by a least squares fit to the experimentally observed distribution of fragment ions.

3.3.4 Adjustable parameters

The adjustable parameters in our model are p_0^{C}, p_0^{O} and the function $g(v)$. As discussed earlier, the function $g(v)$ is taken to be $(1/v)^{1/2}$ to match the model calculation and experimental observation. Since this model does not give the absolute cross-sections, the relative values of p_0^{C} and p_0^{O} matter, and not the absolute values, as long as they are both < 1. For the range of energies covered in the experiment, the ionization cross-sections are nearly independent of the projectile energy for every degree of ionization [94]. Hence, the values of p_0^{C} and p_0^{O} are taken to be independent of projectile energy. The value of p_0^{C} is chosen to be 0.8, based on the recommendation of Caraby *et al.* [62]. We have set the value for the oxygen atom to $0.8\, I_{\mathrm{C}}/I_{\mathrm{O}}$, where I_{C} and I_{O} are the first ionization potential energy of carbon and oxygen atom. The value of the effective ionization radii of carbon and oxygen atoms are calculated using the Slater formula [93]. For double ionization, the value of r_{C} and r_{O} is taken to be equal to the L-shell radius, since the probability of the

participation of the K shell electrons is negligible. For higher degrees of ionization, K-shell electrons can contribute, so the values of r_C and r_O are set equal to the average of K-shell and L-shell radii of the carbon and oxygen atoms, respectively. The value of r_m(ionization radius for the molecule as a whole, needed in equation 3.8) is taken to be $(r_C + r_O)/2$ in all cases.

3.4 Comparison of experimental results and model calculation

In section 1.2.3, we have discussed the experimental results for 100 keV p^+ impact on CO. Experimental data are fitted to equation 3.4 and the values of the asymmetry and anisotropy parameters, β_1 and β_2, are obtained. The calculated value of orientation dependence ionization probability is shown by the continuous curve in Fig 3.1. The calculated distributions agree fairly well with the experimental results. For other energies, we present the results in terms of the asymmetry and anisotropy parameters obtained by fitting equation 3.4 to the experimental and predicted angular distributions. The values of these parameters are shown in Table 3.2.

E_p(keV)	n	β_1		β_2	
		obs.	calc.	obs.	calc.
25	2	0.028 ± 0.008	0.065 ± 0.004	0.164 ± 0.011	0.424 ± 0.006
	3	0.193 ± 0.013	0.127 ± 0.034	0.677 ± 0.018	1.282 ± 0.044
	4	0.377 ± 0.068	0.459 ± 0.089	1.507 ± 0.112	1.915 ± 0.120
50	2	0.026 ± 0.008	0.049 ± 0.003	0.146 ± 0.011	0.339 ± 0.004
	3	0.145 ± 0.012	0.128 ± 0.021	0.643 ± 0.016	0.936 ± 0.027
	4	0.338 ± 0.030	0.369 ± 0.056	1.249 ± 0.045	1.507 ± 0.072
100	2	0.048 ± 0.009	0.040 ± 0.002	0.131 ± 0.013	0.273 ± 0.003
	3	0.117 ± 0.012	0.111 ± 0.014	0.596 ± 0.016	0.679 ± 0.018
	4	0.261 ± 0.042	0.284 ± 0.036	1.024 ± 0.059	1.174 ± 0.046
200	2	0.046 ± 0.009	0.029 ± 0.001	0.148 ± 0.012	0.230 ± 0.002
	3	0.093 ± 0.015	0.087 ± 0.009	0.507 ± 0.020	0.499 ± 0.012
	4	0.068 ± 0.060	0.212 ± 0.023	0.915 ± 0.082	0.919 ± 0.029

Table 3.2: Asymmetry and anisotropy parameters for p^+ projectiles at different energies and different degrees of ionization (n) of target molecule CO. The values of β_1 and β_2 are shown for fit to the observed angular distributions and for model calculation

We see that β_1 and β_2 increase with the degree of ionization for fixed projectile

energy. Experimental results show that a higher degree of ionization is likely to be achieved in the collision when the projectile first encounters the oxygen atom rather than the carbon atom, which is correctly predicted by the model. It is clear from Table 3.2 that for a fixed degree of ionization, asymmetry and anisotropy decrease with an increase in projectile energy. The calculated and experimental distributions follow the same trend.

3.5 Applicability of the model

With this model calculation, we are able to predict the asymmetry for the heteronuclear molecule which was missing in the earlier theoretical works. To further check the applicability of the model, we calculate the orientation dependence of ionization probability of homonuclear molecule, and compare the calculation with earlier works of Siegmann *et al.* [72]. They have reported the anisotropy in the ionization cross-section of N_2, O_2 and CO molecule under different types of projectile in perturbative regime.

The values of r and p_0 (as used in equation 3.5) need not be constant for a given target when it is impinged with projectiles of different velocities or charge. Tonuma *et al.* [46] have experimentally determined the dependence of r and p_0 on the projectile charge, and found that the values of r and p_0 gradually increase with increasing projectile charge. However, they do not suggest any function for the q-dependence of r. In our model, an increase in the value of r results in weaker anisotropy and asymmetry, which is consistent with the results for a highly charged projectile.

In perturbative regime, the single ionization probability of an atom impacted by a projectile of charge q is given as [95]

$$p_q(b) = q^2\, p(b) \tag{3.12}$$

where $p(b)$ is the single ionization probability under p^+ impact (of the same velocity), as given by an expression similar to equation 3.5. For a projectile with large q, the single ionization probability calculated using this formula will be greater than unity for small impact parameters. To avoid the violation of unitarity at large q, a

unitarization method is used , which sets

$$p'_q(b) = 1 - \exp\left[-p_q(b)\right], \tag{3.13}$$

as the ionization probability for $q > 1$. Using this probability function, the orientation dependence ionization probability is calculated in the same manner as discussed in section 3.3 and the value of anisotropy parameter is obtained.

Table 3.3: Comparison of calculated value of anisotropy parameter β_2 from this model with experimentally observed and calculated value of anisotropy parameter by Siegmann *et al.* [72].

	$n=2$			$n=3$			$n=4$		
	Siegmann *et al.* [72]		this	Siegmann		this	Siegmann		this
E (keV)	expt.	calc.	calc.	expt.	calc.	calc.	expt.	calc.	calc.
Collision: D^++CO									
100	0.13	−0.05	0.195	0.35	0.34	0.432	0.86	0.95	0.717
150	0.13	−0.08	0.186	0.33	0.26	0.403	0.68	0.83	0.667
200	0.10	−0.09	0.180	0.33	0.21	0.383	0.80	0.78	0.634
250	0.10	−0.10	0.176	0.27	0.19	0.368	0.71	0.74	0.610
300	0.22	−0.14	0.173	0.26	0.17	0.357	0.67	0.71	0.591
Collision: He^++CO									
100	0.22	−0.04	0.180	0.19	0.33	0.472	0.76	0.95	0.746
150	0.30	−0.11	0.171	0.22	0.15	0.440	0.75	0.62	0.698
200	0.32	−0.13	0.165	0.21	0.06	0.421	0.66	0.45	0.668
250	0.35	−0.12	0.161	0.20	0.01	0.407	0.77	0.35	0.646
300	0.34	−0.12	0.158	0.21	−0.02	0.396	0.63	0.27	0.629
Collision: H^++N_2									
50	−0.26	−0.02	0.248	0.18	0.47	0.472	–	1.25	0.969
100	−0.30	−0.08	0.211	0.16	0.30	0.326	–	0.98	0.749
150	−0.26	−0.10	0.193	0.12	0.24	0.260	–	0.87	0.645
200	−0.26	−0.10	0.182	0.09	0.20	0.220	0.12	0.81	0.579
250	−0.29	−0.11	0.174	0.03	0.19	0.192	–	0.78	0.533
300	−0.25	−0.11	0.168	−0.02	0.18	0.172	0.09	0.76	0.497
Collision: H^++O_2									
50	−0.12	0.00	0.318	0.17	0.57	0.572	–	1.37	1.171
100	−0.10	−0.05	0.276	0.22	0.41	0.409	0.33	1.14	0.918
150	−0.07	−0.07	0.256	0.19	0.34	0.335	0.22	1.04	0.796
200	−0.06	−0.09	0.243	0.15	0.30	0.289	–	0.96	0.719
250	−0.06	−0.09	0.233	0.15	0.27	0.256	–	0.89	0.664
300	−0.08	−0.10	0.226	−0.11	0.26	0.232	–	0.85	0.622

In Table 3.3, the calculated values of anisotropy parameter β_2 for CO, N_2 and O_2 molecules are compared with the experimental and calculated value of Siegmann *et al.* [72]. For CO molecule under D^+ and He^+ impact, for $n = 2$ our model predicts a

positive value of anisotropy parameter β_2 which agrees with the experimental results of Siegmann, while the calculated values using SED model are negative. For higher degrees of ionization, the model predicted values agree fairly well with their results. For homonuclear molecules, the values of r and p_0 will be the same for the two atoms and the asymmetry parameter β_1 will be zero. We set the value of $p_{\mathrm{N}}^0 = 0.8\, I_{\mathrm{C}}/I_{\mathrm{N}}$, and the values of r in the same manner as for CO, using the Slater formula. In Table 3.3, calculated values of the anisotropy parameter for N_2 and O_2 under p^+ impact are compared with the experimental and calculated values, and there is a fairly good agreement with their results.

3.6 Summary

Orientation dependence ionization probability of diatomic molecule CO is discussed under p^+ impact at energy 25-200 keV. We show a higher degree of ionization is likely to be achieved in the collision, when the projectile first encounters the oxygen atom rather than the carbon atom which implies that the orientation effect is not purely a geometric effect but depends on the constituents of the molecule. With an increase in projectile energy, the orientation dependence decreases.

For the perturbative regime, a calculation is performed to obtain the orientation-dependent ionization probability for a diatomic molecule subject to a charged particle. The trajectory is taken to be hyperbolic with a distance of closest approach that depends on the orientation of the molecule. In this model, the interaction between the projectile and the two atoms of the molecule is considered separately under independent atom approximation. The electron-electron correlation is ignored. The heteronuclear nature of the molecule is accounted for by treating the ionization radius and the single ionization probability to be different for the two atoms. Calculated orientation angle-dependent multiple ionization probabilities agree fairly well with the experimental results on the CO molecule. This model is further applied to different systems in the perturbative regime for which data is available and the predicted values show fair agreement with those results. This model can predict the asymmetry for the heteronuclear molecule which was missing in the earlier theoretical works.

Chapter 4

Orientation effect for CO in the intermediate and strong interaction regime

In the previous chapter, we have discussed the orientation effect in multiple ionization of the diatomic molecule CO under the perturbative regime. The orientation effect was parameterized by two parameters β_1 and β_2, which corresponds to the asymmetry and anisotropy in the angular distribution. The values of asymmetry and anisotropy parameters depend on the interaction strength ($k = q/v$) of the projectile. Siegmann *et al.* [74] showed that for a given degree of ionization N_2^{10+}, strong anisotropy was observed for Xe^{18+} (k=1.2) as compare to Xe^{43+}(k=2.8). The energy transfer by the projectile depends approximately on k^2/b^2 [71]. A projectile with a large k can transfer the same amount of energy at a large impact parameter as a projectile with a small k at a small impact parameter. For large impact parameters, the projectile will no longer see a detailed structure of the target molecule. Thus, when integrated over the impact parameter, for a given degree of ionization, the anisotropy will tend to vanish for a projectile with large k but will be significant for a projectile with small k. To systematically study the dependence of orientation effect on projectile interaction strength, further experiments were carried with He^{2+} and Xe^{9+} such that interaction strength for He^{2+} falls under the intermediate regime ($k \approx 1$) and for Xe^{9+}, it falls under strong interaction regime ($k \gg 1$). In this chapter, we will discuss the orientation dependence in multiple ionization of CO

in the intermediate and strong interaction regime.

4.1 CO molecule under He^{2+} impact

In this section, we will discuss the orientation dependence in multiple ionization of CO in the intermediate interaction regime. To achieve the intermediate interaction regime ($k \approx 1$), the experiment was carried out with a He^{2+} beam at different energies. The projectile energy, velocity, and interaction strength (q/v) are tabulated in Table 4.1

Energy (keV)	Velocity (au)	Interaction strength (k)
100	1	2
200	1.41	1.41
300	1.74	1.15
400	2	1
500	2.25	0.89
700	2.63	0.76

Table 4.1: Energy, velocity and interaction strength for He^{2+} beam

4.1.1 Dissociation channels

Dissociation channels can be identified from the time of flight coincidence map. The time of flight coincidence map for CO fragmentation under 100 keV He^{2+} impact is shown in Fig. 4.1. Different islands correspond to different fragmentation channels for multiply ionized CO molecule. Up to a five-fold degree of ionization is observed at all incident energies. Dissociation channels that are observed for various degrees of ionization are

$$CO^{2+} \rightarrow C^{+} + O^{+} \tag{4.1}$$

$$CO^{3+} \rightarrow C^{2+} + O^{+},\ C^{+} + O^{2+} \tag{4.2}$$

$$CO^{4+} \rightarrow C^{2+} + O^{2+},\ C^{3+} + O^{+},\ C^{+} + O^{3+} \tag{4.3}$$

$$CO^{5+} \rightarrow C^{3+} + O^{2+} \tag{4.4}$$

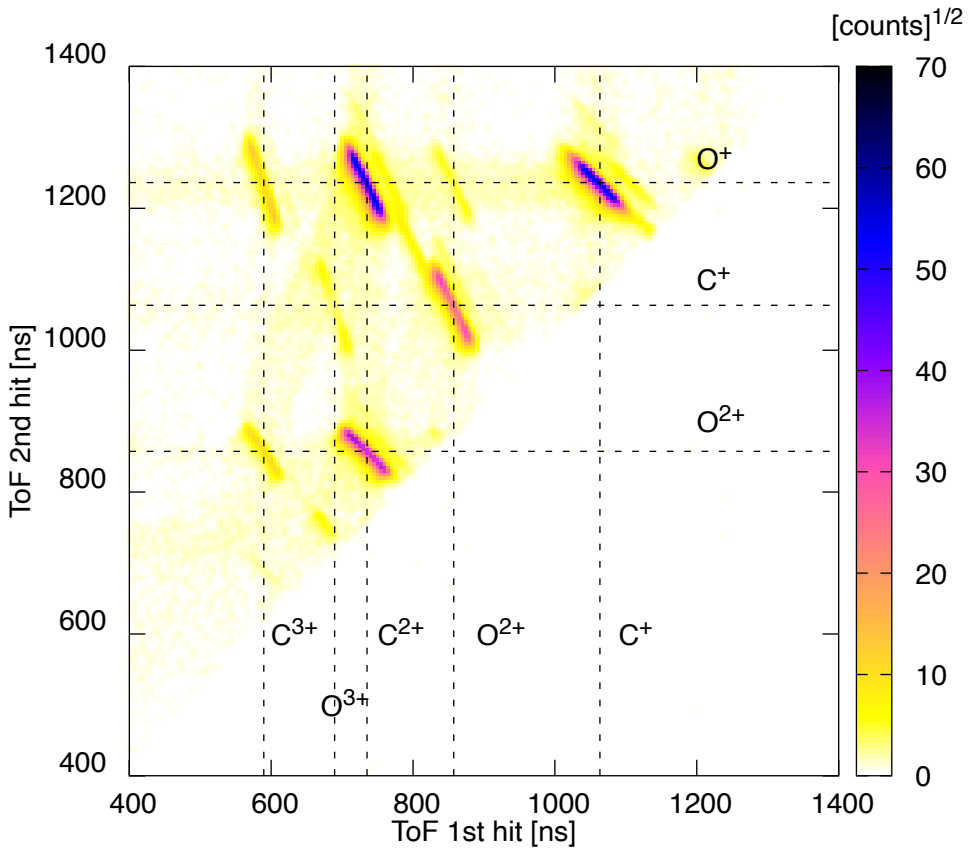

Figure 4.1: Time of flight coincidence map for CO fragmentation under 100 keV He^{2+} impact. Different islands corresponds to different dissociation pathways.

4.1.2 Orientation effect for CO under He^{2+} impact

In our experiment, we have covered the range of k in the intermediate interaction regime ($0.76 \leq k \leq 2$) by choosing He^{2+} projectiles with energies ranging from 100 keV to 700 keV. Experimental data are fitted to equation 4.5 and the values of the asymmetry and anisotropy parameters, β_1 and β_2, are obtained. The observed and fitted angular distributions of multiple ionization of CO under 100 keV He^{2+} impact are shown in Fig. 4.2. The experimentally obtained values of β_1, β_2, from the fit to the experimental data, are shown in Table 4.2 for all the projectile energies.

$$N(\theta) \approx N_0 \Big[1 + \beta_1 P_1(\cos\theta) + \beta_2 P_2(\cos\theta)\Big] \sin\theta \tag{4.5}$$

In Table 4.2, one more parameter A is tabulated,. This parameter is calculated to make a comparative study with the earlier reported results of Kaliman *et al.* [64]

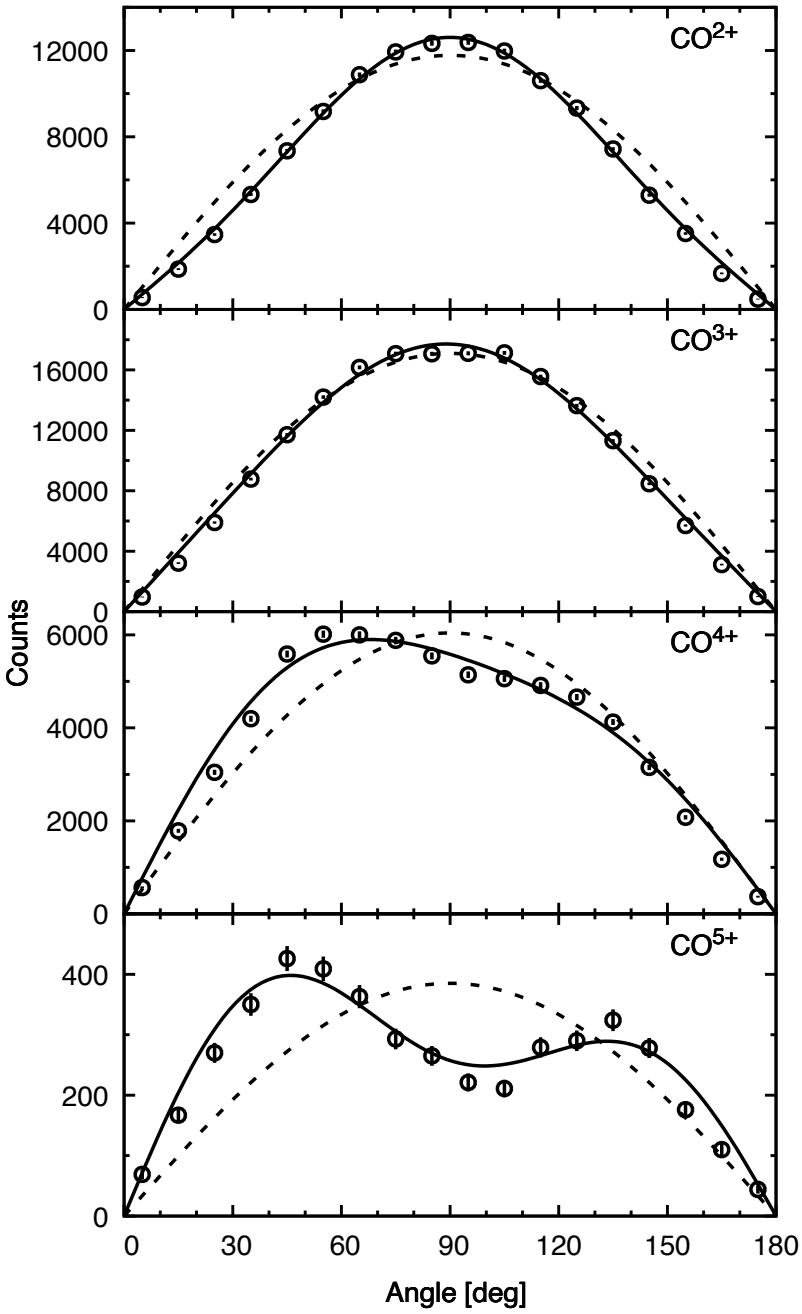

Figure 4.2: Experimental observation [points with error bars] and fitted equation 4.5 [continuous curve] for orientation angle dependence of multiple ionization of CO under 100 keV He^{2+} impact. The dashed curve is $\sin\theta$ distribution, representing the isotropic case.

Table 4.2: Experimentally determined values of the asymmetry and anisotropy parameters, β_1, β_2 and A parameters [64] for different degrees of ionization (n) of CO under He^{2+} impact at different incident energies (E).

E [keV]	n	β_1	β_2	A
100	2	0.000 ± 0.008	-0.278 ± 0.013	-0.224 ± 0.011
	3	0.027 ± 0.011	-0.130 ± 0.016	-0.085 ± 0.013
	4	0.225 ± 0.020	0.198 ± 0.027	0.224 ± 0.017
	5	0.267 ± 0.032	0.747 ± 0.049	0.525 ± 0.023
200	2	-0.011 ± 0.010	-0.199 ± 0.015	-0.163 ± 0.013
	3	-0.005 ± 0.010	-0.194 ± 0.016	-0.156 ± 0.014
	4	0.287 ± 0.014	0.177 ± 0.018	0.232 ± 0.011
	5	0.415 ± 0.041	0.822 ± 0.052	0.583 ± 0.023
300	2	-0.013 ± 0.008	-0.184 ± 0.012	-0.152 ± 0.011
	3	0.007 ± 0.010	-0.159 ± 0.015	-0.120 ± 0.013
	4	0.274 ± 0.018	0.194 ± 0.023	0.238 ± 0.014
	5	0.447 ± 0.039	0.798 ± 0.047	0.577 ± 0.020
400	2	0.007 ± 0.010	-0.173 ± 0.014	-0.131 ± 0.012
	3	0.023 ± 0.011	-0.117 ± 0.016	-0.077 ± 0.013
	4	0.262 ± 0.019	0.222 ± 0.026	0.250 ± 0.016
	5	0.352 ± 0.046	0.826 ± 0.060	0.575 ± 0.027
500	2	0.034 ± 0.008	-0.147 ± 0.012	-0.095 ± 0.010
	3	0.032 ± 0.010	-0.066 ± 0.015	-0.033 ± 0.012
	4	0.244 ± 0.020	0.267 ± 0.026	0.271 ± 0.016
	5	0.362 ± 0.044	0.781 ± 0.056	0.557 ± 0.025
700	2	0.035 ± 0.008	-0.116 ± 0.012	-0.069 ± 0.010
	3	0.056 ± 0.009	-0.002 ± 0.014	-0.025 ± 0.010
	4	0.217 ± 0.020	0.311 ± 0.027	0.288 ± 0.016
	5	0.233 ± 0.041	0.815 ± 0.054	0.551 ± 0.025

and defined as

$$A = \frac{\sigma(0) - \sigma(90)}{\sigma(0) + \sigma(90)} \tag{4.6}$$

From equation 4.5, the parameter A can be written in terms of β_1, β_2 as

$$A = \frac{2\beta_1 + 3\beta_2}{4 + 2\beta_1 + \beta_2} \tag{4.7}$$

We can see that the value of A parameter is based only on the values of the differential cross-section at two angles i.e. $\theta = 0$ and $\theta = 90$ degree, while, the β parameters are based on the entire angular distribution. Kaliman *et al.* have presented the dependence of A on the projectile energy for different degrees of ionization of F_2, CO, and CO_2 under the impact of He^{2+} ions, and the concluded that the observed

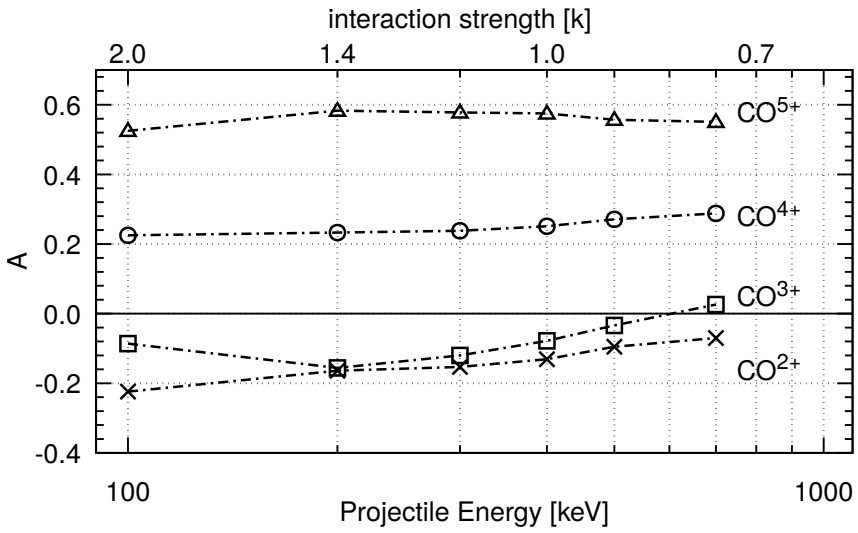

Figure 4.3: Dependence of the parameter A on the projectile energy (lower scale) and the interaction strength (upper scale). The upper scale is shown to enable a comparison with the plots for β_1, β_2 in Fig. 4.4.

anisotropy in the angular distribution is largely independent of the details of the constituents of the molecule, and orientation effect is purely a geometric effect. We have performed an experiment with He^{2+}projectile at different energies. So the A parameter is a better cross-check with the earlier reported theoretical work. In Fig. 4.3, we have plotted the values of A parameter against the projectile energy. For any degree of ionization (n from 2 to 5 in our case), for our data the value of A changes very slowly with the incident energy of the projectile. This dependence does not agree with the predictions of the Kaliman *et al.* model. In their calculation for $n = 4$, for instance, the orientation parameter decreases sharply (for example in their results A changes approximately from 0.6 to 0.2) with an increase in projectile energy. In our observation, the value of A does not change much over the entire energy range span.

The dependence of the asymmetry parameter β_1 and the anisotropy parameter β_2 on the interaction strength ($k = q/v$) of the projectile is shown in Fig. 4.4. The trend is similar to earlier works [74, 72, 73]. We can see that for higher degrees of ionization, the anisotropy parameter β_2, is large and positive, and for low degrees of ionization, it is small and negative. The negative values of β_2 correspond to the case when the differential cross-section is larger at $\theta = \pi/2$ compared to its value at $\theta = 0$. This implies that the ionization cross-section is larger for the perpendicular

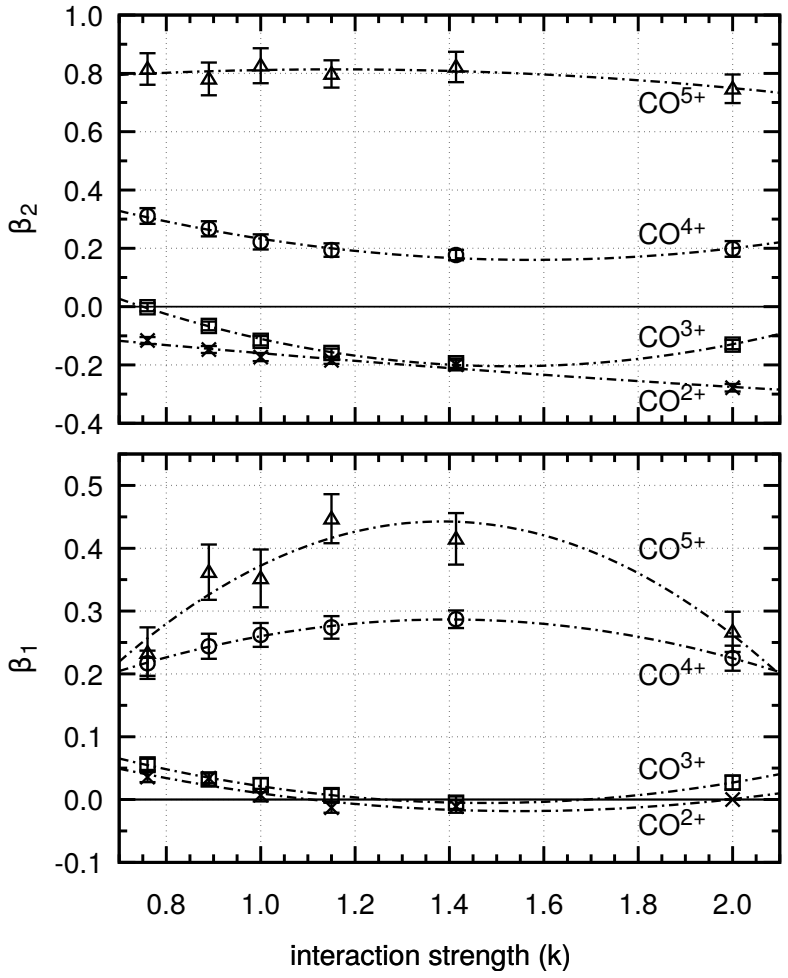

Figure 4.4: Variation of the anisotropy parameter β_2 and asymmetry parameter β_1, with the interaction strength k of the proejctile. The smooth chain curves are shown to guide the eye.

orientation of the molecule to the incident ion beam. For the perpendicular orientation of the molecule, there will be no forward-backward asymmetry. The values of asymmetry parameter β_1 are nearly zero for low degrees of ionization i.e. when the values of β_2 are negative. The high positive values of β_2 imply that the ionization predominantly occurs when the molecule is oriented parallel to the incident ion beam, and forward-backward asymmetry is expected for a heteronuclear molecule. The values of asymmetry parameters are positive and nonzero for positive values of β_2. For interaction strengths around $k = 1.4$ the values of β_1 exhibits a clear maximum for $n = 4, 5$ and a weak minimum for $n = 2, 3$. In the earlier chapter, we have seen that for a given degree of ionization, the values of asymmetry and anisotropy parameters decreases with an increase in projectile energy. In the present experi-

ment, projectiles chosen span a range of interaction strengths from the strong to the perturbative regime. In Fig. 4.4, we can notice a decreasing behavior in the values of beta parameters when we go to the perturbative regime.

4.1.3 Vanishing of anisotropy for a certain degree of ionization

As discussed in the previous chapter, the Wohrer and Watson [58] model suggests that the perpendicular orientation is favorable for a low degree of ionization, and the parallel orientation is more favorable for a high degree of ionization. This implies that the value of parameter A will be slightly less than zero for a low degree and highly positive for a high degree of ionization of the target molecule. In Fig. 4.5, we have shown the dependence of parameter A on the degree of ionization for different projectile energies. As we can see that the value of A flips sign at some *hypothetical* value of n, which we call n_{flip}. The n_{flip} may not be an integer and hence not a direct observable. For a given projectile or a fixed interaction strength, the sign of A would flip when going from a certain degree of ionization ($< n_{\text{flip}}$) to the next higher degree of ionization ($> n_{\text{flip}}$). This interpretation matches the trend of the model of Caraby *et al.* [62] for CO, in which the anisotropy is seen to flip sign in going from $n = 3$ to $n = 4$. This variation is very similar to the variation predicted by the Kaliman *et al.* model for N_2, in which a sign of A is seen to flip around $n = 3$.

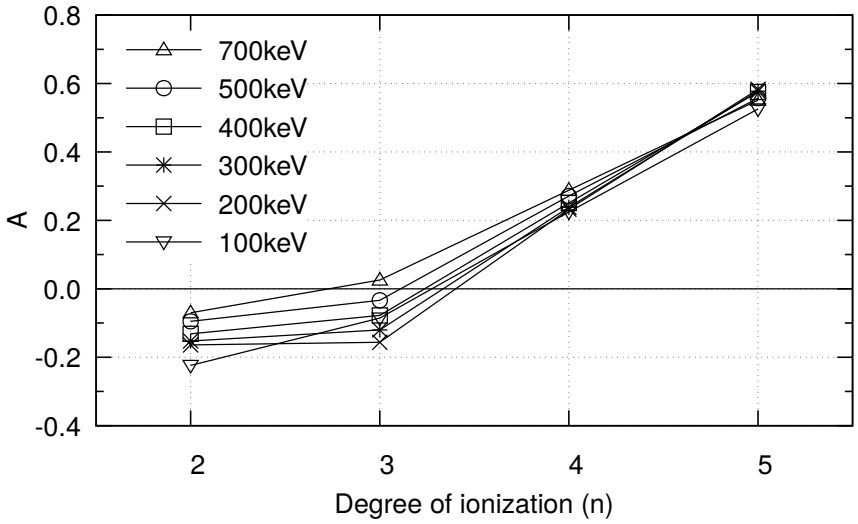

Figure 4.5: Dependence of the parameter A, on the degree of ionization (n) of CO molecule under He^{2+} impact at different energies.

The n_{flip} is called as n_{min} by Kaliman *et al.* and they state it as "the minimal value of n for which we may expect the anisotropy". However, we can see that this is not the minimum values instead this value represents the sign change of anisotropy parameter. We examine the trend in the value of n_{flip} as a function of projectile interaction strength using the formula provided by Kaliman *et al.*. For the perturbative regime, i.e. for $k \ll 1$, that model gives $n_{\text{flip}} \approx (6a^2 v/R_e)^{1/3}$ where a is an effective principal quantum number and R_e is a size parameter of the molecule; for a diatomic molecule, we take this to be the internuclear distance. For the CO molecule the model gives $a \approx 2.7$ and $R_e = 2.13$ a.u., hence $n_{\text{flip}} \approx 2.7\,(kq)^{1/3}$. In the regime of strong interaction ($k \gg 1$), the model gives the value of n_{flip} approximately as $2ak/R_e$, hence $n_{\text{flip}} \approx 2.5\,k$ for $k \gg 1$.

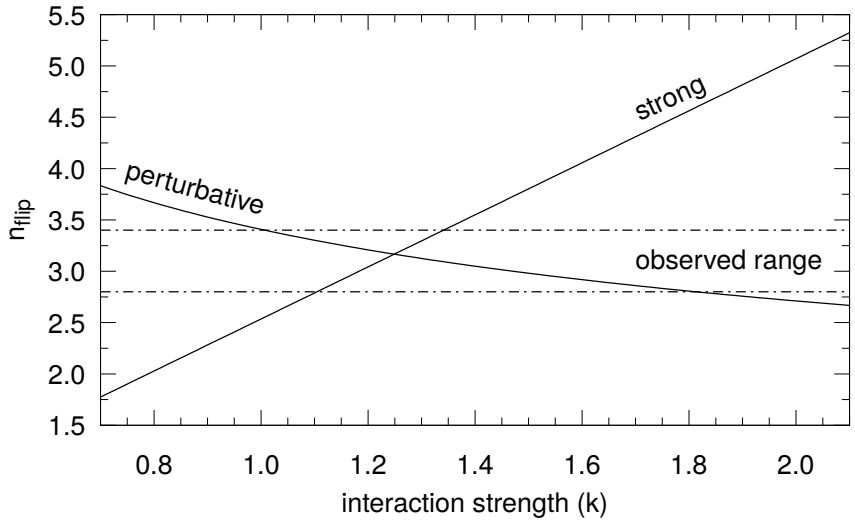

Figure 4.6: The variation of the values of the degree of ionization n_{flip} for which the the sign of A flips. Solid curves are based on the formulae from Kaliman *et al.* model [64] for the strong and the perturbative regimes. Chain lines indicate the range within which the observed values of n_{flip} lie in our experiment.

Since the k parameter or $k = 1$ does not define a sharp transition from one regime to the other, we have calculated the value of n_{flip} using the two separate formulae for a comparison with our results in the range $0.76 \leq k \leq 2.0$. The predicted values of n_{flip} for He^{2+} at different energies and the range of values of n_{flip} extracted from our observations are plotted in Fig. 4.6. We infer that for intermediate interaction strengths, anisotropy nearly vanishes for $n \approx 3$. As we can see the values of n_{flip} increases when go to strong interaction regime or towards the perturbative regime. A large value of n_{flip} represents that the change in sign of anisotropy parameter will

be at a higher degree of ionization.

4.2 CO molecule under Xe^{9+} impact

To study the orientation effect in strong interaction regime, the experiment was carried out with a Xe^{9+} beam at different energy such that the interaction strength lies in the strong interaction regime ($k \gg 1$). The projectile energy, velocity, and interaction strength (q/v) are tabulated in Table 4.3

Energy (keV)	Velocity (au)	Interaction strength (k)
450	0.37	24.12
1170	0.60	14.96
2070	0.79	11.25
3258	1.00	9.00

Table 4.3: Energy, velocity and interaction strength for Xe^{9+} beam

4.2.1 Dissociation channels

The time of flight coincidence map for CO fragmentation under 450 keV Xe^{9+} impact is shown in Fig. 4.7. The time of flight coincidence is map is very dense and upto six-fold degree of ionization is observed at all incident energies. The dissociation channels that are observed for various degrees of ionization are

$$CO^{2+} \rightarrow C^{+} + O^{+} \tag{4.8}$$

$$CO^{3+} \rightarrow C^{2+} + O^{+},\ C^{+} + O^{2+} \tag{4.9}$$

$$CO^{4+} \rightarrow C^{2+} + O^{2+},\ C^{3+} + O^{+},\ C^{+} + O^{3+} \tag{4.10}$$

$$CO^{5+} \rightarrow C^{3+} + O^{2+},\ C^{2+} + O^{3+} \tag{4.11}$$

$$CO^{6+} \rightarrow C^{3+} + O^{3+} \tag{4.12}$$

4.2.2 Orientation effect for CO under Xe^{9+} impact

The observed and the fitted angular distribution for multiple ionization of CO for 450 keV Xe^{9+} ($k \approx 24$) is shown in Fig. 4.8. The distribution is isotropic for all

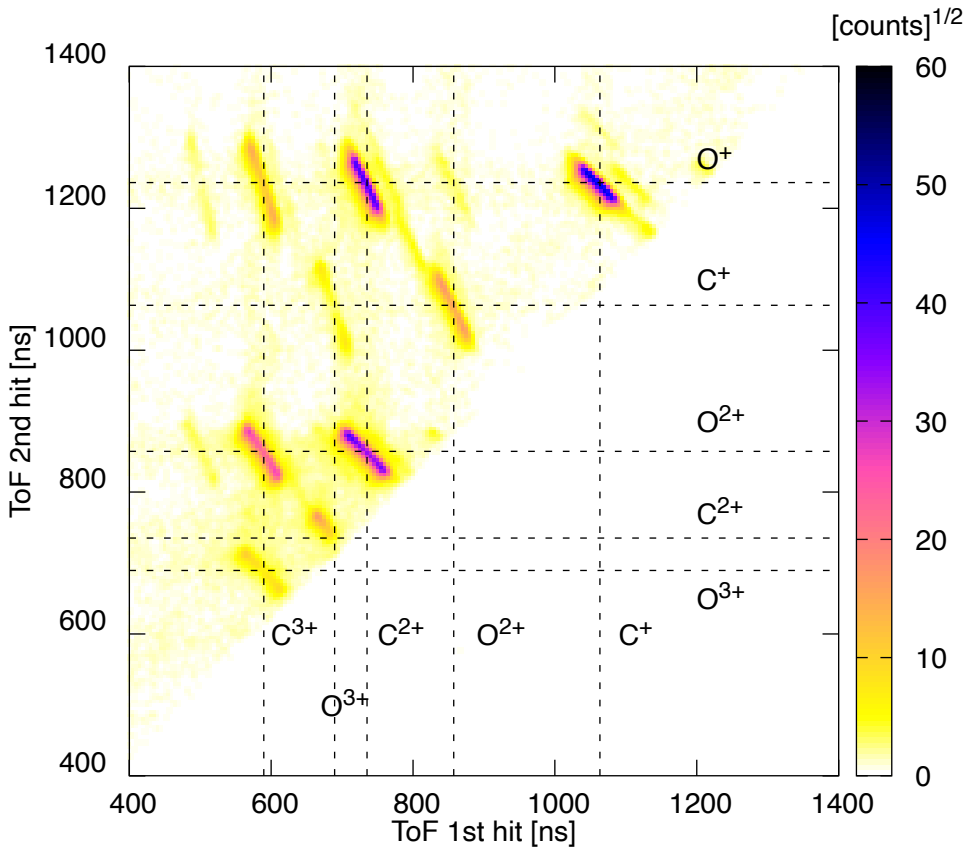

Figure 4.7: Time of fight coincidence map for CO under 450 keV Xe^{9+} impact. Different islands corresponds to different dissociation pathways.

the degrees of ionization. The asymmetry and anisotropy are approximately zero. As discussed earlier, a projectile with a large k can transfer the same energy at a large impact parameter as a projectile with a small k at a small impact parameter. The orientation effect is expected to be strong at small impact parameters since the details of the electron cloud are 'seen' by the projectile. For impact parameters larger than the size of the molecule, the orientation effect would be weak, since the projectile no longer 'sees' the detailed structure of the molecule; the electron cloud appears to be nearly spherical.

4.3 Summary

In this chapter, we have discussed the orientation dependence in multiple ionization of CO molecule in the intermediate and strong interaction regimes. In the intermediate interaction regime, we find that over the entire range of the interaction

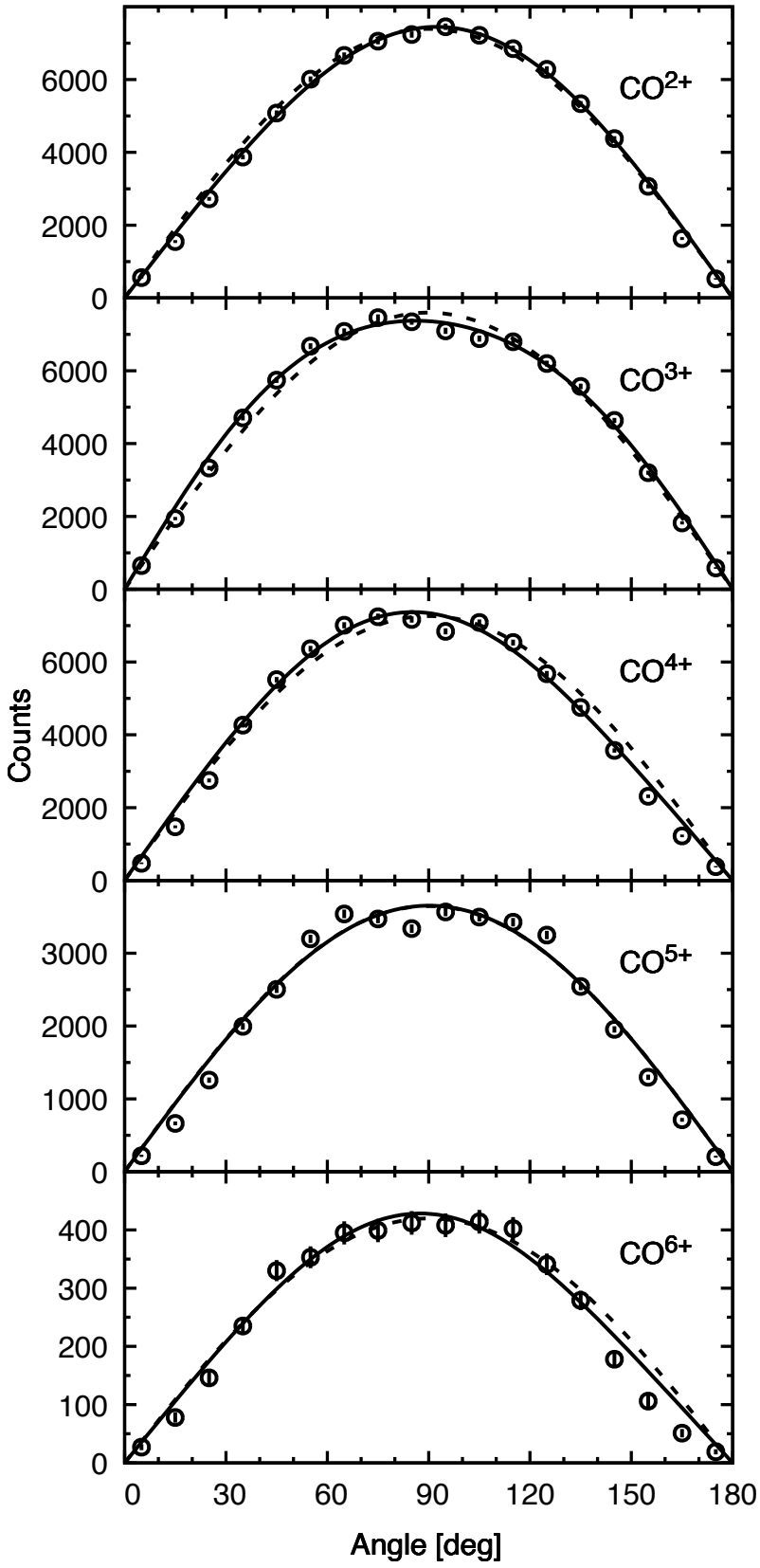

Figure 4.8: Experimental observation [points with error bars] and fitted equation 4.5 [continuous curve] for orientation angle dependence of multiple ionization of CO under 450 keV Xe^{9+} impact. The angular distributions are sum over all fragmentation channels for a given degree of ionization. The dashed curve is $\sin\theta$ distribution, representing the isotropic case.

strength, the anisotropy is strong for the high degree ($n \geq 4$) of ionization and weak for the low degree ($n \leq 3$) of ionization. A simple geometric argument that when the cross-section is higher for perpendicular orientation, there should be little (approx zero) forward-backward asymmetry in the distribution is also verified. When the anisotropy parameter has a positive value, implying that implies that ionization predominantly occurs when the molecule is oriented parallel to the beam, and forward-backward asymmetry is expected for a heteronuclear molecule. This can be verified with for $n \geq 4$ degree of ionization or the results reported in the earlier chapter where β_1 and β_2 are positive under the perturbative regime. As shown in Fig. 4.4, the anisotropy and asymmetry parameters show maxima around $k = 1.4$ and decrease as one goes to the perturbative regime or strong interaction regime. In the earlier chapter, we have discussed the orientation effect under the perturbative regime. With an increase in projectile energy or when $k \ll 1$, the orientation effect decreases. For strong interaction regime, the orientation dependence in multiple ionization of CO molecule was studied under Xe^{9+} impact such that $k \gg 1$. The observed angular distribution was isotropic for all degrees of ionization.

Chapter 5

Orientation effect for triatomic molecule OCS

In the last two chapters, we have discussed the interaction strength dependence of orientation effect in multiple ionization of a diatomic molecule CO. We saw that the orientation effect is not purely a geometric effect but depends on the constituents of the molecule too. The experimental determination of the orientation of the molecule in ionization by charged particle impact exploits the fact that the dissociation products of a diatomic molecule will depart back-to-back along the internuclear axis of the molecule because of linear momentum conservation. The orientation of the molecule is determined from the directions of the momentum vectors of one or both fragment ions. For molecules with differing bond lengths, the longer molecule is likely to show greater asymmetry and anisotropy in the angular distributions of the fragment ions. For this, we choose a triatomic molecule OCS to further extend our study of orientation effect in ion-molecule collisions. For a triatomic molecule, the orientation of the molecule can be determined easily if only one bond is broken (i.e. two-body fragmentation). The orientation can be determined from the emission angle of one of the fragment ions as in the case of a diatomic molecule. But for a three-body breakup, measurement of the fragment emission angle alone is insufficient, because there could be a step-by-step or simultaneous breaking of the two bonds (sequential and concerted fragmentation). The mixing of these two channels makes it challenging to determine the orientation angle of the molecule. Even for a pure concerted channel, the direction of the momentum vector is not a

direct measure of the initial orientation because the angle between the asymptotic momentum vectors of the fragments is different from the initial bond angles of the molecule because of the repulsion between each pair of fragment ions. Zero-point vibrational excitations which give rise to a distribution of bond angles even in the ground electronic state of a triatomic molecule further alter the asymptotic fragment momentum distributions. In continuation of the previous work for diatomic molecule, this chapter deals with the study of interaction strength dependence of orientation effect in multiple ionization of a triatomic molecule OCS.

5.1 OCS molecule

OCS is a linear triatomic molecule with a linear dimension of 272 pm and a molecular mass of 60 amu. Both the oxygen atom and the sulfur atom are more electronegative than the central carbon atom. OCS molecule has a small net dipole moment of 0.714 Debye.

For a triatomic molecule, the main focus of earlier works has been on the separation of dissociation pathways [38, 96–102] and the question of the orientation dependence of multiple ionization is not addressed much. The orientation effect in photoionization and strong-field ionization has been addressed in various studies [103–105]. Under photon or laser impact, the polarization of the external field offers a natural direction relative to which angular distributions of the fragment ions or electrons are measured. The measurements of angular distributions of photoelectrons in the molecular reference frame have usually relied on processes in which ionization is followed by fragmentation. Holmegaard [106] studied the angular distribution of photoelectrons from OCS and showed that the orientation dependence of the ionization process causes an asymmetry in the angular distribution of photoelectrons. Sakemi *et al.* [107] studied the two-body dissociation of OCS^+ brought about by elliptically polarised laser pulses and showed the asymmetry in the fragmentation pathways. Here, we will look at the orientation effect in multiple ionization of OCS in ion-molecule collisions.

5.2 Experimental results

The experiment was carried out with p^+ and C^{2+} projectiles at different energy so as to access the perturbative regime ($k < 1$) and strong interaction regime ($k > 1$). The projectile energy, velocity, and interaction strength are tabulated in Table 5.1

Projectile	Energy (keV)	Velocity (au)	Interaction strength (k)
p^+	50	1.42	0.74
C^{2+}	50	0.41	4.87

Table 5.1: Energy, velocity and interaction strength for p^+ and C^{2+} projectiles

5.2.1 Dissociation channels

When a molecule breaks into two fragments, the linear momentum of the two fragments are equal and opposite. The time of flight of the two fragments is anti-correlated and an island appears in the time of flight coincidence map. The shape of the island will be a narrow bar with a negative slope depending on the charge states of the fragments ions. The time of flight coincidence map for first and second ion from the dissociation of OCS molecule is shown in the lower panel of Fig 5.1. The two-body dissociation channels that are observed for multiply ionized OCS molecule are:

$$OCS^{2+} \rightarrow O^+ + CS^+ \tag{5.1}$$

$$OCS^{2+} \rightarrow OC^+ + S^+ \tag{5.2}$$

$$OCS^{3+} \rightarrow OC^+ + S^{2+} \tag{5.3}$$

For a triatomic molecule like OCS, depending on the charge state and stability of parent molecular ions, there can be three body dissociation. The three body dissociation channel that is observed for triply ionized OCS molecule is:

$$OCS^{3+} \rightarrow O^+ + C^+ + S^+ \tag{5.4}$$

The signature of high degree of ionization of OCS molecule (correlation between C^{2+}:O^+ and C^{2+}:S^+) can also be seen in the time of flight coincidence map. But the

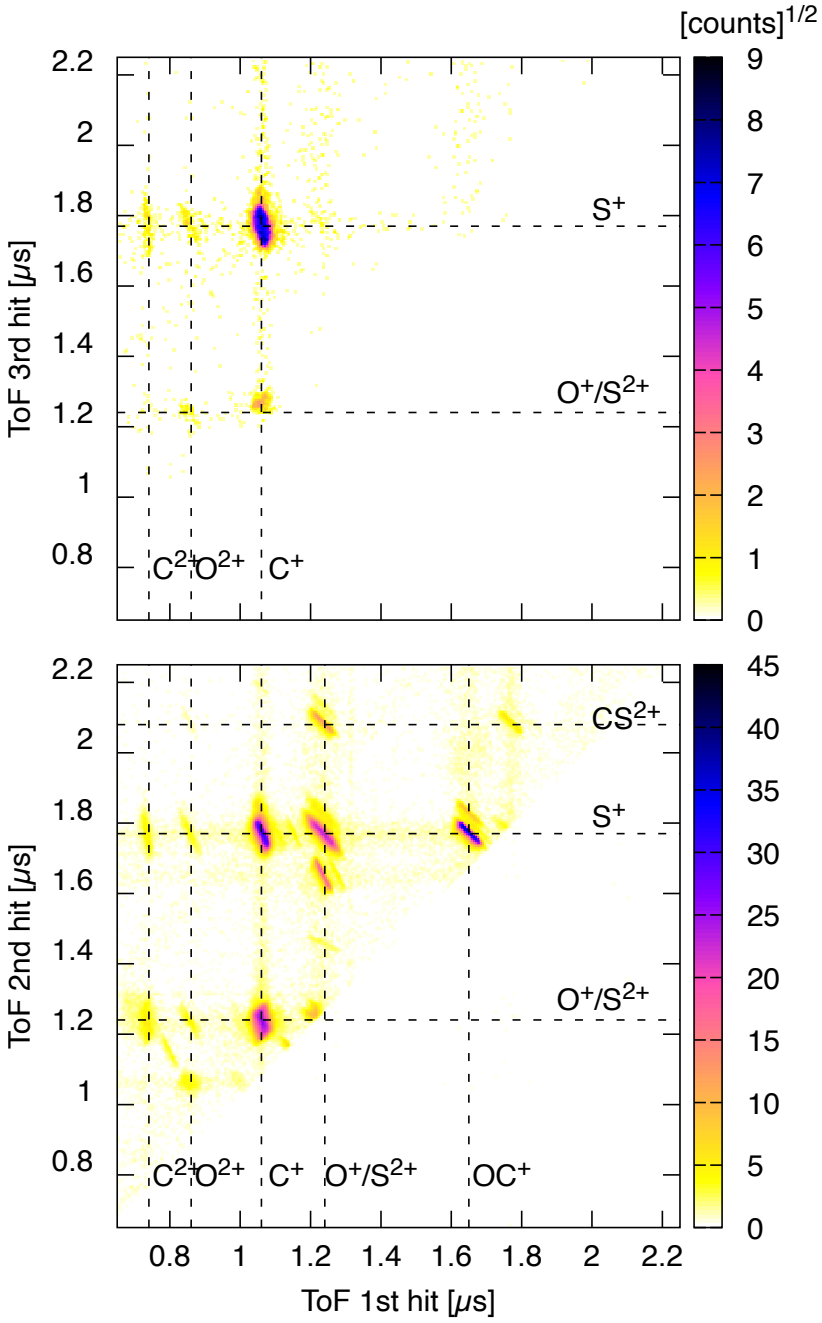

Figure 5.1: Time of flight coincidence map for OCS fragmentation under 50 keV p^+ impact. Different islands correspond to different dissociation pathways.

counts are not enough for the analysis. In the chapter, we will discuss the orientation effect in double and triple ionization of OCS.

5.3 Orientation effect for two body breakup

As discussed earlier, the measurement of the orientation of the molecule is straightforward for two-body dissociation. The momentum vector of one of the fragment ions can be used to calculate the orientation of the molecule with respect to the incident beam. In this section, we will discuss the orientation effect for doubly and triply ionized OCS molecule dissociating into two fragment ions. The angular distribution of one of the fragments ion (eg. OC^+ for OC^+:S^+ and O^+ for O^+:CS^+) is fitted to equation 5.5 and the values of asymmetry and anisotropy parameters are obtained.

$$N(\theta) \approx N_0 \Big[1 + \beta_1 P_1(\cos\theta) + \beta_2 P_2(\cos\theta)\Big] \sin\theta \tag{5.5}$$

5.3.1 OCS^{2+}

In Fig. 5.2, the angular distributions of one of the fragment ion from the dissociation of OCS^{2+} to OC^+:S^+ and O^+:CS^+ are shown for p^+ and C^{2+} impact. The experimentally observed values of anisotropy and asymmetry parameters are listed in Table 5.2.

Projectile	Fragment ion	β_1	β_2
p^+	OC^+	0	-0.15
	O^+	0	-0.20
C^{2+}	OC^+	0	-0.16
	O^+	0	-0.18

Table 5.2: The value of asymmetry and anisotropy parameters for two body dissociation of OCS^{2+} under p^+ and C^{2+} impact

The angular distribution shows maxima at 90 degrees and the value of the anisotropy parameter β_2 is negative. It implies the enhancement in the ionization probability for perpendicular orientation of the molecule. The angular distributions of fragment ions are symmetric and the observed values of asymmetry parameter β_1 are zero for both the projectiles.

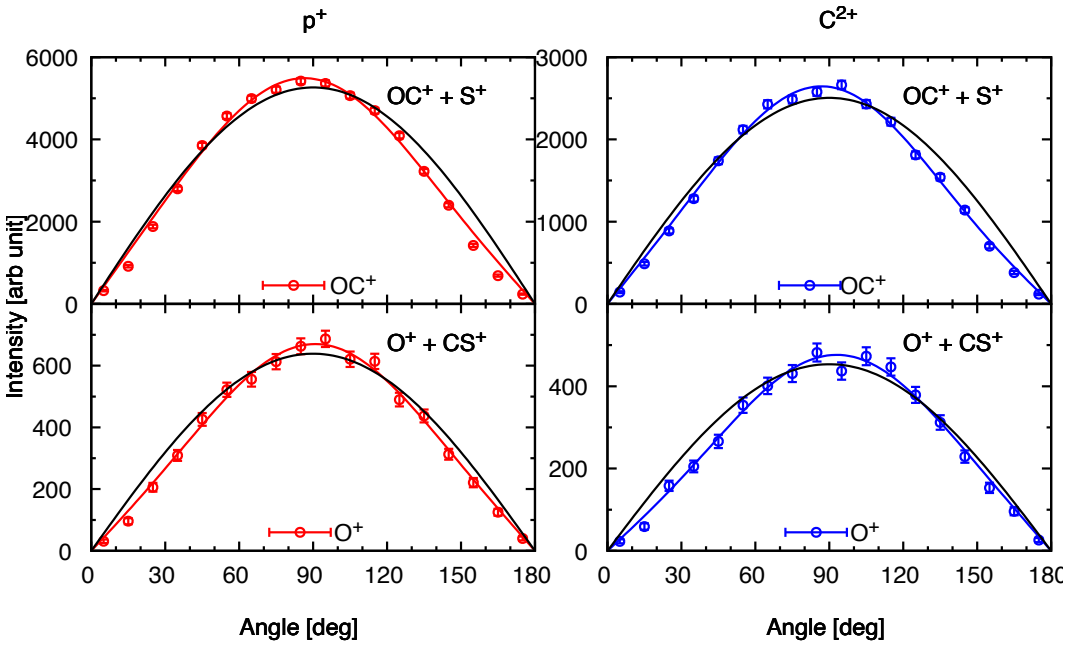

Figure 5.2: Angular distribution of fragments from dissociation of OCS^{2+} to OC^{+}+S^{+} and O^{+}+CS^{+} channels. (Left): for p^{+} impact, (Right): for C^{2+} impact. Black curve represents the isotropic distribution and continuous cure is the fitted function (equation 5.5).

5.3.2 OCS^{3+}

In Fig. 5.3, the angular distributions of the fragments ion OC^{+} for dissociation channel OC^{+}:S^{2+} are shown. The observed values of the anisotropy and asymmetry parameters are listed in Table 5.3.

Projectile	Fragment ion	β_1	β_2
p^{+}	OC^{+}	0	0.24
C^{2+}	OC^{+}	0	-0.23

Table 5.3: The value of asymmetry and anisotropy parameters for dissociation of OCS^{3+} to OC^{+}:S^{2+} under p^{+} and C^{2+} impact

The angular distribution of the fragment ions is symmetric with $\beta_1 \approx 0$ for both projectiles. The distribution shows a very weak anisotropy for both the projectiles. It is clear from Table 5.3, the sign of anisotropy parameter is positive for p^{+} impact: $\beta_2 \approx 0.24$, and negative for carbon impact $\beta_2 \approx -0.23$. A positive value of β_2 implies an enhancement in the ionization cross-section for parallel orientation and a negative value of β_2 implies an enhancement of the ionization cross-section for the perpendicular orientation of the molecule with respect to the incident projectile.

This is in agreement with our study of diatomic molecule CO and with the earlier works [108, 72] for diatomic molecules: for a given degree of ionization, β_2 changes sign from positive to negative as the projectile interaction strength q/v increases [64, 74]. For p^+ impact, the value of the anisotropy parameter is negative for OCS^{2+} and positive for OCS^{3+}. This effect is also similar to what is observed for diatomic molecules: with an increase in the degree of ionization, anisotropy increases. For projectile with high interaction strength, the change in β_2 values from negative to positive occurs at higher degrees of ionization. For doubly and triply ionized OCS, the anisotropy parameters are negative for C^{2+} impact.

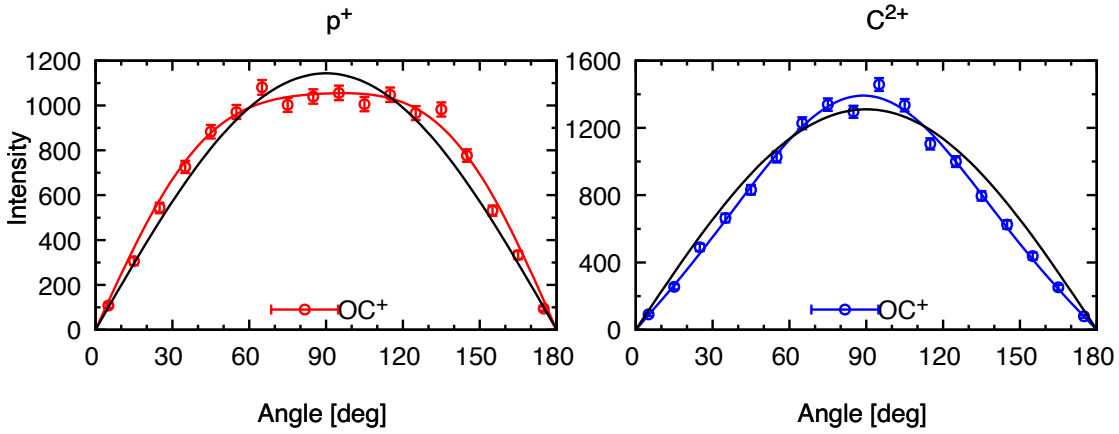

Figure 5.3: Angular distribution of fragments from dissociation of OCS^{3+} to OC^++S^{2+}. (Left): for p^+ impact, (Right): for C^{2+} impact.

5.4 Three body dissociation

The following channels are possible for the three-body fragmentation of OCS^{3+}, with equal sharing of charge between the three fragments. Apart from the concerted fragmentation, two sequential fragmentation channels are possible. The concerted fragmentation is a one-step process where all the bonds break simultaneously. The sequential fragmentation is a two-step process where one of the bonds breaks first leaving behind an ion and molecular dication. The intermediate molecular dication can rotate and dissociate after some time. The concerted and sequential channels for dissociation of OCS^{3+} are

$$OCS^{3+} \rightarrow O^{+} + C^{+} + S^{+} \tag{5.6}$$

$$OCS^{3+} \rightarrow OC^{2+} + S^{+} \rightarrow O^{+} + C^{+} + S^{+} \tag{5.7}$$

$$OCS^{3+} \rightarrow O^{+} + CS^{2+} \rightarrow O^{+} + C^{+} + S^{+} \tag{5.8}$$

An exact separation of concerted and sequential channels is not possible. The experimentally measured parameters are the momentum vector of the fragment ions, but the fragment could be from a concerted channel or sequential channel. The mixing of the concerted and sequential pathways makes it challenging to determine the orientation angle of the molecule from the momentum vector of one of the fragment ions. In the next section, very well known and widely used methods of visualization of a three-body breakup are discussed. These methods are used to distinguish between dissociation pathways for the three-body breakup.

5.4.1 Newton diagram and Dalitz plot

For the three-body breakup process, a visual impression of the distribution of events can be obtained by the use of a Dalitz plot or a Newton diagram. In the Dalitz plot, the correlated KE after normalization to the total KER of three fragments are transformed to Cartesian coordinates x and y given by

$$x = \frac{E_{O^+} - E_{S^+}}{\sqrt{3}E_k} \tag{5.9}$$

$$y = \frac{E_{C^+}}{E_k} - \frac{1}{3} \tag{5.10}$$

where E_k is the total kinetic energy release. Each point in the Dalitz plot corresponds to a specific fragmentation pattern. In Fig. 5.4, the Dalitz plots for the fragmentation of OCS^{3+} in under of p^+ and C^{2+} impact are shown. The intense area in the plot, located away from and above the point $(0.1, -0.3)$ represents the pure Coulombic explosion and linear dissociation of the molecule. The asymmetric cross structure corresponds to sequential breakup. It is clear from the plots that the sequential fragmentation channels are quite weak and, more likely in the case of C^{2+} impact than for p^+ impact. The leftward propensity of the distribution is on account of the

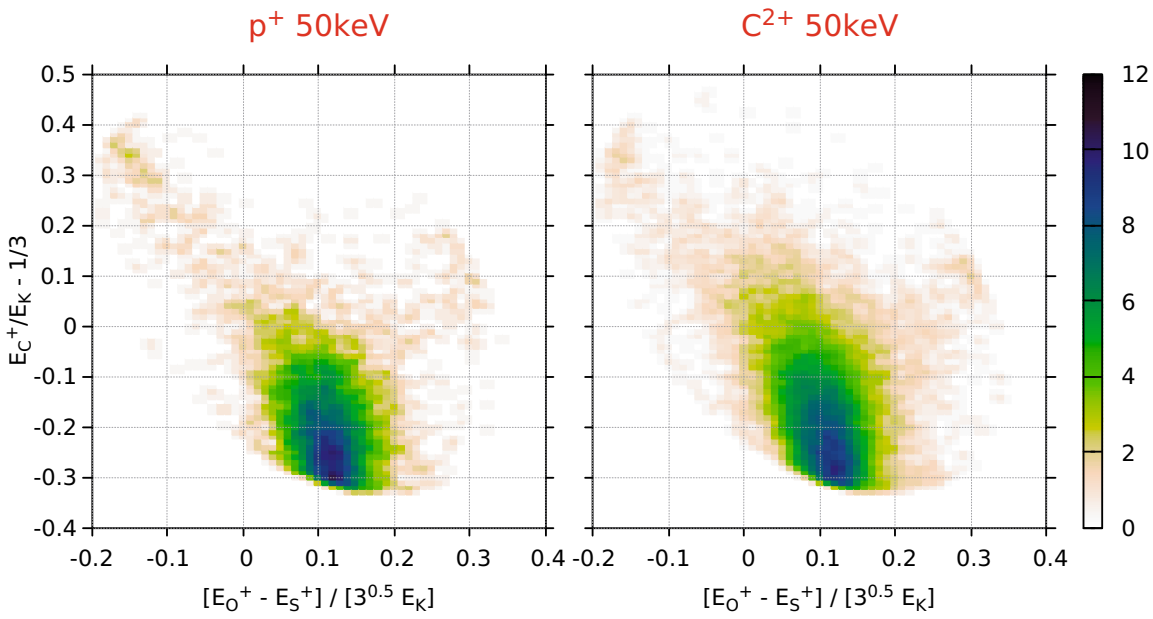

Figure 5.4: Dalitz plots for three-body fragmentation of OCS^{3+} for p^+ and C^{2+} impact. The false colour scale represents the square-root of the counts in the bin. The high intensity region away from$(0.1, -0.3)$ corresponds to concerted fragmentation, while the rest of the events falling roughly around an asymmetric cross structure, are from sequential fragmentation.

asymmetry of the masses of O^+ and S^+.

The Newton diagram for three-body dissociation is shown in Fig. 5.5. We have taken the direction of the normalised O^+ momentum to be the reference direction and the relative momentum of C^+ and S^+ are plotted in upper and lower quadrant respectively. The two major intense lobes correspond to the concerted pathways. The signature of sequential pathways for which the intermediate molecular ion can rotate and dissociate can be seen as the circular structure in the diagram. This diagram can be used to calculate the molecular geometry and angular correlation between the fragment ions.

These methods are provide an effective visual representation of the data but the exact separation of the dissociation pathways is not possible. No methods are available to separate events arising from the three channels based on a single parameter. The mixing of these pathways makes the measurement of the orientation angle of the molecule very difficult. Even for a pure concerted channel, the Coulombic repulsion between the fragments alters the measurement of the actual bond angle of the molecule and so does the measurement of the orientation angle. In the next section,

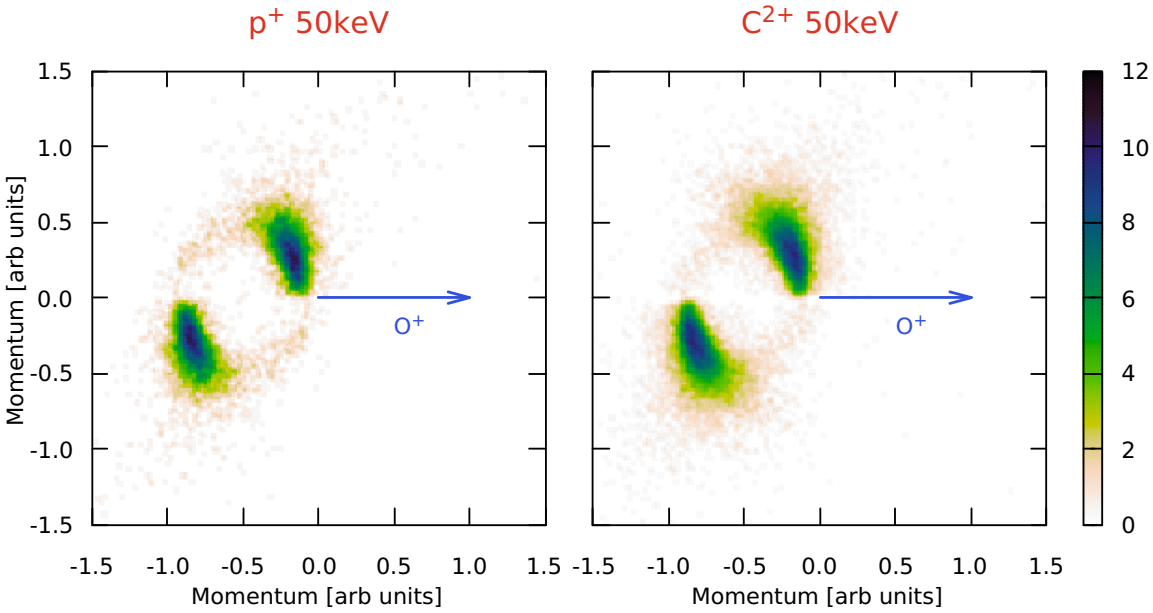

Figure 5.5: Newton diagram for three-body fragmentation of OCS^{3+} for p^+ and C^{2+} impact. The false colour scale represents the square-root of the counts in the bin. C^+ and S^+ momentum distribution are plotted in upper and lower quadrant. The high intensity region corresponds to the concerted and circular structure corresponds to sequential pathways.

the angular correlation between outer fragment ions is discussed.

5.5 Angular correlation between fragments

In its ground vibrational state, the most probable bond angle of neutral OCS is 175°. Zero-point vibrational excitations give rise to a distribution of bond angles in the ground electronic state and the probability of the bond angle being 180° is zero. So, when the triply ionized OCS molecule undergoes concerted fragmentation, where all the bonds break simultaneously, the terminal ions do not depart back-to-back. The initial Coulomb repulsion between the ionic fragments alters the final asymptotic angle between their momentum vectors. Within the framework of the simple Coulomb explosion model of three charged particles departing apart, the asymptotic angle between the momentum vectors of the terminal ions O^+ and S^+ can be calculated for a given initial bond angle. This angle will be smaller than the actual bond angle of the molecule, which is observed in our case too. The experimentally observed angular distributions between the terminal fragment ions are shown in Fig. 5.6.

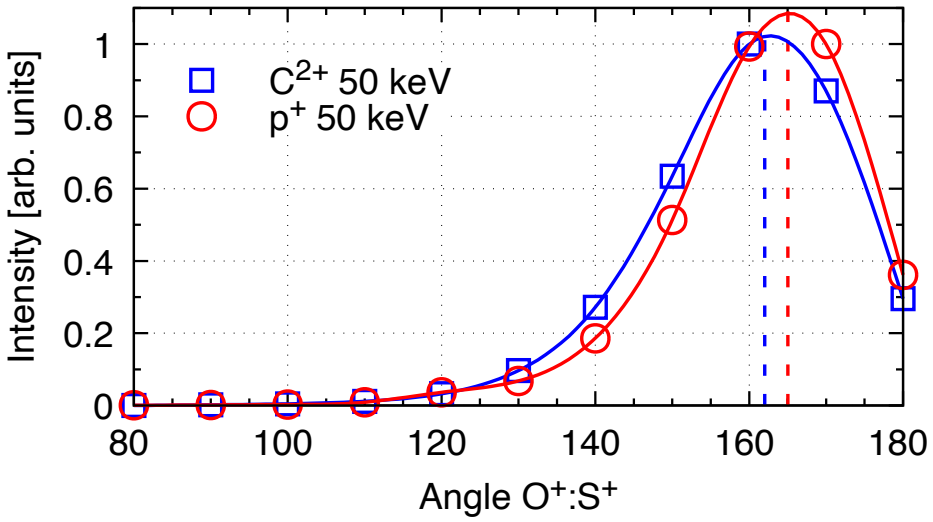

Figure 5.6: Distribution of the asymptotic angle between O^+ and S^+ momentum vectors for the case of p^+ and C^{2+} impact. The smooth curve is a cubic spline intended to guide the eye.

The distribution peaks at 165° for p^+ impact and at 162° for C^{2+} impact with a long tail for both the projectiles. This peak value is smaller than the most probable bond angle of the OCS molecule. Using the simple Coulomb explosion model, we can map the asymptotic angle between the terminal fragments to the initial bond angles. For a concerted process, all the bonds break simultaneously and for a sequential process, the intermediate molecular ion can rotate and dissociate after some time leading to a nearly unrestricted distribution of the O^+:S^+ angle. A rough separation of concerted and sequential channels can be made from angular distribution of terminal fragment ions. Based on the simple Coulomb explosion model and earlier studies [109], we may regard all events with the O^+:S^+ angle falling in the range 180°–150° as arising from concerted fragmentation of OCS^{3+}. Any asymptotic O^+:S^+ angle smaller than this must arise from sequential events. For sequential channels, the orientation effect can be examined by measuring the angle between the first fragment ion and incident projectile. But our data statistics are too low to permit analysis for these channels.

5.6 Orientation effect for three body breakup: OCS^{3+}

We have discussed the two major challenges for estimating the orientation angle of the molecule for three-body breakup. The first one is the mixing of concerted and sequential dissociation pathways. The second one is the bond angle distribution in the ground electronic state of the molecule, which results in the asymptotic angular distribution to be different than the actual bond angle of the molecule. It is clear from Fig. 5.6 that both of these challenges can be addressed in one diagram.

For concerted fragmentation, for which the asymptotic O^+:S^+ angles lie in the range 180°–150°, the orientation dependence of triple ionization may be discerned by merely observing the angular distribution of the terminal fragments ions with respect to the projectile direction. Compared to terminal ions, the central C^+ ion will always have a small momentum, and hence the determination of the orientation dependence has to rely on the terminal ions. In Fig. 5.7, we show a two-dimensional plot of the triple ionization and fragmentation of OCS molecule as a function of the emission angle of the terminal fragment ions and the asymptotic O^+:S^+ angle. As expected, the distributions of O^+ and S^+ are complementary to each other. If S^+ ions are emitted in the forward direction (along the projectile i.e. $\theta < 90°$), the O^+ ions are emitted in the backward direction.

The two-dimensional plots between the asymptotic O^+:S^+ angles and the angle of emission of any one of the terminal fragments with respect to the projectile direction are shown in Fig. 5.7 for both the projectiles, p^+ and C^{2+}. Since in the case of OCS^{3+} triple fragmentation is a necessary consequence of triple ionization, the plots in Fig. 5.7 give us a direct impression of the anisotropy and asymmetry in the triple ionization of OCS molecule. For p^+ impact, there is a small asymmetry as well as anisotropy in the distribution. For C^{2+} impact, there is no forward-backward asymmetry in the angular distribution of either of terminal ions. The distribution is nearly isotropic with a slightly enhanced probability at 90°. In other words, for p^+ impact, the orientation in which the O atom point towards the projectile (i.e. $\theta \gg 90°$) or, equivalently, when the S atom along the projectile, is the favored orientation for the triple ionization.

The asymmetry and anisotropy parameters, β_1 and β_2, for the orientation dependence of triple ionization are calculated by fitting the equation 5.5 to the data

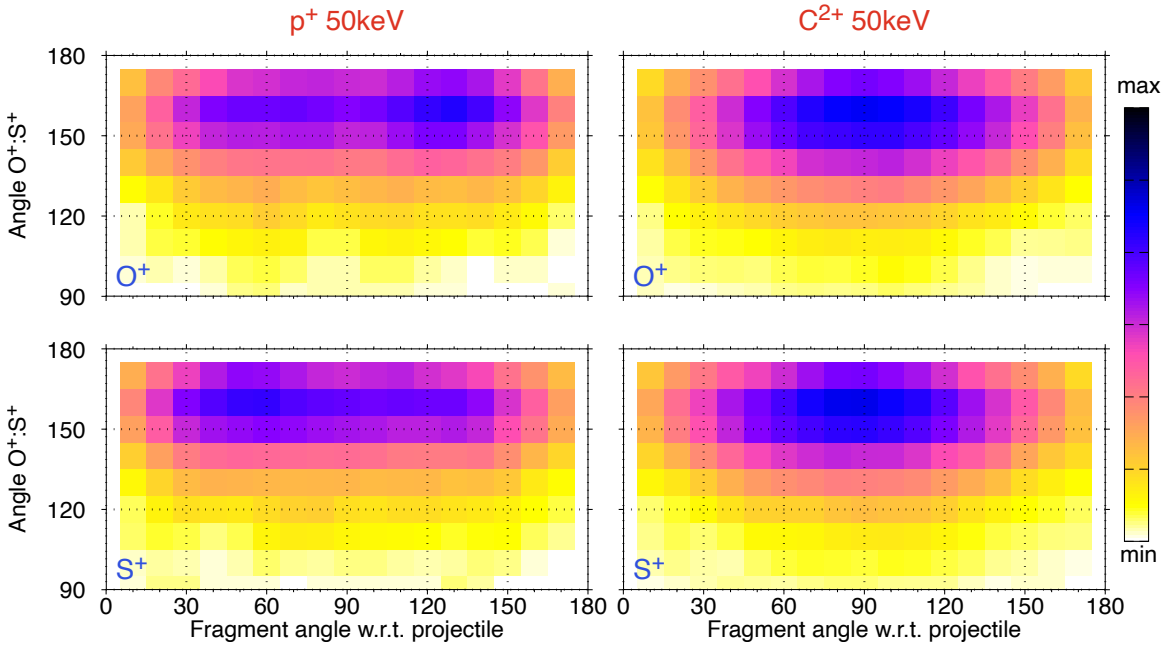

Figure 5.7: The distribution of angle of emission (relative to the projectile) of the two terminal ions as a function of the asymptotic angle between them in three-body fragmentation of OCS^{3+}. The false colour scale represents the square-root of the counts in the bin. The counts scale in each colour map is individually normalised to the maximum counts. The intense region (Angle $O^+ : S^+ > 150°$) corresponds to concerted fragmentation. The forward–backward asymmetry in the fragmentation w.r.t. the projectile is readily seen for p^+ impact.

for O^+:S^+ angle integrated over the range 180°–150°. The values of asymmetry and anisotropy parameters are shown in Table 5.4.

Projectile	Fragment	β_1	β_2
p^+	O^+	-0.21	0.47
	S^+	0.21	0.40
C^{2+}	O^+	-0.08	-0.41
	S^+	0.11	-0.47

Table 5.4: The value of asymmetry and anisotropy parameters for angular distribution of fragments from dissociation of OCS^{3+} under p^+ and C^{2+} impact

The value of the anisotropy parameter β_2 is higher and more positive for p^+ impact as compared to C^{2+} impact. It implies that ionization probability is higher for the parallel orientation than perpendicular orientation of the molecules. For parallel orientation, the asymmetry parameter is expected to be non-zero. It is clear from the angular distribution of O^+ and S^+ that ionization probability is high for the orientation in which the oxygen atom points towards the projectile. For

C^{2+} impact, a high negative value of the anisotropy parameter indicates a higher ionization probability for the perpendicular orientation of the molecule, and thus in this case no forward-backward asymmetry can be expected. It is clear from the Table 5.4 that the values of the asymmetry parameters for O^+ and S^+ are indeed very small.

5.7 Summary

In this chapter, we have discussed the orientation effect in multiple ionization of a triatomic molecule OCS under p^+ impact ($q/v = 0.7$) and C^{2+} impact ($q/v = 4.9$). For a two-body breakup, the measurement of the orientation angle is straightforward. The angular distribution of one of the fragment ions can be used to determine the orientation of the molecule with respect to the projectile beam. Under p^+ impact, the anisotropy parameter β_2 changes sign from negative to positive with an increase in the degree of ionization. Under C^{2+} impact, the anisotropy parameter is negative for both cases. For a three-body breakup, we have discussed the challenges for estimating the orientation of the molecule. By examining the angular distribution of the terminal ions (O^+ and S^+) as a function of the angle between their asymptotic momentum vectors, we are able to obtain the anisotropy and asymmetry parameters for the orientation dependence of triple ionization (three-body breakup). A strong anisotropy is observed in the angular distributions for p^+ impact compared to C^{2+} impact. This dependence of the anisotropy parameter on the projectile interaction strength is similar to that observed in diatomic molecules i.e. for higher interaction strengths the anisotropy is weaker. For p^+ impact, experimental results show that the ionization probability is higher when the oxygen atom point towards the projectile. For C^{2+} impact, the triple ionization probability is higher for perpendicular orientation of the molecule. The anisotropy as well as asymmetry are greater for triple ionization than for double ionization. In the case of p^+ impact, there is a forward-backward asymmetry in the angular distribution of the terminal fragments ions while in the case of C^{2+} impact the distribution is symmetric.

Chapter 6

Summary and outlook

6.1 Summary of the current work

In ion–molecule collisions, based on the anisotropy of the electron distribution in the molecule, the probability of multiple ionization of a molecule is expected to depend on the orientation of the molecule with respect to the incident ion beam. The main focus of the present work has been on the study of interaction strength dependence of the orientation effect in multiple ionization of the diatomic molecule CO and the triatomic molecule OCS under charged particle impact. This dependence has widely been studied, starting as early as 1935 for the simplest H_2 molecule and in the last 20 years for more complex molecules: N_2, O_2, and CO. No distinctions had been made between homonuclear and heteronuclear molecules, and the orientation dependence has been attributed purely to the geometry of the molecule. The orientation effect also depends on the interaction strength of the projectile which is parameterized by the ratio of q (charge of the projectile) to v (velocity of the projectile) in atomic units.

In this work, the orientation dependence of ionization for diatomic molecule CO and triatomic molecule OCS resulting from collisions with a variety of ion beams, e.g. p^+, He^{2+}, C^{2+}, and Xe^{9+} is discussed. The main purpose of using different types of projectile is to systematically study the dependence of orientation effect on the interaction strength of the projectile. All of the experiments were performed at the Low Energy Ion Beam Facility at the Inter-University Accelerator Center (IUAC) New Delhi, India, and the experimental setup used for this study was a Recoil Ion

Momentum Spectrometer.

For heteronuclear diatomic molecule CO, spatial anisotropy accompanied by a forward-backward asymmetry in the multiple ionization cross-sections with respect to the projectile direction is observed and quantified. We find that over the entire range of the interaction strengths the anisotropy is strong for a high degree of ionization and weak for a low degree of ionization. We further show that the difference in the nature of the two atoms in the case of CO gives rise to an asymmetry in the ionization process which was missing in the earlier studies. A higher degree of ionization is likely to be achieved in the collision when the projectile first encounters the oxygen atom rather than the carbon atom. Thus, the orientation effect is not purely a geometric effect but depends on the atomic species in the molecule also.

The orientation dependence is studied in perturbative, intermediate, and strong interaction regime. We show that the orientation effect depends on the interaction strength ($k = q/v$) of the projectile. If one goes to the perturbative regime ($k < 1$) or strong interaction regime ($k > 1$), orientation effect decreases. A model calculation is performed for obtaining the orientation-dependent ionization probability for a diatomic molecule subject to charged particle impact in the perturbative regime. The trajectory of the projectile is taken to be hyperbolic with a distance of closest approach that depends on the orientation of the molecule. The interaction between projectile and the two atoms of the molecule is considered separately under the independent electron approximation. The heteronuclear nature of the molecule is accounted for by treating the ionization radius and the single ionization probability to be different for the two atoms. Calculated orientation angle-dependent multiple ionization probabilities agree fairly well with the experimental results on the CO molecule. We show that modification to the straight-line trajectory is needed to bring the asymmetry parameter in the calculation.

In continuation of the orientation dependence ionization study in the case of a diatomic molecule CO, we extend our study to triatomic molecule OCS. For molecules with differing bond lengths, the longer molecule is likely to show greater asymmetry and anisotropy in the angular distributions of the fragment ions. But, for OCS, it is difficult to determine the orientation of the molecule with respect to the ion beam because of additional degrees of freedom. For two-body dissociation, the mea-

surement of the orientation angle is simple as in the case of a diatomic molecule. But, for three-body dissociation additional difficulties arise due to the mixing of sequential and concerted channels and the fact that the bond angle in the ground state has a distribution. The angle between the asymptotic momentum vectors of the fragments (which can be measured) is different from the initial bond angles of the molecule because of the repulsion between each pair of fragment ions, and zero-point vibrational excitations which give rise to a distribution of bond angles even in the ground electronic state of a triatomic molecule further alter the asymptotic fragment momentum distributions. By examining the angular distribution of the terminal ions (O^+ and S^+) with respect to the projectile as a function of the angle between their asymptotic momentum vectors, we are able to obtain the anisotropy and asymmetry parameters for the orientation dependence of triple ionization. This dependence of the orientation effect on the projectile interaction strength is similar to that for diatomic molecules i.e. for higher interaction strengths the anisotropy is weaker. Greater anisotropy is observed for p^+ impact compared to C^{2+} impact. For p^+ impact, experimental results show that the triple ionization probability is higher when the projectile is faced with an oxygen atom. For C^{2+} impact, the triple ionization probability is higher for perpendicular orientation of the molecule.

6.2 Outlook

In this work, we have presented the study of orientation effect in multiple ionization of a diatomic molecule CO and triatomic molecule OCS. The effect of projectile interaction strength is studied systematically. Following this work, one can proceed in three major directions as follows:

1. The perturbative regime can be attained for highly charged ($q \gg 1$) and highly energetic ($v \gg 1$) projectile such that $k \leq 1$. For $q \gg 1$, there will be charge exchange processes and orientation effects in those will be more interesting, and perhaps stronger. It will be interesting to look at the orientation dependence in multiple ionization of diatomic molecule under such projectile and compare the results with those presented in this work. We will be able to answer the dependence of orientation effect on charge state of the projectile under perturbative regime.

2. For the perturbative regime, a semiclassical model is presented. The applicability of the model is checked with earlier studies. While this model makes reasonable predictions about orientation-dependent anisotropy and asymmetry, it is a simple empirical model with a crude approximation of the trajectories. One can look into the modification of the trajectory. The ionization radius r calculated using Slater formula is found to affect the results strongly. For higher degrees of ionization we have taken the mean of k-shell and l-shell radius. A better and efficient approach can be used to estimate the ionization radius r.

3. For a three-body breakup of triatomic molecule OCS, quantifying the orientation effect is very difficult. By using a new representation, we can obtain the anisotropy and asymmetry parameters. A theoretical approach can be used to predict the angular distribution between terminal fragments ions and compare with experimental observations. That will be more helpful to determine the orientation angle of the molecule. For a more complex molecule, where the dissociation products are three or more than that, the situation will be more complex. It will be interesting to study the orientation effect for those molecules under the perturbative regime.

This work is focused on the total ionization of the molecule. For a given degree of ionization, all the dissociation channels are added. It will be interesting to study the orientation effect on individual dissociation channels. One would be able to answer the question that can the orientation of the molecule be used to dissociate into a particular channel? This type of study will be useful in surface chemistry, stereochemistry, selective bond breaking etc.

Conference contributions

1. 8th Topical Conference on Atomic and Molecular Collisions for Plasma Applications, 3 - 5 March 2020, IIT Roorkee, India
   P1. Orientation effect in multiple ionization of OCS under proton and C2+ impact at 50 keV

2. 31st International Conference on Photonic, Electronic and Atomic Collisions, 23 - 30 July 2019, Deauville, France
   P1. Orientation effects in ionization of CO by proton and ion impact
   P2. Electron Beam Ion Trap/Source for ion–molecule collisions in the non-perturbative regime

3. 22nd National Conference on Atomic and Molecular Physics, 25 - 28 March 2019, IIT Kanpur, India
   P1. Model Calculation To Study The Orientation Effect In Multiple Ionization Of Diatomic Molecule
   P2. Electron Beam Ion Source (EBIS) Facility at IISER, Pune

4. 13th Asian International Seminar on Atomic and Molecular Physics, 3 - 8 December 2018, IIT Bombay, India
   P1. Interaction Strength Dependence Of Orientation Effect In Multiple Ionization Of CO

5. 7th Topical Conference of the Indian Society of Atomic and Molecular Physics, 6 - 8 January 2018, Tirupati, India
   P1. Orientation effects in ionization of CO by proton and ion impact

Bibliography

1. J. Dalton, *A New System of Chemical Philosophy*, English, Courtesy of Science History Institute. Rights: Public Domain Mark 1.0 (Executors of S. Russell, Manchester, England, 1808), (https://digital.sciencehistory.org/works/ff365590j).

2. J. J. T. M. F.R.S., *The London, Edinburgh, and Dublin Philosophical Magazine and Journal of Science* **44**, 293–316, eprint: https://doi.org/10.1080/14786449708621070, (https://doi.org/10.1080/14786449708621070) (1897).

3. H. Gegier, E. Marsden, *Proc. R. Soc. Lond.* **82**, 495–500, eprint: https://doi.org/10.1098/rspa.1909.0054, (https://doi.org/10.1098/rspa.1909.0054) (1909).

4. P. E. R. F.R.S., *The London, Edinburgh, and Dublin Philosophical Magazine and Journal of Science* **21**, 669–688, eprint: https://doi.org/10.1080/14786440508637080, (https://doi.org/10.1080/14786440508637080) (1911).

5. N. B. D. phil., *The London, Edinburgh, and Dublin Philosophical Magazine and Journal of Science* **26**, 1–25, eprint: https://doi.org/10.1080/14786441308634955, (https://doi.org/10.1080/14786441308634955) (1913).

6. W. Heisenberg, *Zeitschrift für Physik* **33**, 879–893, ISSN: 0044-3328, (https://doi.org/10.1007/BF01328377) (1925).

7. *NIST database* (https://www.nist.gov/pml/atomic-spectra-database).

8. H. D. Hagstrum, *Rev. Mod. Phys.* **23**, 185–203, (https://link.aps.org/doi/10.1103/RevModPhys.23.185) (3 1951).

9. C. J. Powell, *Rev. Mod. Phys.* **48**, 33–47, (https://link.aps.org/doi/10.1103/RevModPhys.48.33) (1 1976).

10. E. Everhart, Q. C. Kessel, *Phys. Rev. Lett.* **14**, 247–249, (https://link.aps.org/doi/10.1103/PhysRevLett.14.247) (8 1965).

11. M. A. Coplan, J. H. Moore, J. P. Doering, *Rev. Mod. Phys.* **66**, 985–1014, (https://link.aps.org/doi/10.1103/RevModPhys.66.985) (3 1994).

12. J. B. Furness, I. E. McCarthy, *Journal of Physics B: Atomic and Molecular Physics* **6**, L204–L207, (https://doi.org/10.1088/0022-3700/6/8/004) (1973).

13. D. Wolfgang, *Atoms, Molecules and Photons*, English (Springer, Springer Heidelberg Dordrecht London New York, 2010), (https://link.springer.com/book/10.1007/978-3-642-10298-1#toc).

14. M. Born, R. Oppenheimer, *Annalen der Physik* **389**, 457–484, eprint: https://onlinelibrary.wiley.com/doi/pdf/10.1002/andp.19273892002, (https://onlinelibrary.wiley.com/doi/abs/10.1002/andp.19273892002) (1927).

15. A. C. Wahl, *Science* **151**, 961–967, ISSN: 0036-8075, eprint: https://science.sciencemag.org/content/151/3713/961.full.pdf, (https://science.sciencemag.org/content/151/3713/961) (1966).

16. L. Keldysh, *JETP* **20**, 1307, (http://www.jetp.ac.ru/cgi-bin/e/index/r/47/5/p1628?a=list) (1965).

17. K. Saha, S. Banerjee, B. Bapat, *Chemical Physics Letters* **607**, 85 –91, ISSN: 0009-2614, (http://www.sciencedirect.com/science/article/pii/S0009261414004126) (2014).

18. S. S. Kumar, P. C. Deshmukh, R. K. Kushawaha, V. Sharma, I. A. Prajapati, K. P. Subramanian, B. Bapat, *Phys. Rev. A* **78**, 062706, (https://link.aps.org/doi/10.1103/PhysRevA.78.062706) (6 2008).

19. J. A. Samson, *Physics Reports* **28**, 303 –354, ISSN: 0370-1573, (http://www.sciencedirect.com/science/article/pii/0370157376900120) (1976).

20. M. Wollenhaupt, V. Engel, T. Baumert, *Annual Review of Physical Chemistry* **56**, PMID: 15796695, 25–56, eprint: https://doi.org/10.1146/annurev.physchem.56.092503.141315, (https://doi.org/10.1146/annurev.physchem.56.092503.141315) (2005).

21. A. Assion, M. Geisler, J. Helbing, V. Seyfried, T. Baumert, *Phys. Rev. A* **54**, R4605–R4608, (https://link.aps.org/doi/10.1103/PhysRevA.54.R4605) (6 1996).

22. L. Fang *et al.*, *Phys. Rev. Lett.* **109**, 263001, (https://link.aps.org/doi/10.1103/PhysRevLett.109.263001) (26 2012).

23. I. I. Fabrikant, S. Eden, N. J. Mason, J. Fedor, *Chapter Nine - Recent Progress in Dissociative Electron Attachment: From Diatomics to Biomolecules* (Academic Press, 2017), vol. 66, pp. 545 –657, (http://www.sciencedirect.com/science/article/pii/S1049250X17300034).

24. J. N. Bardsley, F Mandl, *Reports on Progress in Physics* **31**, 471–531, (https://doi.org/10.1088%2F0034-4885%2F31%2F2%2F302) (1968).

25. L. J. KIEFFER, G. H. DUNN, *Rev. Mod. Phys.* **38**, 1–35, (https://link.aps.org/doi/10.1103/RevModPhys.38.1) (1 1966).

26. K. H. Becker, V Tarnovsky, *Plasma Sources Science and Technology* **4**, 307–315, (https://doi.org/10.1088%2F0963-0252%2F4%2F2%2F015) (1995).

27. P. L. Bartlett, A. T. Stelbovics, *Nuclear Instruments and Methods in Physics Research Section A: Accelerators, Spectrometers, Detectors and Associated Equipment* **619**, Frontiers in radiation physics and applications:Proceedings of the 11th International Symposium on Radiation Physics, 1 –6, ISSN: 0168-9002, (http://www.sciencedirect.com/science/article/pii/S0168900209020117) (2010).

28. V. Sharma, B. Bapat, J. Mondal, M. Hochlaf, K. Giri, N. Sathyamurthy, *The Journal of Physical Chemistry A* **111**, 10205–10211, ISSN: 1089-5639, (https://doi.org/10.1021/jp070257k) (2007).

29. X. Wang, Y. Zhang, D. Lu, G. C. Lu, B. Wei, B. H. Zhang, Y. J. Tang, R. Hutton, Y. Zou, *Phys. Rev. A* **90**, 062705, (https://link.aps.org/doi/10.1103/PhysRevA.90.062705) (6 2014).

30. V. Krishnamurthi, I Ben-Itzhak, K. D. Carnes, *Journal of Physics B: Atomic, Molecular and Optical Physics* **29**, 287, (http://stacks.iop.org/0953-4075/29/i=2/a=016) (1996).

31. H. O. Folkerts, R. Hoekstra, R. Morgenstern, *Phys. Rev. Lett.* **77**, 3339–3342, (https://link.aps.org/doi/10.1103/PhysRevLett.77.3339) (16 1996).

32. G. Handke, F. Tarantelli, L. S. Cederbaum, *Phys. Rev. Lett.* **76**, 896–899, (https://link.aps.org/doi/10.1103/PhysRevLett.76.896) (6 1996).

33. I. Ben-Itzhak, S. G. Ginther, K. D. Carnes, *Phys. Rev. A* **47**, 2827–2837, (https://link.aps.org/doi/10.1103/PhysRevA.47.2827) (4 1993).

34. E. Wells, V. Krishnamurthi, K. D. Carnes, N. G. Johnson, H. D. Baxter, D. Moore, K. M. Bloom, B. M. Barnes, H. Tawara, I. Ben-Itzhak, *Phys. Rev. A* **72**, 022726, (https://link.aps.org/doi/10.1103/PhysRevA.72.022726) (2 2005).

35. M Tarisien *et al.*, *Journal of Physics B: Atomic, Molecular and Optical Physics* **33**, L11, (http://stacks.iop.org/0953-4075/33/i=1/a=102) (2000).

36. E. Wells, T. Nishide, H. Tawara, R. L. Watson, K. D. Carnes, I. Ben-Itzhak, *Phys. Rev. A* **77**, 064701, (https://link.aps.org/doi/10.1103/PhysRevA.77.064701) (6 2008).

37. L Adoui, C Caraby, A Cassimi, D Lelièvre, J. P. Grandin, A Dubois, *Journal of Physics B: Atomic, Molecular and Optical Physics* **32**, 631, (http://stacks.iop.org/0953-4075/32/i=3/a=008) (1999).

38. N. Neumann *et al.*, *Phys. Rev. Lett.* **104**, 103201, (https://link.aps.org/doi/10.1103/PhysRevLett.104.103201) (10 2010).

39. R. K. Kushawaha, S. S. Kumar, M. R. Jana, I. A. Prajapati, C. P. Safvan, B Bapat, *Journal of Physics B: Atomic, Molecular and Optical Physics* **43**, 205204, (http://stacks.iop.org/0953-4075/43/i=20/a=205204) (2010).

40. M. R. Jana, P. N. Ghosh, B. Bapat, R. K. Kushawaha, K. Saha, I. A. Prajapati, C. P. Safvan, *Phys. Rev. A* **84**, 062715, (https://link.aps.org/doi/10.1103/PhysRevA.84.062715) (6 2011).

41. T. Weber *et al.*, *Phys. Rev. Lett.* **90**, 153003, (https://link.aps.org/doi/10.1103/PhysRevLett.90.153003) (15 2003).

42. R. Shingal, C. D. Lin, *Phys. Rev. A* **40**, 1302–1309, (https://link.aps.org/doi/10.1103/PhysRevA.40.1302) (3 1989).

43. Y. D. Wang, J. H. McGuire, *Phys. Rev. A* **44**, 367–372, (https://link.aps.org/doi/10.1103/PhysRevA.44.367) (1 1991).

44. S. Corchs, H. Busnengo, R. Rivarola, J. McGuire, *Nuclear Instruments and Methods in Physics Research Section B: Beam Interactions with Materials and Atoms* **117**, 41 –46, ISSN: 0168-583X, (http://www.sciencedirect.com/science/article/pii/0168583X96002340) (1996).

45. C. A. Tachino, M. E. Galassi, R. D. Rivarola, *Journal of Physics: Conference Series* **58**, 271, (http://stacks.iop.org/1742-6596/58/i=1/a=059) (2007).

46. T. Tonuma, H. Shibata, S. H. Be, H. Kumagai, M. Kase, T. Kambara, I. Kohno, A. Ohsaki, H. Tawara, *Phys. Rev. A* **33**, 3047–3053, (https://link.aps.org/doi/10.1103/PhysRevA.33.3047) (5 1986).

47. I. Ben-Itzhak, J. H. McGuire, *Phys. Rev. A* **38**, 6422–6423, (https://link.aps.org/doi/10.1103/PhysRevA.38.6422) (12 1988).

48. N. SASAKI, T. NAKAO, *Proceedings of the Imperial Academy* **11**, 138–140 (1935).

49. N. SASAKI, T. NAKAO, *Proceedings of the Imperial Academy* **11**, 413–415 (1935).

50. N. SASAKI, T. NAKAO, *Proceedings of the Imperial Academy* **17**, 75–77 (1941).

51. E. H. Kerner, *Phys. Rev.* **92**, 1441–1447, (https://link.aps.org/doi/10.1103/PhysRev.92.1441) (6 1953).

52. G. H. Dunn, *Phys. Rev. Lett.* **8**, 62–64, (https://link.aps.org/doi/10.1103/PhysRevLett.8.62) (2 1962).

53. G. H. Dunn, L. J. Kieffer, *Phys. Rev.* **132**, 2109–2117, (https://link.aps.org/doi/10.1103/PhysRev.132.2109) (5 1963).

54. T. A. Green, J. M. Peek, *Phys. Rev.* **183**, 166–179, (https://link.aps.org/doi/10.1103/PhysRev.183.166) (1 1969).

55. R. J. Van Brunt, L. J. Kieffer, *Phys. Rev. A* **2**, 1293–1304, (https://link.aps.org/doi/10.1103/PhysRevA.2.1293) (4 1970).

56. A Crowe, J. W. McConkey, *Journal of Physics B: Atomic and Molecular Physics* **6**, 2088–2107 (1973).

57. Y. D. Wang, J. H. McGuire, O. L. Weaver, S. E. Corchs, R. D. Rivarola, *Phys. Rev. A* **47**, 3966–3975, (https://link.aps.org/doi/10.1103/PhysRevA.47.3966) (5 1993).

58. K. Wohrer, R. L. Watson, *Phys. Rev. A* **48**, 4784–4786, (https://link.aps.org/doi/10.1103/PhysRevA.48.4784) (6 1993).

59. J. H. McGuire, L. Weaver, *Phys. Rev. A* **16**, 41–47, (https://link.aps.org/doi/10.1103/PhysRevA.16.41) (1 1977).

60. I. Ben-Itzhak, T. J. Gray, J. C. Legg, J. H. McGuire, *Phys. Rev. A* **37**, 3685–3691, (https://link.aps.org/doi/10.1103/PhysRevA.37.3685) (10 1988).

61. O. Heber *et al.*, *Phys. Rev. A* **39**, 4898–4901, (https://link.aps.org/doi/10.1103/PhysRevA.39.4898) (9 1989).

62. C. Caraby, A. Cassimi, L. Adoui, J. P. Grandin, *Phys. Rev. A* **55**, 2450–2452, (https://link.aps.org/doi/10.1103/PhysRevA.55.2450) (3 1997).

63. V. Horvat, O Heber, R. Watson, R. Parameswaran, J. Blackadar, *Nuclear Instruments and Methods in Physics Research Section B: Beam Interactions with Materials and Atoms* **99**, Application of Accelerators in Research and Industry '94, 94 –97, ISSN: 0168-583X, (http://www.sciencedirect.com/science/article/pii/0168583X94005532) (1995).

64. Z. Kaliman, N. M. Kabachnik, H. O. Lutz, *Phys. Rev. A* **65**, 012708, (https://link.aps.org/doi/10.1103/PhysRevA.65.012708) (1 2001).

65. N. M. Kabachnik, V. N. Kondratyev, Z. Roller-Lutz, H. O. Lutz, *Phys. Rev. A* **56**, 2848–2854, (https://link.aps.org/doi/10.1103/PhysRevA.56.2848) (4 1997).

66. N. M. Kabachnik, V. N. Kondratyev, Z. Roller-Lutz, H. O. Lutz, *Phys. Rev. A* **57**, 990–996, (https://link.aps.org/doi/10.1103/PhysRevA.57.990) (2 1998).

67. G. Schiwietz, P. Grande, *Nuclear Instruments and Methods in Physics Research Section B: Beam Interactions with Materials and Atoms* **153**, 1 –9, ISSN: 0168-583X, (http://www.sciencedirect.com/science/article/pii/S0168583X98009811) (1 1999).

68. A. K. Edwards, R. M. Wood, R. L. Ezell, *Phys. Rev. A* **31**, 99–102, (https://link.aps.org/doi/10.1103/PhysRevA.31.99) (1 1985).

69. A. K. Edwards, R. M. Wood, R. L. Ezell, *Phys. Rev. A* **31**, 3972–3973, (https://link.aps.org/doi/10.1103/PhysRevA.31.3972) (6 1985).

70. S. Varghese, C. Cocke, S. Cheng, E. Kamber, V. Frohne, *Nuclear Instruments and Methods in Physics Research Section B: Beam Interactions with Materials and Atoms* **40-41**, 266 –269, ISSN: 0168-583X, (http://www.sciencedirect.com/science/article/pii/0168583X89909750) (1 1989).

71. N. Bohr, *K. Dan. Vidensk. Selsk. Mat. Fys Medd.* **18**, 1–144, (https://link.aps.org/doi/10.1103/PhysRevA.65.012708) (1 1948).

72. B. Siegmann, U. Werner, Z. Kaliman, Z. Roller-Lutz, N. M. Kabachnik, H. O. Lutz, *Phys. Rev. A* **66**, 052701, (https://link.aps.org/doi/10.1103/PhysRevA.66.052701) (5 2002).

73. B Siegmann, U Werner, H Lebius, B Huber, H. Lutz, R Mann, *Nuclear Instruments and Methods in Physics Research Section B: Beam Interactions with Materials and Atoms* **205**, 11th International Conference on the Physics of Highly Charged Ions, 629 –633, ISSN: 0168-583X, (http://www.sciencedirect.com/science/article/pii/S0168583X03005937) (1 2003).

74. B. Siegmann, U. Werner, R. Mann, Z. Kaliman, N. M. Kabachnik, H. O. Lutz, *Phys. Rev. A* **65**, 010704, (https://link.aps.org/doi/10.1103/PhysRevA.65.010704) (1 2001).

75. Z. Man, Z. Xian-Rong, Z. Lei, C. Xi-Meng, W. Shi-Yao, Z. Wang, S. Jian-Xiong, *Chinese Physics B* **22**, 103402, (http://stacks.iop.org/1674-1056/22/i=10/a=103402) (1 2013).

76. M. Zhou, X. Zou, S. Wang, H. Zang, S. Niu, W. Liu, X. Chen, J. Shao, *International Journal of Mass Spectrometry* **357**, 45 –50, ISSN: 1387-3806, (http://www.sciencedirect.com/science/article/pii/S1387380613003473) (1 2014).

77. S. Cheng, C. L. Cocke, V. Frohne, E. Y. Kamber, J. H. McGuire, Y. Wang, *Phys. Rev. A* **47**, 3923–3929, (https://link.aps.org/doi/10.1103/PhysRevA.47.3923) (5 1993).

78. T Mizuno, T Majima, H Tsuchida, Y Nakai, A Itoh, *Journal of Physics: Conference Series* **58**, 173, (http://stacks.iop.org/1742-6596/58/i=1/a=034) (1 2007).

79. H. J. Lüdde, T. Spranger, M. Horbatsch, T. Kirchner, *Phys. Rev. A* **80**, 060702, (https://link.aps.org/doi/10.1103/PhysRevA.80.060702) (6 2009).

80. X. Hong, F. Wang, Y. Wu, B. Gou, J. Wang, *Phys. Rev. A* **93**, 062706, (https://link.aps.org/doi/10.1103/PhysRevA.93.062706) (6 2016).

81. K. Sarvesh, K. P, L. P. S, R. G, S. C. P, M. A, K. D, *Design of new low energy ion beam facility at IUAC*, 2009, (https://www.osti.gov/etdeweb/biblio/22322014).

82. W. C. Wiley, I. H. McLaren, *Review of Scientific Instruments* **26**, 1150–1157, eprint: https://doi.org/10.1063/1.1715212, (https://doi.org/10.1063/1.1715212) (1 1955).

83. J Ullrich, R Moshammer, R Dörner, O Jagutzki, V Mergel, H Schmidt-Böcking, L Spielberger, *Journal of Physics B: Atomic, Molecular and Optical Physics* **30**, 2917–2974, (https://doi.org/10.1088%2F0953-4075%2F30%2F13%2F006) (1 1997).

84. R. Dörner, V. Mergel, O. Jagutzki, L. Spielberger, J. Ullrich, R. Moshammer, H. Schmidt-Böcking, *Physics Reports* **330**, 95 –192, ISSN: 0370-1573, (http://www.sciencedirect.com/science/article/pii/S037015739900109X) (1 2000).

85. A. Kumar, J. Rajput, T. Sairam, M. Jana, L. Nair, C. Safvan, *International Journal of Mass Spectrometry* **374**, 44 –48, ISSN: 1387-3806, (http://www.sciencedirect.com/science/article/pii/S1387380614004035) (1 2014).

86. D. D. D. Manura, *SIMION User Manual* (Scientific Instrument Services, Inc., 8.0, 2008), vol. 65, p. 012708, (https://link.aps.org/doi/10.1103/PhysRevA.65.012708).

87. A. Czasch, J. Milnes, N. Hay, W. Wicking, O. Jagutzki, *Nuclear Instruments and Methods in Physics Research Section A: Accelerators, Spectrometers, Detectors and Associated Equipment* **580**, Imaging 2006, 1066 –1070, ISSN: 0168-9002, (http://www.sciencedirect.com/science/article/pii/S0168900207013241) (1 2007).

88. I. Ali *et al.*, *Nuclear Instruments and Methods in Physics Research Section B: Beam Interactions with Materials and Atoms* **149**, 490 –500, ISSN: 0168-583X, (http://www.sciencedirect.com/science/article/pii/S0168583X98009161) (1 1999).

89. D. Sankar, PhD dissertation, University of Calcutta, 2006, p. 012708, (https://link.aps.org/doi/10.1103/PhysRevA.65.012708).

90. K. Ajit, PhD dissertation, Jamia Millia Islamia University, 2014, p. 012708, (https://link.aps.org/doi/10.1103/PhysRevA.65.012708).

91. Z. Kaliman, N. M. Kabachnik, H. O. Lutz, *Phys. Rev. A* **65**, 012708, (https://root.cern) (1 2001).

92. J. H. D. Eland, *Laser Chemistry* **11**, 717149, ISSN: 0278-6273, (https://doi.org/10.1155/LC.11.259) (1 1991).

93. J. C. Slater, *Phys. Rev.* **36**, 57–64, (https://link.aps.org/doi/10.1103/PhysRev.36.57) (1 1930).

94. E. Wells, V. Krishnamurthi, K. D. Carnes, N. G. Johnson, H. D. Baxter, D. Moore, K. M. Bloom, B. M. Barnes, H. Tawara, I. Ben-Itzhak, *Phys. Rev. A* **72**, 022726, (https://link.aps.org/doi/10.1103/PhysRevA.72.022726) (2 2005).

95. V. Krishnamurthi, I Ben-Itzhak, K. D. Carnes, *Journal of Physics B: Atomic, Molecular and Optical Physics* **29**, 287–297, (https://doi.org/10.1088/0953-4075/29/2/016) (1 1996).

96. B. Wales *et al.*, *Journal of Electron Spectroscopy and Related Phenomena* **195**, 332 –336, ISSN: 0368-2048, (http://www.sciencedirect.com/science/article/pii/S0368204814001121) (1 2014).

97. A. Ramadhan, B. Wales, R. Karimi, I. Gauthier, M. MacDonald, L. Zuin, J. Sanderson, *Journal of Physics B: Atomic, Molecular and Optical Physics* **49**, 215602, (https://root.cern) (1 2016).

98. Z. Shen, E. Wang, M. Gong, X. Shan, X. Chen, *The Journal of Chemical Physics* **145**, 234303, (https://doi.org/10.1063/1.4972064) (1 2016).

99. A. Khan, L. C. Tribedi, D. Misra, *Phys. Rev. A* **96**, 012703, (https://link.aps.org/doi/10.1103/PhysRevA.96.012703) (1 2017).

100. T. Jiang, B. Wang, Y. Zhang, L. Wei, S. Chen, W. Yu, Y. Zou, L. Chen, B. Wei, *Phys. Rev. A* **100**, 022705, (https://link.aps.org/doi/10.1103/PhysRevA.100.022705) (2 2019).

101. J. Rajput *et al.*, *Phys. Rev. Lett.* **120**, 103001, (https://link.aps.org/doi/10.1103/PhysRevLett.120.103001) (10 2018).

102. H. Kumar, P. Bhatt, C. P. Safvan, J. Rajput, *The Journal of Chemical Physics* **148**, 064302, (https://doi.org/10.1063/1.5001121) (1 2018).

103. P. Erman, A. Karawajczyk, E. Rachlew, M. Stankiewicz, K. Yoshiki Franzén, *Phys. Rev. A* **56**, 2705–2712, (https://link.aps.org/doi/10.1103/PhysRevA.56.2705) (4 1997).

104. J.-i. Adachi, N. Kosugi, E. Shigemasa, A. Yagishita, *The Journal of Chemical Physics* **107**, 4919–4926, (https://doi.org/10.1063/1.474855) (1 1997).

105. J. Laksman, D. Céolin, M. Gisselbrecht, S. L. Sorensen, *The Journal of Chemical Physics* **133**, 144314, (https://doi.org/10.1063/1.3502116) (1 2010).

106. L. Holmegaard *et al.*, *Nature Physics* **6**, 428–432, ISSN: 1745-2481, (https://doi.org/10.1038/nphys1666) (1 2010).

107. Y. Sakemi, S. Minemoto, H. Sakai, *Phys. Rev. A* **96**, 011401, (https://link.aps.org/doi/10.1103/PhysRevA.96.011401) (1 2017).

108. U. Werner, N. M. Kabachnik, V. N. Kondratyev, H. O. Lutz, *Phys. Rev. Lett.* **79**, 1662–1665, (https://link.aps.org/doi/10.1103/PhysRevLett.79.1662) (9 1997).

109. B. Wales, T. Motojima, J. Matsumoto, Z. Long, W.-K. Liu, H. Shiromaru, J. Sanderson, *Journal of Physics B: Atomic, Molecular and Optical Physics* **45**, 045205, (https://root.cern) (1 2012).